In vitro studies of NOS inhibitors using purified human NOS isozymes

by

Danica Estavillo

A thesis
presented to the University of Waterloo
in fulfillment of the
thesis requirement for the degree of
Master of Science
in
Chemistry

Waterloo, Ontario, Canada, 2017

Author's Declaration

I hereby declare that I am the sole author of this thesis. This is a true copy of the thesis, including any required final revisions, as accepted by my examiners.

I understand that my thesis may be made electronically available to the public.

Abstract

Endogenous nitric oxide (NO) is derived from L-arginine via a chemical reaction catalyzed by nitric oxide synthases (NOS). Three NOS isozymes are found in humans: neuronal NOS (nNOS), endothelial NOS (eNOS) and inducible NOS (iNOS). Over-activation of NOS enzymes lead to pathologies due to excessive NO production. In particular, nNOS and iNOS are implicated in serious neurodegenerative and inflammatory diseases, and are hence attractive pharmacological targets. However, off-target inhibition of eNOS results in adverse effects such as hypertension and atherosclerosis. To complicate drug design, the NOS active site sequence is highly conserved across isozymes. Most of the currently available NOS inhibitors have been designed through and assayed against non-human mammalian NOS isozymes but the recent publication of the human nNOS oxygenase crystal structures showed minute differences in structure between human NOS and their non-human counterparts. Oxyhemoglobin capture assays were performed to determine the specific activity of each NOS isoform and plot the corresponding Michaelis-Menten curves to determine their relative affinity towards the substrate L-arginine. These assays, which are performed in quadruplicates, show significant difference in the activity of human NOS and non-human NOS. Furthermore, discrepancies in the K_m values of human NOS and non-human NOS were observed.

Inhibition studies using first generation active site inhibitors were performed in quadruplicates to confirm their isoform selectivity as previously determined using non-human NOS isoforms. L-arginine based inhibitors L-NMMA, L-ALA and L-NNA were shown to be non-selective over eNOS. However, the affinity ranking (in terms of K_i) of human NOS toward these L-ALA and L-NNA did not agree with the affinity rankings for non-human NOS. The K_i values of the cyclic aromatic compound 3-bromo-7-nitroindazole did not vary among isoforms for both human and non-human NOS, as previously available data. In contrast, the iNOS selective isoform 1400W showed significantly higher affinity towards iNOS over nNOS and eNOS. Given these preliminary results, the minute differences in sequence and structure between human and non-human NOS appear to have substantial effects on the selectivity of first generation inhibitors. However, it is important to note that these results need to be verified by structural studies, which can be used to pinpoint the differences in the binding of these inhibitors between human and non-human NOS.

To determine if human and non-human NOS are affected by calmodulin-binding inhibitors differently, inhibition assays were performed with trifluoperazine (TFP) and melatonin. Since both of these inhibitors bind CaM instead of NOS, it is expected that their IC50s for human and non-human NOS isoforms would be similar. Furthermore, the fact that these compounds bind CaM in a similar manner suggests that TFP and melatonin would have similar dose-inhibition curves. However, only TFP exhibited dose-dependent inhibition of NOS, while melatonin did not inhibit NOS at all. In any case, the inhibition assay results for both did not show differences between human and non-human NOS.

Acknowledgements

Firstly, I express my deepest gratitude to my supervisor, Dr. Guy Guillemette, for his exemplary guidance and erstwhile support over the course of this project. The man's patient encouragement through years of frustration and, eventually, satisfaction is insurmountable. It is a pleasure to learn under his tutelage. I extend my thanks to the members of my supervisory committee, Dr. Thorsten Dieckmann and Dr. Gary Dmitrienko, for their helpful suggestions and constructive criticisms. Having them as mentors has benefited me a lot, not just academically but also in other aspects in life.

Many, many thanks to all my friends and colleagues. To the members of the Guillemette, Dieckmann and Dmitrienko labs: Dr. Mike Piazza, John Lape, Volition La, Kyle Piccolo and Carol Tanner for their keen assistance in my research. Their company and the interesting conversations about science and life made my experience so valuable. To my CGSS co-execs, for the time spent planning and organizing events which proved how important and how fun breaks can be. Free food, it turns out, is a great vehicle for building community among stressed out graduate students. To my fellow volunteers at the UWaterloo Science Outreach, for giving me the opportunity to teach kids science. It was very fulfilling to see the wonder in their eyes when they realize how cool and not scary science can be.

Finally, a whole lot of thanks to Christy, Danny and Dyan, for the unconditional love and support, endless encouragements and the best *kaldereta* in the whole wide universe. I wouldn't be where I am without you. I couldn't have done this without you.

Dedication

To the revolution!

Table of Contents

List of Figures

List of Tables

List of Abbreviations

1400W	N-(3-(aminomethyl)benzyl)acetamidine
3Br7NI	3-bromo-7-nitroindazole
5C HS	five-coordinated high spin
6C LS	six-coordinated low-spin
ACh	acetylcholine
ADP	adenosine diphosphate
AI	autoinhibitory loop
ATP	adenosine triphosphate
BSA	bovine serum albumin
CaM	calmodulin
cGMP	cyclic guanosine monophosphate
cNOS	constitutive NOS
CO	carbon monoxide
CT	C-terminal tail
Cyt C	cytochrome C
DDAH-1	dimethylarginine dimethylaminohydrolase-1
DMSO	dimethyl sulfoxide
DTT	dithiothreitol
EDTA	ethylenediaminetetraacetic acid
eNOS	endothelial NOS
EtBr	ethidium bromide
FAD	flavin adenine dinucleotide
$FeCN_6$	ferricyanide
FMN	flavin mononucleotide
FPLC	fast protein liquid chromatography
GTP	guanoside triphosphate
H_4B	tetrahydrobiopterin
HO-1	heme oxygenase-1
IFN	interferon
iNOS	inducible NOS
IPTG	β-D-1-thiogalactopyranoside
L-ALA	N^G-allyl-L-arginine
LB	Luria-Bertani broth
L-NMMA	N^G-methyl-arginine
L-NMMA	N^G-monomethyl-L-arginine
L-NNA	N^G-nitro-L-arginine
L-NOHA	N^ω-hydroxy-L-arginine

Abbreviations continued

LTP	long-term potentiation
metHb	methemoglobin
MLCK	myosin light chain kinase
NADPH	reduced nicotinamide adenine dinucleotide phosphate
NMDA	*N*-methyl-D-aspartate
nNOS	neuronal NOS
NO	nitric oxide
NOS	nitric oxide synthase
oxyHb	oxyhemoglobin
PCR	Polymerase Chain Reaction
PDZ	PSD-95 discs large/ZO-1
PKG	protein kinase G
PMSF	phenylmethylsulfonyl fluoride
RNS	reactive nitrogen species
ROS	reactive oxygen species
SB	super broth
SDS-PAGE	sodium dodecyl sulfate polyacrylamide gel electrophoresis
TB	terrific broth
TFP	trifluoroperazine
TNF	tumour necrosis factor
UV	ultraviolet
δ-ALA	δ-aminolevulinic acid

Chapter 1

1. Literature review

1.1 Nitric oxide physiology

Nitric oxide (NO) is a signalling molecule that plays a critical role in the maintenance of normal physiology in mammals, including humans. NO is small and gaseous, and thus, diffuses freely across membranes. Its short half-life allows for its short range of action. Primarily, NO induces the conversion of guanosine triphosphate into cyclic guanosine monophosphate (cGMP) by binding and activating soluble guanylyl cyclase in the target cell. cGMP is a secondary intracellular molecule and it is involved in most physiological pathways, e.g. cardiovascular regulation, immune response and neurotransmission. cGMP binds and activates cGMP-dependent protein kinase or protein kinase G, which initiates a signalling cascade, the effects of which are dose-dependent and tissue-specific.(Alderton, Cooper, & Knowles, 2001) NO functions in neurotransmission, cardiovascular regulation and immune response.

Given its role in normal physiology and short half-life ($t_{1/2}$ = 5 s), NO is constantly produced at low levels in the body, except during disease.(Alderton et al., 2001; Joubert & Malan, 2011) However, overproduction of NO leads to serious pathological conditions, some of which could be fatal. NO overproduction has been implicated in neurodegenerative diseases. It has also been shown that high levels of NO causes uncontrolled inflammation. Furthermore, NO can react with other physiological compounds to form reactive nitrogen species (RNS) that are detrimental to cell growth and development. Peroxynitrite ($ONOO^-$) is an RNS that is highly reactive with various biological targets. As such, regulation of NO synthesis is an important field in pharmacological research.

1.2 Nitric oxide synthase

Endogenous NO is derived from L-arginine via a chemical reaction catalyzed by nitric oxide synthase (NOS).(Alderton et al., 2001) There are three known NOS isozymes found in mammals: neuronal NOS (nNOS), endothelial NOS (eNOS) and inducible NOS (iNOS).(Alderton et al., 2001) The first two are constitutively expressed, i.e. exist at a constant level at normal physiological state, and are sometimes collectively referred to as constitutive NOS (cNOS).(Alderton et al., 2001) nNOS is primarily found in the neuronal cells and is involved in NO-mediated neurotransmission. eNOS is expressed in endothelial cells and is essential to cardiovascular regulation through NO-induced vasodilation.(Alderton et al., 2001) Meanwhile,

iNOS expression is induced by inflammatory cytokines during diseased state and is highly linked to immune response.(Alderton et al., 2001) NOS enzyme catalysis is activated upon binding of the protein cofactor, calmodulin (CaM).

1.2.1 NOS isoforms, related physiology and pathophysiology

As mentioned above, there are three known mammalian NOS isozymes and the effects of NO signalling are dependent on which NOS enzyme synthesized the NO molecule. The differences among nNOS, eNOS and iNOS are discussed in this section.

1.2.1.1 Neuronal nitric oxide synthase (nNOS)

As suggested by its name, nNOS is constitutively expressed in neurons of the nervous system. Even so, nNOS expression can be affected by neurotransmitter and steroid hormone signalling.(Joubert & Malan, 2011) Furthermore, gene regulation may induce nNOS alternative splicing, which results in the selective expression of nNOS isoforms: nNOS-α, nNOS-β, nNOS-γ and nNOS-μ.(Eliasson, Blackshaw, Schell, & Snyder, 1997; Joubert & Malan, 2011) nNOS-α refers to the full-length nNOS peptide. Unlike eNOS and iNOS, the nNOS isozyme has the 220 amino acid-long PSD-95 discs large/ZO-1 (PDZ; PSD stands for post-synaptic density protein 95) homology domain. The PDZ domain mediates the anchoring of nNOS to the neuronal membrane and the C-terminus of the N-methyl-D-aspartate (NMDA) receptor.(Alderton et al., 2001) In general, nitrergic signalling begins with the activation of the NMDA receptor by the neurotransmitter glutamate. NMDA is a ligand-gated calcium channel, whose activation triggers an influx of calcium ions. The subsequent increase in intracellular calcium then activates CaM proteins. Activated CaM binds and activates nNOS as described before, causing an increase in NO production. NO activates soluble GC, causing an increase in intracellular cGMP, which then activates PKG. In nitrergic neurons, PKG phosphorylates and activates potassium ion channels. Furthermore, since NO can diffuse freely across membranes, it can travel to neighbouring neurons and activate the soluble GCs in those cells as well where other ion channels are also activated by PKG.(Mukherjee, Cinelli, Kang, & Silverman, 2014; Taqatqeh et al., 2009)

NO neurotransmission has been implicated in the learning process and memory formation, particularly in long-term potentiation (LTP).(Hopper & Garthwaite, 2006; Taqatqeh et al., 2009) Increased levels of NO have been shown to improve memory and restore observable LTP in nNOS knockout rats.(Hopper & Garthwaite, 2006) However, increased NO production in neurons could lead to neurotoxicity and given the free diffusion of NO across membranes, these neuronal deaths

are not confined within a single cell only. NO-induced neurotoxicity is linked to neurodegenerative diseases such as Alzheimer's and Huntington's diseases.(Mukherjee et al., 2014) In both cases, neuronal deaths are caused by oxidative damage in cellular organelles due to NO over-excitation. In the case of Parkinson's disease, tyrosine nitration of select proteins causes the formation of inclusion bodies that are insoluble and resistant to normal degradation pathways thereby preventing normal neuron function.(Mukherjee et al., 2014)

1.2.1.2 Endothelial nitric oxide synthase (eNOS)

NO is involved in the maintenance of vascular tone; eNOS constitutively produces low levels of NO to balance adrenergic vasoconstriction and prevent hypertension. Under normal physiological conditions, eNOS in vascular endothelial cells are stimulated by the parasympathetic nervous system through the neurotransmitter acetylcholine (ACh).(Kellogg, Zhao, Coey, & Green, 2005) ACh binds and activates M3 receptors in endothelial cells, which are Gq-protein coupled receptors. Activation of this signalling pathway increases the intracellular calcium concentration, which causes the activation of the NOS cofactor CaM.(Kellogg et al., 2005) CaM then activates eNOS, as described above, and the NO produced by eNOS freely diffuses into adjacent vascular smooth muscle cells, where it activates soluble GC.(Palmer, Ashton, & Moncada, 1988) In this case, cGMP binds and inactivates calcium ions, thus causing a decrease in the intracellular calcium concentration of vascular smooth muscles. In addition, cGMP activates PKG, which phosphorylates and inactivates myosin light chain kinase (MLCK), thereby preventing contraction of the smooth muscle cells. Vasodilation reduces the blood pressure. Indeed, exogenous NO, derived from nitroglycerin and other nitrates, have been used in the pharmacological treatment of hypertension. A caveat, however, is that soluble GC in the vasculature is prone to desensitization of NO. As such, NO loses potency if given at doses higher than the physiological levels. To counter this, NO production by eNOS is regulated via a negative feedback loop; NO inhibits its own production by S-nitrosylation of select tyrosine residues in the eNOS enzyme.(Joubert & Malan, 2011; Kellogg et al., 2005) This mechanism ensures tight regulation of NO activity in the cardiovascular system. NO also inhibits platelet aggregation, which has direct effects on the prevention of atherosclerosis and increased blood pressure.

1.2.1.3 Inducible nitric oxide synthase (iNOS)

Unlike nNOS and eNOS, iNOS is not constitutively expressed. Rather, its expression is triggered as part of immune response, hence the term inducible. As well, the iNOS control

mechanism is at the gene level owing primarily to its tight and calcium-independent interaction with CaM. During microbial infections, proinflammatory cytokines such as tumour necrosis factors (TNF) and interferons (IFN) bind the iNOS gene promoter in macrophage cells and trigger iNOS transcription.(Green et al., 1994) TNFs and IFNs are regulated by a positive feedback loop, causing a dramatic increase in iNOS expression during immune response. Macrophages and other phagocytic immune cells contain a considerable amount of reactive oxygen species (ROS) to aid in processing and clearance of infections. Since NO is a radical, it could react with ROS to form RNS such as peroxynitrite ($ONOO^-$) and nitrogen dioxide (NO_2).(Alderton et al., 2001) Both ROS and RNS induce damage to microbes which causes apoptotic cell death. Immune cells employ a cytoprotective system against ROS and RNS because they also pose danger to host cells in the same manner.(Joubert & Malan, 2011; Okamoto et al., 2010) Recall that NO activation of soluble GC increases intracellular cGMP levels. RNS react with cGMP to form the nitrated nucleotide 8-nitro-cGMP, which then induce heme oxygenase (HO)-1. HO-1 has been shown to reduce host cell apoptosis.(Okamoto et al., 2010) In the event of NO overproduction by iNOS under normal physiological conditions, the HO-1-mediated cytoprotective mechanism gets overwhelmed and unnecessary cell death occurs and the increased activity of the immune system leads to symptoms akin to auto-immune diseases, including uncontrolled inflammation.(Okamoto et al., 2010)

1.2.2 NOS structure and NO synthesis

All NOS isozymes contain the same major domains: an N-terminal oxygenase domain and a C-terminal reductase domain that are connected by a CaM binding site.(Alderton et al., 2001; Stuehr, Santolini, Wang, Wei, & Adak, 2004) Figure 1.1a shows the crystal structure of the iNOS holoenzyme. The major domains are conserved across isozymes, consistent with the 50-57% sequence identity among them (Figure 1.1b). Additionally, NOS isozymes have similar quaternary shape, cofactor orientation and active site conformation. The reductase domain contains sites for the binding of cofactors flavin adenine dinucleotide (FAD), flavin mononucleotide (FMN) and reduced nicotinamide adenine dinucleotide phosphate (NADPH), whereas the oxygenase domain has binding sites for (6R)-5,6,7,8-tetrahydrobiopterin (H_4B), heme propionate and L-arginine.(Alderton et al., 2001; Stuehr et al., 2004) NOS requires both dimerization and binding of the aforementioned cofactors for enzymatic activity to proceed.(Alderton et al., 2001; Stuehr et al., 2004) Both domains are catalytically active, allowing for biophysical studies to elucidate the

reduction and oxidation reactions of NOS enzymes separately.(Alderton et al., 2001; Stuehr et al., 2004)

a

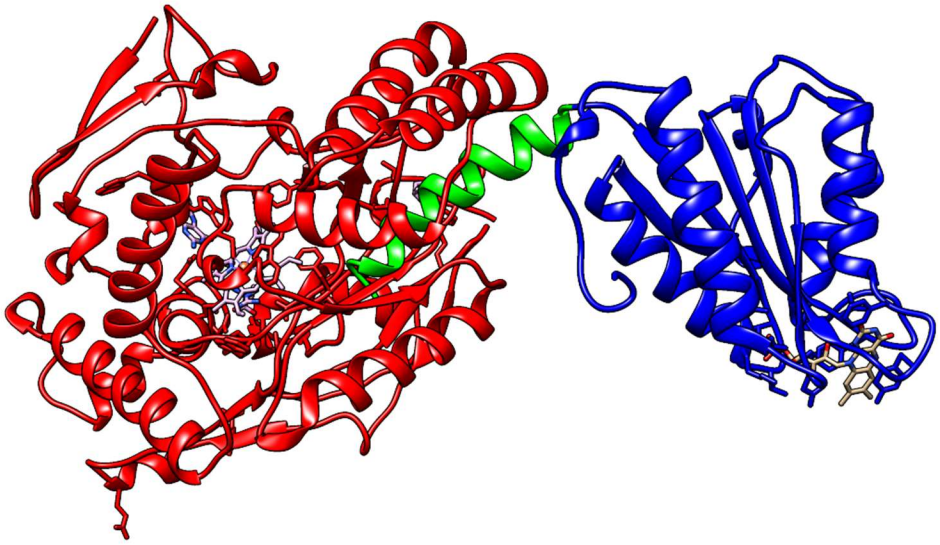

b

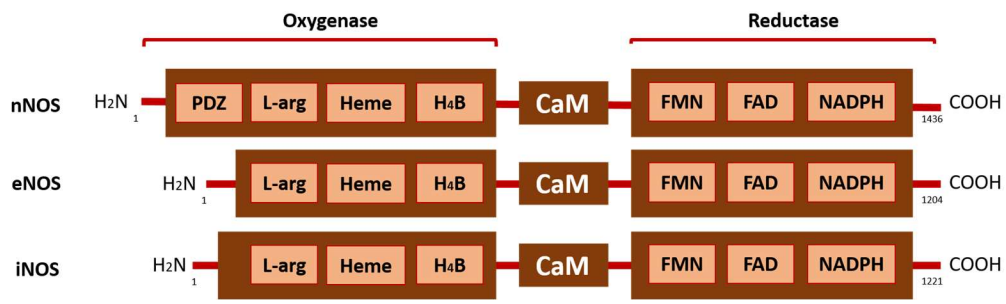

Figure 1.1. NOS holoenzyme structure. (a) Crystal structure of the published segments of the human iNOS. Note that the domain structures are obtained separately due to the highly dynamic nature of NOS. This image is a composite of the oxygenase (red, PDB ID: 1NSI) and the reductase (blue, PDB ID: 3HR4) structures aligned using Chimera. These domains are linked by the CaM binding region (green). At the time of writing, there is no complete NOS holoenzyme structure available. (b) NOS isoform sequences are highly conserved; they contain the same domains and subdomains.

Active NOS enzymes exist as homodimers; dimerization is required for function and binding of other cofactors. Once the dimer is formed, dissociating NOS into monomers requires a huge amount of energy (Mukherjee et al., 2014). As such, the NOS dimer is unlikely to separate unless subjected to heat or a denaturing agent. The importance of dimerization is highlighted by the fact that the amino acid residues involved in dimerization are highly conserved across isozymes. Each NOS subunit requires one molecule of H_4B; H_4B binds NOS at the dimer interface. It interacts with one NOS monomer via a conserved Trp residue through π-π stacking. H_4B forms H-bonds with the backbone carbonyl groups of conserved Ser112 and Ile456, as well as the Arg

side chain.(Tejero & Stuehr, 2013) For the other NOS monomer, it coordinates water in an H-bond network with conserved Trp and Phe in the oxygenase domain.(Tejero & Stuehr, 2013) Its position near the active site allows H_4B to function as an electron donor and acceptor during the NOS catalytic cycle.(Lang, Santolini, & Couture, 2011) It is important to note that the chirality of H_4B affects its affinity towards NOS. The naturally occurring R isomer binds NOS at 17 times higher affinity than the S isomer.(Gross, Stuehrt, Jaffet, & Griffitho, 1990)

Roman et al.'s crystal structure of the truncated domain showed that the rat nNOS reductase dimerize in addition to the oxygenase domains. This was similarly observed in Volkmann et al.'s cryo-EM studies of the full-length eNOS holoenzyme.(Volkmann et al., 2014) In contrast, Campbell et al.'s cryo-EM images of the full-length human iNOS holoenzyme show that only the oxygenase domains dimerize.(Campbell, Smith, Potter, Carragher, & Marletta, 2014) For all three isoforms, CaM appears to stabilize the dimer formation via its interactions with both subunits in addition to the CaM binding sites.

1.2.2.1 NOS activation by CaM

In addition to dimerization, all NOS isoforms also require CaM binding to produce NO. The 25-residue sequence between the reductase and oxygenase domains of a NOS monomer is a conserved region, to which CaM binds.(Curtin, Kinsella, & Stephens, 2015) The CaM binding regions of mammalian NOS isoforms follow a 1-5-8-14 motif, where the first, fifth, eighth and fourteenth residues in the binding sequence interact non-covalently with the CaM protein. (Figure 1.2)(Curtin et al., 2015) In cNOS, these residues are conserved as Phe, Ala, Val and Leu, whereas in iNOS, the first two residues are replaced with Leu and Val.(Curtin et al., 2015) Furthermore, the iNOS CaM binding sequence itself contains more hydrophobic residues than those of cNOS. This increase in hydrophobicity is linked to the increased affinity of CaM for iNOS compared to cNOS. Indeed, CaM binds iNOS regardless of intracellular calcium concentration so that iNOS always exists as a tetramer (one NOS dimer, with CaM bound to each monomer).(Alderton et al., 2001) Meanwhile, CaM binding to cNOS requires calcium to form the active tetramer. Previous studies have shown that nNOS and eNOS require 200-300 nM Ca^{2+} to achieve half maximal NO synthesis activity; physiological [Ca^{2+}] is 225 nM.(Piazza, Guillemette, & Dieckmann, 2015)

```
nNOS          R R A I G F K K L A E A V K F S A K L M     731 - 750
eNOS          T R K K T F K E V A N A V K I S A S L M     491 - 510
iNOS          R R E I P L K L K V K A V L F A C M L M     510 - 529
                          1       5    8          14
```

Figure 1.2. CaM binding sequence. Human NOS isoforms contain a conserved 1-5-8-14 CaM binding motif.

The mechanism of NOS activation by CaM is currently not fully understood. However, recent studies using fluorescence, cryo-EM, pulsed electron resonance and spectroscopic techniques have shown that CaM promotes the electron flow from the reductase domain to the oxygenase heme by facilitating the interactions between these two domains.(Campbell et al., 2014; Volkmann et al., 2014)

1.2.2.2 Catalytic mechanism

An invariant Glu residue in the L-arginine binding site was found in all isozymes across species. Two guanidino nitrogens of the L-arginine substrate form a hydrogen bond with the carboxylate moiety of the conserved Glu residue at the NOS active site, in addition to a hydrogen bond with the carbonyl of the conserved Trp.(Fan, Stuehr, & Rousseau, 2009; Mukherjee et al., 2014; Stuehr et al., 2004) The L-arginine substrate interacts with the heme propionate through its third guanidino nitrogen.(Mukherjee et al., 2014; Stuehr et al., 2004) Additionally, the π electrons of the guanidino group have stacking interactions with the heme rings to further stabilize the ligand-enzyme interaction.(Li et al., 2014; Mukherjee et al., 2014) These interactions, and thus the catalytic conversion of L-arginine into L-citrulline and radical NO powered by coupled electron transfers carried out by nNOS is similar to that of eNOS and iNOS.

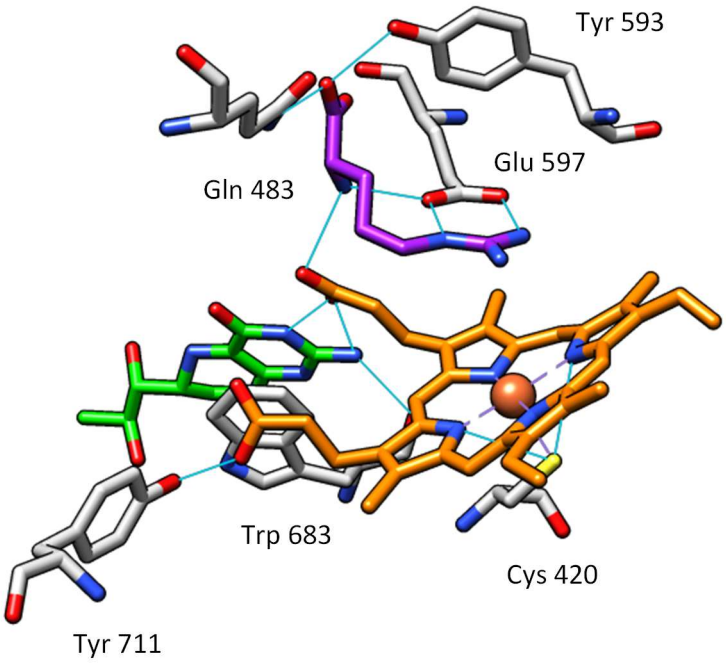

Figure 1.3. NOS active site. In human nNOS, L-arginine (purple) is anchored to the active site by conserved Gln, Tyr and Glu residues (white). It also interacts with the heme (orange) via H bonding and π stacking interactions. The interaction of the heme propionate and active site residue Trp with the cofactor H_4B (green) promotes the correct orientation of the substrate for oxidation. This active site was obtained from the crystal structure of the human nNOS oxygenase domain on PDB (4D1N). This image was created using Chimera.

The intradomain electron flow from NADPH to FAD to FMN in the reductase domain involves a complicated conformational change that culminates in the inter-subunit reduction of the heme Fe(III) by FMN. To understand the different steps of the interflavin electron flow, the NOS reductase can be further divided into two subdomains: the NADPH/FAD subdomain and the FMN subdomain. The FMN subdomain is separated from the rest of the reductase via a 23-25 residue hinge sequence. This hinge region is flexible and facilitates the movement of the FMN domain to deliver the flavin to the appropriate redox partner.

Prior to NADPH binding, the NOS dimer adopts an "open" state, in which the NADPH/FAD subdomain and the FMN subdomain are in an extended conformation. A conserved Phe reside (Phe1395 in nNOS) rotates such that NADPH directly sits on top the bound FAD molecule(Campbell et al., 2014; Leferink, Hay, Rigby, & Scrutton, 2014) As shown in Figure 1.4, NADPH donates a hydride ion to FAD and the $NADP^+$-$FADH_2$ complex is formed.(Yamamoto, Kimura, Shiro, & Iyanagi, 2005) The rotation by Phe then causes the NOS dimer to be in a "closed" state, in which the FMN subdomain is buried onto the NADPH and FAD interface. Arg1400 in the

C-terminal tail of the nNOS reductase domain has been shown to form a salt bridge with the negatively charged 2' phosphate group of NADPH.(Tiso et al., 2005) This electrostatic interaction orients NADPH in such a way that it interacts with both the C-terminal end of the reductase and the FMN binding site, stabilizing the "closed" state of the NOS dimer. In this conformation, $FADH_2$ quickly transfers an electron to FMN, forming the reduced FMNH.(Yamamoto et al., 2005) The electron flow through the reductase domain occurs relatively quickly compared to the inter-domain electron transfer from FMN to the heme. Indeed, this is the rate limiting step in the NO biosynthesis. As shown in Figure 1.4b, the FMN subdomain becomes "unburied" from the rest of the reductase domain and "swings" toward the oxygenase heme.(Campbell et al., 2014) This conformational change requires CaM binding.

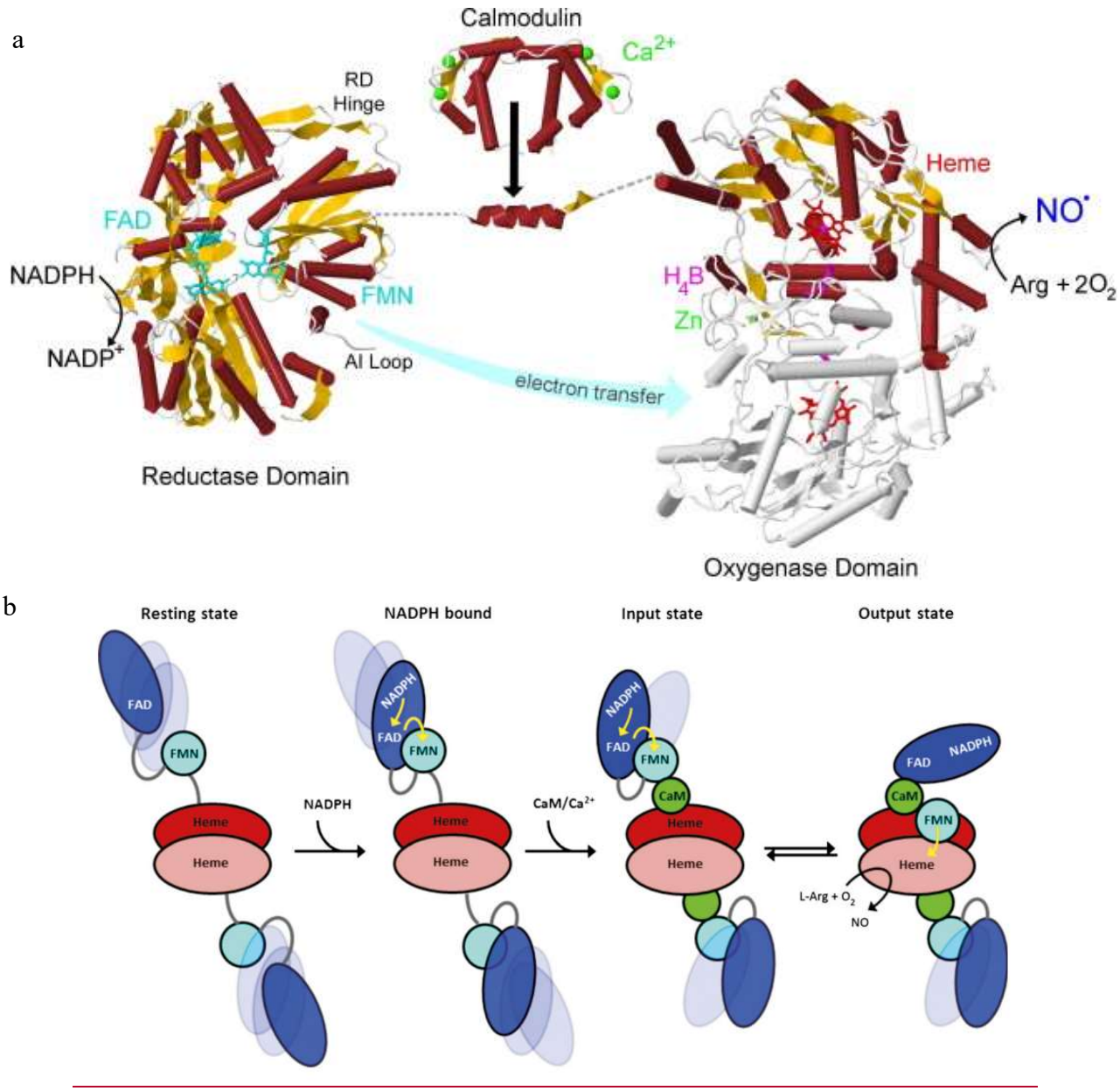

Figure 1.4. Electron transfer in the NOS from the reductase domain to the oxygenase domain. (a) Crystal structures of NOS domains showing the electrons flow from NADPH to FAD to FMN in the reductase domain of NOS. The heme iron of the adjacent monomer (shown in white) acts as the last electron acceptor and facilitates the catalytic conversion of L-arginine into L-citrulline and NO. Reprinted from Nitric Oxide 23 (1) Daff, S. "NO synthase: Structures and mechanisms," 1-11, 2010, with permission from Elsevier. (b) Proposed model of CaM activation and electron transfer showing both NOS monomers. Reprinted from FEBS Journal 282 (16) Leferink, N. et al. "Towards the free energy landscape for catalysis in mammalian nitric oxide synthases," 3016-3029, 2015, with permission from John Wiley and Sons.

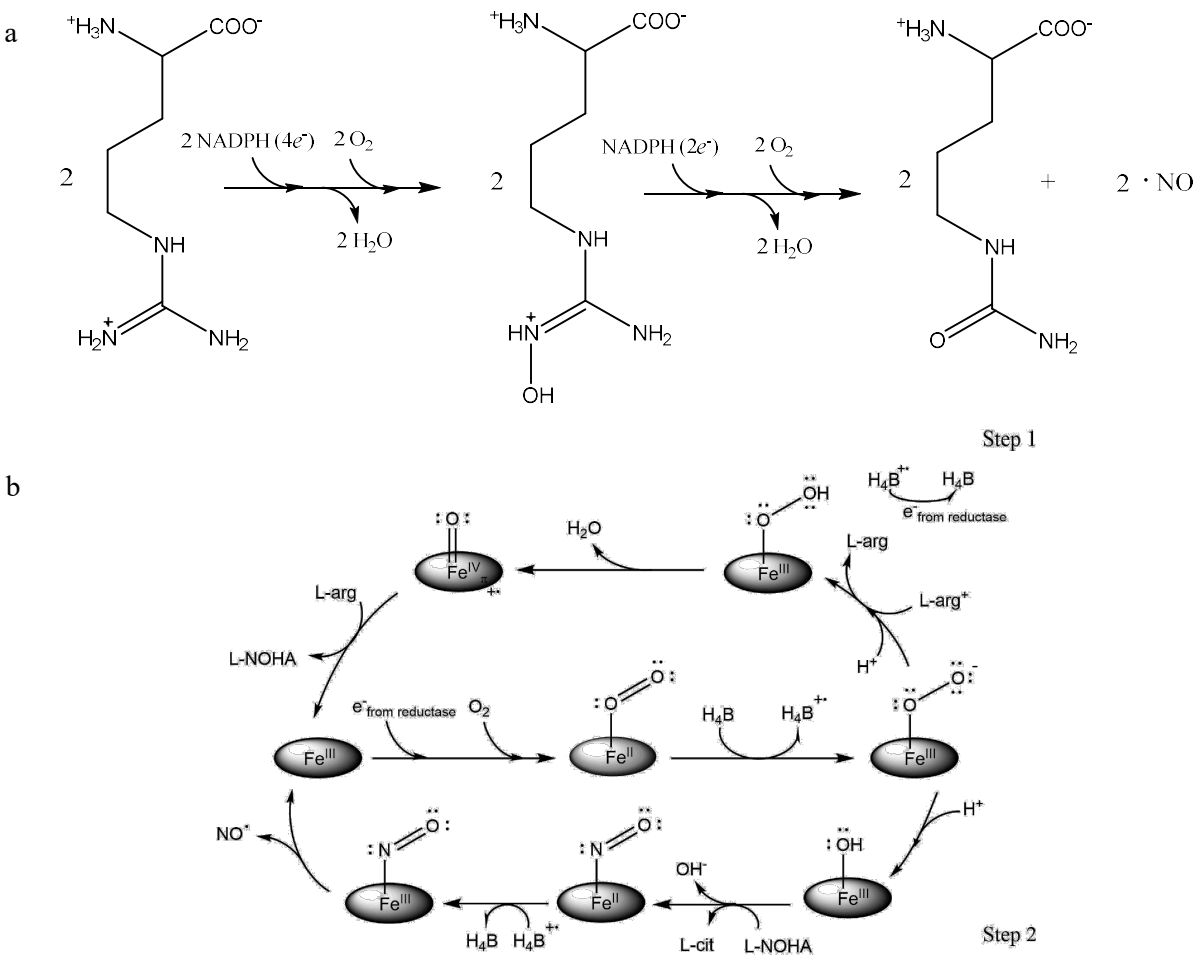

Figure 1.5. NOS enzyme catalysis. (a) The catalytic conversion of L-arginine into L-citrulline and NO involves two monooxygenation steps. (b) Both steps involve coupled electron and proton transfers to and from the heme iron.

The catalytic conversion of L-arginine into L-citrulline and NO that occurs at the oxygenase domain is a two-step reaction (Figure 1.5), fueled by tightly coupled redox reactions. In a comprehensive review, Santolini presented different scenarios for the proton and electron transfers for both catalytic steps.(Santolini, 2011) Results from Brunel et al.'s study provide evidence supporting the most commonly accepted pathway, shown in Figure 1.5b and discussed below.(Brunel et al., 2016) It is important to note, however, that the exact mechanism of proton and electron transfers (and their respective donors) remains a point of contention in NOS research.

The first step of the reaction begins with the reduction of the heme Fe(III) into Fe(II); the FMN domain swings toward the heme to deliver an electron from the reductase domain. Following this, O_2 binds the heme iron to form an unstable Fe(II)-O_2. This complex is rapidly reduced into Fe(III)-OO^{2-} by H_4B, which gets oxidized into $H_4B\cdot^+$. Note that this cation radical is transient, as

it is immediately reduced back into H_4B by the reductase domain.(Ramasamy, Haque, & Gangoda, 2016) Next, Fe(III)-OO^{2-} accepts two protons; the first proton comes from the L-arginine substrate while the second is from the distal H_2O molecule in the H-bond network with the substrate and the heme.(Brunel et al., 2016; Santolini, 2011) The resulting Fe(III)-OOH loses water via heterolytic cleavage and collapses into Fe(IV)=O$\pi\cdot^{+}$, referred to as Compound I. Compound I then hydroxylates L-arginine via radical rebound and form N^{ω}-hydroxy-L-arginine (L-NOHA).

The second monooxygenase reaction proceeds similarly as the first step up until the protonation due to the lack of a distal H_2O molecule in an H-bonding network with the substrate. Additionally, $H_4B\cdot^{+}$ was not immediately re-reduced. The oxidation of L-NOHA involves the formation of a tetrahedral intermediate that is covalently bound to Fe(III)-OOH. What follows is the formation of Fe(II)-N=O and L-citrulline, and the loss of a hydroxide ion. At this point, NO remains covalently linked to the heme. Its release requires the oxidation of Fe(II) into Fe(III) by $H_4B\cdot^{+}$ from before.

1.3 NOS regulation

All NOS isoforms contain structures that facilitate internal regulation, i.e. without the aid of external cofactors. These regulatory factors are the C-terminal (CT) tail and the autoinhibitory (AI) loop. Both of these block heme reduction by interfering with CaM binding, thereby preventing heme reduction.

The C-terminal (CT) tail, which is a sequence of 21 to 42 amino acids at the C-terminus of NOS.(Roman, Marta, Sue, Masters, & Domain, 2002) The CT tail is thought to inhibit the NOS reductase activity. In eNOS, the CT tail is subject to another layer of regulation, by way of post-translational modification. Ser1179 in the CT tail is a conserved residue is phosphorylated upon shear stress stimuli due to a local increase in blood pressure.(Fleming & Busse, 2003) This phosphorylation allows eNOS to bind CaM at resting [Ca^{2+}], which results in an increase in NO production to counter the increase in blood pressure. Studies with the phosphomimetic mutation Ser1179Asp showed that CaM binding and Ser1179 phosphorylation have equivalent effects on the rate of electron transfer, as evidenced by NADPH-dependent flavin reduction.(Haque, Ray, & Stuehr, 2016) Furthermore, Ser1179Asp has higher NO production than the wild type eNOS with and without CaM binding. As such, Ser phosphorylation appears to have an additive effect to CaM binding with regard to heme reduction.

The AI loop found between the FMN binding domain and the CaM binding region.(Weissman, Jones, Liu, & Gross, 2002) This AI loop locks the FMN in its electron accepting state, i.e. "buried" in the FAD/NADPH subdomain, at low [Ca^{2+}]. In other words, the AI loop prevents the electron flow to the oxygenase heme when CaM is not bound to nNOS or eNOS. Relatedly, the removal of this AI loop in nNOS results in a decrease in Ca^{2+}-dependence of NOS activity.(Montgomery, Romanov, & Guillemette, 2000) Furthermore, when the AI loop sequence was inserted into iNOS, there was a 1/3 decrease in NO production.(Weissman et al., 2002) Such results imply that the AI loop interferes with CaM binding and its role on the electron flow.

1.4 NOS inhibition

As mentioned previously, the endogenous NO exists in tightly controlled levels during normal physiological state. Overproduction of NO leads to a wide array of pathologies. As such, the development of NOS inhibitors that are selective towards either nNOS or iNOS, which have been implicated in NO-related pathologies. Recall that eNOS activity is necessary for normal physiological processes and, hence, must not be inhibited. Indeed, most adverse effects associated with NOS inhibitors are cardiovascular-related and are due to off-target inhibition of eNOS. However, the high similarity among the isoforms (especially at the active site) presents a problem in designing selective inhibitors. Yang et al.'s recent review reports that more than 100 patents have been filed for NOS inhibitor compounds from 2011-2014 alone, in addition to the already existing parents from the discovery of the NOS enzymes.(Yang et al., 2014) Unfortunately, at the time of writing, none of the isoform-specific NOS inhibitors in development have been approved for clinical trials. Note, however, that some non-selective first generation inhibitors have been used as eNOS blockers to induce peripheral hypertension in clinical trials (Víteček, Lojek, Valacchi, & Kubala, 2012).

1.4.1 Classes of NOS inhibitors

NOS inhibitor compounds can be categorized according to their binding targets on the holoenzyme structure. Most of these compounds target the active site to directly compete with substrate binding and prevent catalysis. These mechanism-based inhibitors include L-arginine derivatives and compounds that contain moieties that mimic the guanidine group and ionisable amines of L-arginine. However, owing to the highly conserved active site, these compounds tend to be non-selective.

Non-mechanism based inhibitors are also being developed. These compounds target the binding sites for cofactors H_4B, CaM and NADPH.(Curtin et al., 2015; Mukherjee et al., 2014) Heme-Fe blockers, which disrupt the metal-poryphyrin coordination at the active site, are also being developed.(Mukherjee et al., 2014) Furthermore, NOS dimerization blockers have been investigated because NOS monomers are inactive.(Mukherjee et al., 2014) However, these binding targets contain motifs for H_4B, CaM and NADPH that also occur in other proteins. As such, off-target inhibition may occur, which can lead to adverse effects. For instance, the cofactor CaM is known to bind and activate over 300 different proteins, some of which contain the 1-5-8-14 binding motif. One such protein is troponin C in cardiac and smooth muscle cells. Blocking CaM binding to these proteins could lead to serious cardiovascular effects. As a result, the majority of NOS inhibitors in development target the active site of the enzyme.

1.4.2 Approaches in isoform-selective inhibitor design

The problem of NOS selectivity arises from the fact that currently targeted binding sites are highly conserved across all three isozymes, particularly the catalytic active site that contains an invariant Glu residue. Despite some variation in the amino acid sequence, crystal structure alignments of the NOS isozymes suggest that the overall molecular shapes of these enzymes are nearly identical (Figure 1.6). This identity in domains is consistent with the fact that all NOS enzymes utilize the same cofactors and bind the same substrate L-arginine with similar affinity.

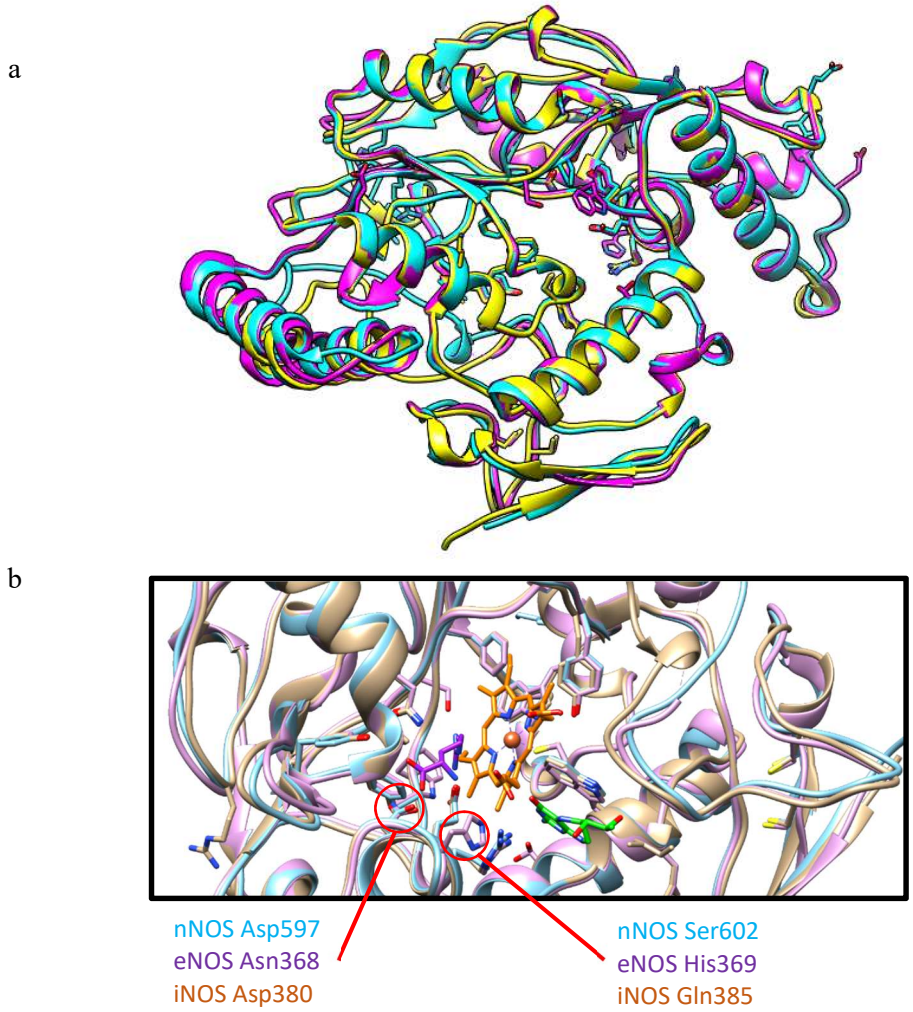

Figure 1.6. Human NOS oxygenase structures are highly conserved across isoforms. (a) Aligned crystal structures of the human NOS oxygenase doimain show highly conserved domain structures of NOS isozymes. (b) NOS isoforms exhibit single residue differences in the active site and vicinal structures. Human nNOS (cyan; PDB: 4D1N), human eNOS (magenta; PDB: 4D1O) and human iNOS (yellow; PDB: 1NSI) oxygenase domains aligned using Chimera.

In their patent review, Yang et al. (2014) listed the major classes of core structures for isoform-selective NOS inhibitors. Selective NOS inhibitors are generally based on pyrrolidine, quinoline, indole, pyrazole and aminopyridines.(Yang et al., 2014) These inhibitor cores are all cyclic and contain ionisable amines that can be H-bond donors or acceptors; all except pyrrolidine are also aromatic (Figure 1.7). Over the years, the design of selective NOS inhibitors progressed towards bulkier compounds that contain guanidino and amino moieties, and more extended conformation with hydrophobic and hydrogen bonding sites.(Joubert & Malan, 2011) Guanidino and amino moieties contain ionisable amines which mimic L-arginine binding to position and stabilize the compound at the active site.(Fan et al., 2009; Joubert & Malan, 2011) Yang et al.

(2014) report that inhibitor design follow different trends depending on the targeted NOS isoform. For example, the Poulos and Silverman groups from University of California Irvine and Northwestern University, respectively, have independently and jointly developed double-headed symmetric and asymmetric compounds that appear to be selective towards nNOS. The compound "heads" are rings, usually pyrrolidine or quinolone, which interact with the heme and side chains conserved aromatic residues. Meanwhile, iNOS selective inhibitors, such as those developed by the pharmaceutical company Kalypsys, are pyrimidine derivatives with heteroalkyl moieties. In any case, the extended conformations of these bulky compounds are designed to target remote isoform specific binding sites, which increase inhibitor selectivity.(Garcin et al., 2008; Joubert & Malan, 2011) Combining these two properties, Garcin et al.'s anchored plasticity approach in drug design exploits the formation of isoform-specific binding sites.(Garcin et al., 2008; Maddaford, 2012)

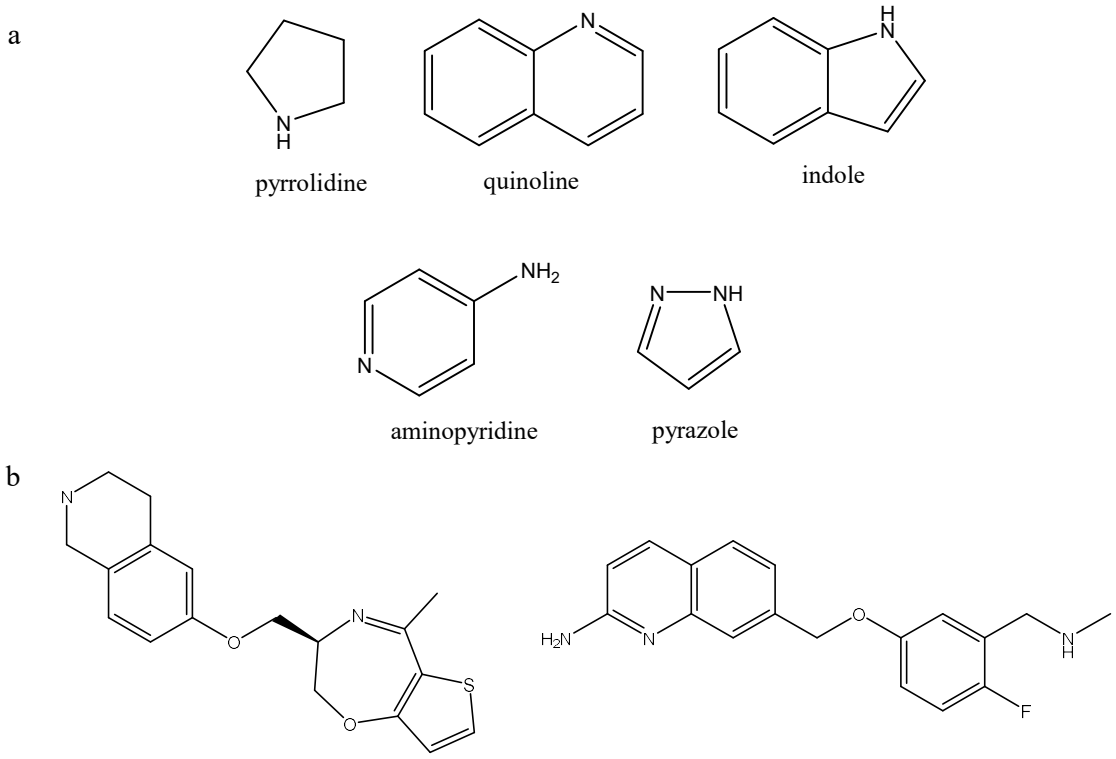

Figure 1.7. Chemical structures of major NOS inhibitor cores and examples of novel selective inhibitors. (a) From Yang et al.'s (2014) patent review, selective NOS inhibitors are based on pyrrolidine, quinoline, indole, aminopyridine and pyrazole. (b) Garcin et al.'s (2008) Novel iNOS selective inhibitor based on bicyclic thienooxapenzine from (left) and Cinelli et al.'s (2015) novel nNOS selective inhibitor derived from aminoquinoline (right).

In anchored plasticity, an inhibitor core is "anchored" at the conserved active site.(Garcin et al., 2008) An inhibitor tail is extended to sites just outside the binding pocket and access residues that can form new sites for inhibitor-binding. Garcin et al. identified first-, second- and third-shell amino acids that change conformation upon ligand-binding at the NOS active site. These so-called "plastic residues" change side chain conformation when the inhibitor binds at the active site.(Garcin et al., 2008) Some of these residues outside the active site vary across isoforms; after all, they do not directly participate in NOS catalysis and, hence, are less likely to be conserved. Novel selective NOS inhibitors could then be designed to take advantage of these isoform-specific plastic residues in the second and third shells (Figure 1.8).

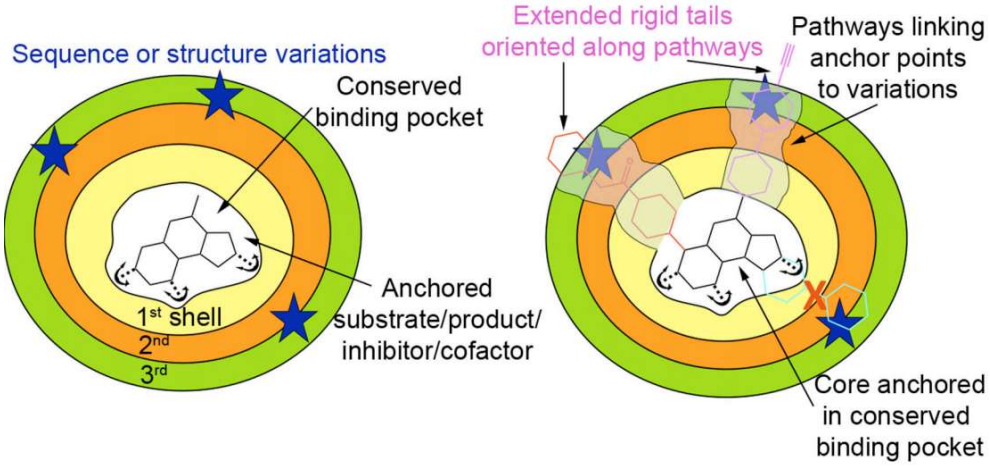

Figure 1.8. Anchored plasticity. Plastic residues in the vicinity of the conserved active site can be used as targets for isoform selective inhibition. Reprinted from the supplementary material of Nat. Chem. Biol. (4) Garcin, E. D. et al. "Anchored plasticity opens doors for selective inhibitor design in nitric oxide synthase." 700–707, 2008, with permission from Nature Publishing Group.

Using this approach, Garcin et al. discovered a Gln specificity pocket in human and murine iNOS which is an extended pocket next to the heme pocket, composed of the first shell Gln, Tyr and Arg residues.(Garcin et al., 2008) This pocket forms when a bulky inhibitor, i.e. ones with rigid and extended tails, forces the first shell Gln residue to rotate away from its neighbouring Tyr residue; this rotation then causes the formation of a new H-bond with another Arg residue, also in the first shell.(Garcin et al., 2008) The Arg side chain rotates towards and pushes away the second shell Asn.(Garcin et al., 2008) Note that the inhibitor tail must be hydrophobic so that hydrophobic interactions with the specificity pocket stabilizes the complex. Binding of the same inhibitor to eNOS does not cause the formation of this Gln pocket because the third shell residues of eNOS, Leu and Ile, prevents the movement of the second shell Asn; specificity pocket formation was

observed in the eNOS mutant with the third shell residues of iNOS, Phe and Val.(Garcin et al., 2008) The Gln specificity pocket allowed Garcin et al. to design a series of novel human and murine iNOS inhibitors with 125- to 3000-fold selectivity over bovine eNOS.(Garcin et al., 2008)

Using similar concepts, Cinelli et al. reported a series of aminoquinoline-derived nNOS selective inhibitors.(Cinelli et al., 2015) These compounds contain ionizable amines that H-bonds with the invariant active site Glu and extended tails that are long enough to access a hydrophobic pocket proximal to the heme and the H_4B binding sites.(Cinelli et al., 2015) These compounds also have central aromatic rings that have π-stacking interactions with the nNOS active site Tyr.(Cinelli et al., 2015) Further, inhibitor binding at the nNOS active site induces the formation of a hydrophobic pocket with residues Tyr, Leu and Met, which does not occur in eNOS due to the difference in Tyr conformation between nNOS and eNOS.(Cinelli et al., 2015) In eNOS, the Tyr phenyl ring is perpendicular to the plane of the heme, so steric interactions prevent rotation of the Tyr side chain that would cause the formation of the hydrophobic pocket.(Cinelli et al., 2015)

1.4.3 Human and non-human NOS isoforms

Human NOS holoenzymes are difficult to isolate due to their instability. As well, the expression and purification of these human cNOS are, as of yet, quantitatively inferior to that of the rat nNOS and bovine eNOS. These non-human cNOS have well-established expression systems that provide yields quantitatively superior to their human counterparts.(Huang et al., 2012) Non-human NOS have a high sequence similarity with human NOS (96%, 95% and 87% for nNOS, eNOS and iNOS, respectively) and as such, they have been used extensively as model systems for inhibitor design.

Until recently, the eNOS and iNOS oxygenase domain was the only available crystal structure for human NOS (Fischmann et al., 1999). The crystal structures of the human nNOS and eNOS have only been published in 2014 (Li et al., 2014). Furthermore, there are no published crystal structures for the full-length NOS, owing to the highly dynamic nature of the holoenzymes. Relatedly, drug development research (both experimental and theoretical) relied on the crystal structures of the rat nNOS and bovine eNOS oxygenase domains, instead of the human cNOS. However, structure alignments of the human and non-human NOS oxygenase domains reveal that the minute differences in the amino acid sequence correspond to differences in structure (Figure 1.9 Figure 1.10). Li et al. report that while human cNOS exhibit the similar helix structures and disordered loops, the active sites of the human isoforms show minute disparities.(Li et al., 2014)

Specifically, there are single amino acid differences in the active and its vicinity, which tend to form isoform-specific hydrophobic pockets. Hence, these structural differences result in differences in the kinetics of enzyme catalysis. The Michaelis constants K_m for the NOS substrate L-arginine have been shown to vary between human and non-human NOS. Other kinetic parameters, such as V_{max} and specific activity, also vary. These discrepancies affect the selectivity of NOS inhibitors; novel inhibitor-enzyme bonding interactions may occur and alter affinity and selectivity.(Boer et al., 2000; Cinelli et al., 2014) Cinelli et al. directly compared the inhibitory activity of the selective nNOS inibitors that they have synthesized on rat and human nNOS; their results show a consistently higher K_i values, i.e. lower potency, in human nNOS than in rat nNOS.(Cinelli et al., 2015; Cinelli et al., 2014) The decreased affinity may be a consequence of designing the compounds using non-human NOS enzymes, specifically because the single residue difference of Leu (rat) to His (human) at the hydrophobic pocket near the active site that forms upon inhibitor binding.(Cinelli et al., 2015; Cinelli et al., 2014)

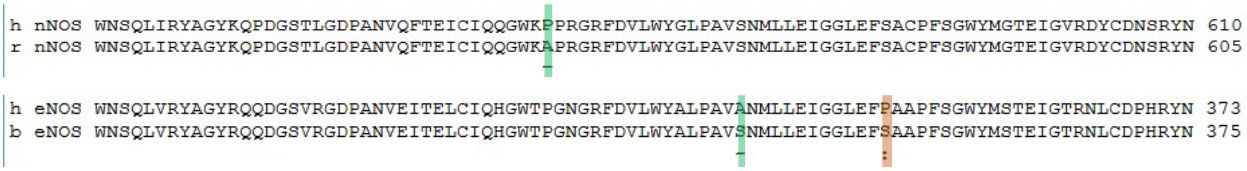

Figure 1.9. Sequence alignment of active site residues of human and non-human cNOS. Residues highlighted in green correspond to different amino acidsl red, chemically similar amino acids.

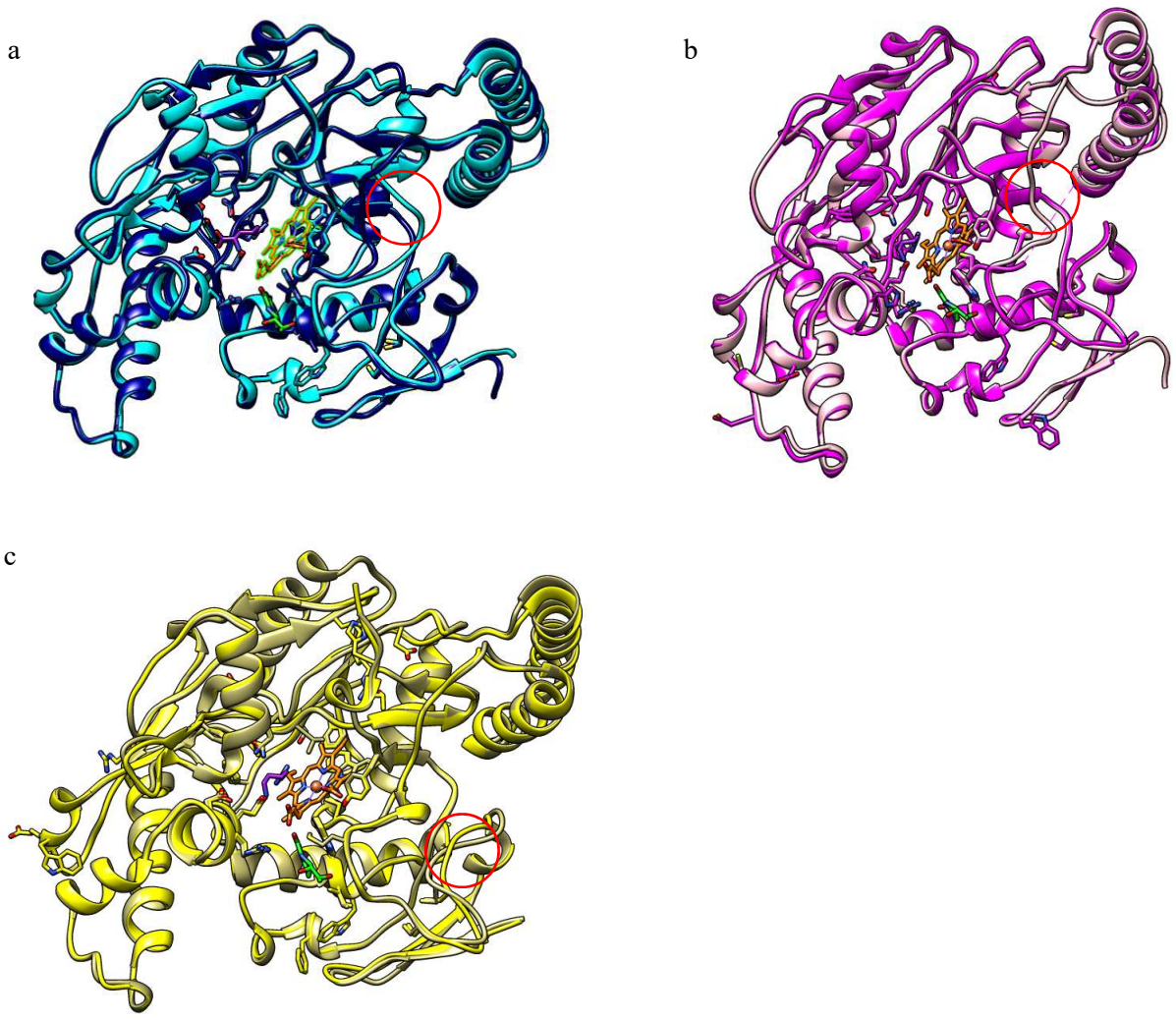

Figure 1.10. Alignment of human and non-human NOS oxygenase domains. (a) nNOS, (b) eNOS and (c) iNOS. The darker colours represent the human NOS and lighter colours refer to non-human NOS. The structural differences between human and non-human NOS are evident in the disordered loop sections, as highlighted. These structures are aligned using Chimera.

1.4.4 Inhibitors used in this study

This project presents a systematic approach on studying the differences in inhibition kinetics between human and non-human NOS. Preliminary experiments are performed using first generation active site inhibitors. These include non-selective inhibitors N^G-monomethyl-L-arginine (L-NMMA), N^G-nitro-L-arginine (L-NNA) and N^ω-allyl-L-arginine (L-ALA), all of which are L-arginine derivatives. Bulky compounds 3-bromo-7-nitroindazole and 1400W (N-(3-(aminomethyl)benzyl)acetamidine). These compounds have been reported to be selective towards

nNOS and iNOS, respectively. In addition to active site inhibitors, CaM binding inhibitors trifluoroperazine (TFP) and melatonin are also examined.

1.5 Purpose of study

Despite the high homology with their human counterparts, conclusions drawn from studies of the non-human NOS may not be reasonably translatable to humans, given the small differences that might lead to isoform-specificity. As previously mentioned, the slight differences in structure may be the cause of kinetic differences in the activity of human and non-human NOS. Hence, it is important to determine these differences using a uniform study. As Curtin et al. recently pointed out, there is not yet a consistent human NOS isozyme assay system for studying the inhibitory activity of NOS inhibitors.(Curtin et al., 2015) BRENDA (The Comprehensive Enzyme Information System; formerly, Braunschweig Enzyme Database) lists an array of K_m values for L-arginine for different NOS isoforms, as well as K_i and IC50s. These values were acquired via different methods: either directly through radiolabeled L-arginine or indirectly via the Griess reaction or the oxyhemoglobin capture assay. Furthermore, the NOS protein sources were not uniform either. Some were purified heterologously expressed proteins, while some were isolated from tissue extracts. Others even utilized crude lysates. Without the uniformity in activity assay methods, the inhibitors cannot be compared directly. As such, the main objectives of this master's thesis are to:

1. Develop heterologous human NOS holoenzyme expression systems with comparable quantitative and qualitative yields to established non-human NOS expression systems
2. Assess the NOS inhibition kinetics of first generation active site inhibitors and CaM-blockers using a uniform assay method

Chapter 2

2. Enzymatic activity of human and non-human NOS holoenzymes

2.1 Introduction

Although the gene sequences of the human constitutive NOS isozymes have been isolated and cloned since the mid-90s, the structure-based design of NOS inhibitors still relies on non-human NOS models. Non-human NOS expression systems, such as rat nNOS and bovine eNOS, have well-established growth and purification methods that give high protein yields. In contrast, current human NOS expression systems yield less proteins than their non-human counterparts. This chapter describes the development of optimal expression systems for human constitutive NOS enzymes.

2.1.1 Vector selection

The choice of plasmid vector dictates the efficiency of heterologous protein expression. To optimize the expression of NOS, two vectors are considered: pCWori and PDS-78. Both vectors utilize IPTG induction to effect protein synthesis.

pCWori (4955 bp) contains the tac promoter, which is a hybrid of the trp and lacUV5 promoters. The tac promoter is a favourable binding site for the *E. coli* RNA polymerase, which is readily expressed by most *E. coli* strains. The *E. coli* RNA polymerase binds the tac promoter and initiate gene transcription upon the addition of IPTG. IPTG de-represses the tac promoter by allosterically modifying the lac repressor that constitutively inhibits the binding of RNA polymerases to the promoter region. pCWori is a commonly used vector for the heterologous expression of oxidoreductases such as NOS and cytochrome P450 (Roman et al., 1995).

Meanwhile, PDS-78 (5488 bp) is a high-expression derived from pET28a. This vector contains a T7 promoter region, which binds the T7 RNA polymerase. The T7 RNA polymerase is a highly efficient polymerase that is not normally expressed in *E. coli*. Once T7 RNA polymerase is synthesized upon induction by IPTG, it binds the T7 promoter and effect the transcription of the protein of interest. Heterologous proteins tend to be over-expressed because the T7 RNA polymerase is highly efficient, especially compared with the native *E. coli* polymerase.

The full-sequence human nNOS and eNOS holoenzymes have been cloned into PDS-78 (pHnNOShisKan and pHeNOShisKan, respectively), but have not yet been purified using established protocols in the lab.

2.1.2 *E. coli* strain

Heterologous protein expression may be hindered by codon usage incompatibility between the host organism and the gene donor. Although the genetic code is redundant, some species favour specific codons over others. For example, *E. coli* exhibit codon usage bias. *E. coli* does not produce tRNA that correspond to codons that rarely appear in its genome. In contrast, the human genome does not exhibit such bias. Hence, codons that do not appear in the *E. coli* genome may be in the transplanted human gene. Genes that contain rare *E. coli* codons have been reported to have reduced synthesis rates, and contain frameshift mutations and mistranslations. Codon usage bias could also negatively affect protein folding.

In this project, both the human nNOS and eNOS holoenzyme genes each contain more than 10 instances of the Arg rare codons AGA, AGG and CGA. Thus, the *E. coli* strain BL21 (DE3) may be unsuitable for human nNOS and eNOS expression. The modified strain BL21 (DE3) CodonPlus RP could suffice, since its phenotype includes tRNA for rare codons AGA, AGG and CGA (Arg) and CCC (Pro).

2.1.3 Chaperone proteins

High concentrations of heterologous protein in bacterial cells are susceptible to aggregation due to protein misfolding. Aggregation presents challenges to protein purification, especially in chromatographic techniques. For gel filtration, the formation of inclusion bodies changes the elution time of the protein. Additionally, aggregation prevents the adsorption of the protein via specific binding sites if these sites are buried into the core of the aggregate. These problems can be overcome by the co-expression of chaperone proteins such as Gro-ES and Gro-EL. Gro-ES and Gro-EL encapsulate a protein and help it refold into its native state, and thus reducing its aggregation propensity.

2.1.4 Use of truncated NOS holoenzymes

Removing the first several amino acids of human NOS holoenzymes have been shown to improve yields from heterologous expression systems. Truncated NOS are less prone to proteolysis. Indeed, the human iNOS expression system used by the Guillemette group lacks the first 70 amino acids at the N-terminal. The yields in this expression system are comparable to the long established rat nNOS and bovine eNOS expression systems. In this project, 290 N-terminal amino acids of the human nNOS are removed; the human eNOS lacks the first 66 amino acids.

This truncation may be especially important with regard to the nNOS isoform. Recall that the nNOS holoenzyme contains an additional PDZ domain that is absent in both the eNOS and

iNOS. The PDZ domain is 220 amino acid long and thus, presents more sequences that can be targeted by proteases. Furthermore, the PDZ domain acts as an anchoring domain, which may promote troublesome protein-protein interactions that can lead to aggregation. If so, then the inclusion of this domain could decrease not only the protein yield, but also the catalytic activity of the enzyme.

2.2 Methods

2.2.1 Subcloning human NOS holoenzymes into pCWori

The pCWori vector is not commercially available, so the linearized vector is obtained from pBeNOShisAmp, which is a plasmid that was constructed by the Guillemette group. Polymerase chain reaction (PCR) was used to truncate and amplify the full NOS sequences. Both the forward and reverse primers contain 5'. These restriction sites allow for insertion into the desired vector via ligation.

Successful constructs were verified via analytical restriction digests and nucleotide sequencing. The Guillemette group avails sequencing services from The Centre for Applied Genomics Sanger Sequencing Facility in Toronto, ON.

2.2.1.1 Competent *E. coli* cell transformation

In this project, two cell transformation methods were employed: electroporation and $CaCl_2$ heat shock. Both methods require aseptic conditions. In electroporation, electrocompetent cells were transformed by adding 0.3 µL of plasmid DNA sample into 40 µL of cell stock. The cell and DNA mixture was transferred into 0.1-cm gap electroporation cuvettes (Bio-Rad), and pulsed with approximately 1800 V for about 5 ms. The pulsed cells were then suspended in 500 µL non-selective Luria-Bertani (LB) broth and incubated at 37 ˚C for 1 hour at 250 rpm. 100 µL of the cell suspension was spread-plated onto a selective LB-agar plate. The plates were stored in a 37 ˚C incubator for 16 hours, after which they were checked for visible colonies.

For the $CaCl_2$ heat shock method, 5 µL of the plasmid DNA sample was added into 100 µL of chemically competent cells in a microfuge tube. The cell and DNA mixtures were incubated on ice for 30 minutes. These were then heat shocked via a 2-minute water bath at 42 ˚C, which was immediately followed by a 2-minute incubation on ice. Afterwards, 100 µL of LB broth was added into the mixture and the tubes were incubated in a 37 ˚C water bath for 1 hour without shaking. 100 µL of the cell suspension was plated onto a selective LB-agar plate, as above. The plates were stored in a 4 ˚C refrigerator when not in use.

2.2.1.2 Plasmid DNA sample preparation

To obtain DNA plasmid samples, competent *E. coli* DH5α cells were transformed and plated onto selective LB-agar media. Distinct colonies were used to inoculate 2 mL terrific broth (TB) with the appropriate antibiotics and grown for 16 hours at 225 rpm at 37 ˚C. Plasmid DNA were extracted using silica resin spin columns according to manufacturer instructions (BioBasic). DNA were eluted with and stored in 2 mM Tris buffer (pH 8.0-8.5) and concentrations were determined using the NanoDrop 2000 (ThermoScientific). Samples were stored in –20 ˚C.

2.2.1.3 pCWori vector preparation

The pCWori vector in pBeNOShisAmp contains the ATG start codon and a poly-histidine tag in its 3' end, upstream of an NdeI restriction site. Meanwhile, the 5' end contains an EcoRI recognition sequence. Hence, pBeNOShisAmp was digested with both NdeI and EcoRI (Thermo Fisher) to isolate the 4955-bp fragment. To maximize the fragment yields, the enzymatic reactions were scaled up, such that approximately 5 µg of plasmid DNA was digested in each reaction tube. The reaction was allowed to progress through incubation at 37 ˚C for 1 hour and then stopped via heat inactivation at 65 ˚C. Agarose gel electrophoresis was used to separate the fragments according to size (See Section 2.2.1.5 for more details).

2.2.1.4 PCR amplification of gene inserts

As mentioned previously, the constitutive NOS genes were truncated at the N-termini to improve protein yields. Hence, the forward primers for each the nNOS and eNOS were designed such that the NdeI restriction site was followed by the codons for 291st and 67th amino acids, respectively. These primers are complementary to eight codons on the original template. Note that the ATG start codon is already in the vector fragment, so it was not added. The reverse primers were the complementary sequence to the final nine codons, including the stop codon, plus the EcoRI restriction site. The following table shows the primer specifications (Integrated DNA Technologies):

Table 2.1. Forward and reverse primers (FP and RP) for PCR amplification of truncated human nNOS and eNOS with GC content and melting temperatures (T_m). Highlighted sequences correspond to the restriction sites for NcoI (cyan), NdeI (yellow) and EcoRI (green).

Primer	Sequence	GC	T_m[a]
hnNOSΔ290FP	5′ CCACCATGGTCATATGGGAAAACAGTCCCCCACAAAGAATGGC 3'	51.2%	75.9 ˚C
hnNOSholoRP	5′ GCGGAATTCTTAGGAGCTGAAAACCTCATCGGTGTC 3′	50.0%	72.8 ˚C
heNOSΔ66FP	5′ CCACCATGGTCATATGCCCAAGTTCCCTCGTGTGAAGAACTGG 3′	53.5%	76.1 ˚C
heNOSholoRP	5′ GCGGAATTCTCAGGGGCTGTTGGTGTCTGAGCCGGG 3′	63.9%	77.7 ˚C

[a] T_m values were calculated with the primer concentration at 0.5 µM, [NaCl] at 0 mM, [$MgCl_2$] at 2 mM and [dNTPs] at 200 µM using the IDT OligoAnalyzer®.

PCR amplification of the truncated human nNOS and eNOS sequences were performed using the pHnNOShisKan and pHeNOShisKan as templates, respectively. The reactions were performed using high-fidelity polymerase Phusion® (Thermo Fisher). In addition to 0.02 U/µL Phusion® enzyme and the provided high-fidelity buffer, each 50 µL reaction mixture contained about 10 ng of template DNA, 0.5 µM of forward primer, 0.5 µM of reverse primer, 200 µM dNTP mixture and 2 mM $MgCl_2$. Since the T_m values are above the optimal extension temperature of the Phusion® polymerase, a two-step PCR program was utilized:

Table 2.2. Two-step PCR program for amplification of truncated human nNOS and eNOS sequences.

PCR Step	Temperature	Duration, mm:ss	Cycles
Initial Denaturation	98 ˚C	05:00	1
Denaturation	98 ˚C	00:10	35
Annealing/Extension	72 ˚C	06:00	
Final Extension	72 ˚C	10:00	1
Hold	4 ˚C	Indefinite	-

Ligation into the pCWori vector requires the generation of complementary 5' sticky ends for the inserts. The PCR products were digested with EcoRI and NdeI directly without purification: 2 µL of the FastDigest Green Buffer, 1 µL of EcoRI and NdeI each, and 16 µL of MQW were added into 10 µL of the PCR mixture. This 30 µL reaction mixture was incubated in a 37 ˚C water bath for 1 hour. The reaction was stopped by heat inactivation at 65 ˚C for 15 minutes. The human nNOSΔ290 sequence was expected to be 3441 bases long, while the human eNOSΔ66 should have 3417 bases. The digested insert sequences were separated from non-specifically amplified fragments via agarose gel electrophoresis (see Section 2.2.1.5).

2.2.1.5 DNA fragment isolation

Once the vector and insert fragments were digested with the appropriate restriction enzymes, the fragments of interests were separated by electrophoresis using 1% agarose gel in pH 8.3 TBE buffer (89 mM Tris-borate, 89 mM boric acid, 2 mM ethylenediaminetetraacetic

[EDTA]). The agarose gels were cast with large wells (approximately 5 cm by 1 mm) to allow for loading large volumes of restriction digest mixtures. The DNA fragments were visualized under ultraviolet (UV) light using ethidium bromide (EtBr).

Sections of the agarose gel containing the fragments of interest were excised using a clean blade and transferred into 1.5 mL microfuge tubes. The DNA fragments were extracted using silica resin spin columns per manufacturer instructions (BioBasic). The DNA concentrations were estimated using NanoDrop 2000, and the fragment lengths were verified by agarose gel electrophoresis. Samples, which were eluted with 2 mM Tris buffer (pH 8.0-8.5), were stored in –20 ˚C.

2.2.1.6 Ligation into pCWori

The nNOS and eNOS inserts were subcloned into the linearized pCWori vector via ligation using the T4 DNA ligase (Thermo Fisher). The ligation reactions were performed at 20 µL volumes, each containing 50 ng of pCWori, 1 U of T4 DNA ligase, excess ATP (at least 2.5 mM) and MQW. The amount of insert sequence added into the reaction was varied from 1:1 to 3:1 molar ratio over the vector.

The ligation reactions were incubated at 16 ˚C for either 1 hour or 16 hours. For both cases, the reactions were stopped via heat inactivation at 65 ˚C for 5 minutes. The ligation mixtures were used to transform competent DH5α cells (see Section 2.2.1.1) directly without purification. Visible colonies were used to inoculate TB media for plasmid DNA preparation (see Section 2.2.1.2). Successful constructs are heretofore referred to as pHnNOSΔ290hisAmp and pHeNOSΔ66hisAmp.

2.2.1.7 PCR-based site directed mutagenesis

PCR was used to reverse spontaneous mutations that arose during the amplification process. Sequencing information show that the human nNOSΔ290 holoenzyme amplicon (pHeNOShisKan) was found to have three spontaneous mutations, only one of which occurs naturally and is considered benign.(C. (Erica) Lee, 2015) One mutation, a G to A base change, caused Gly to become Arg. Because this amino acid is within the NADPH-binding site of the human nNOS reductase domain, this mutation may have negative effects in expression and activity of the enzyme. Hence, site-directed mutagenesis was performed to reverse this mutation on the pHnNOSΔ290hisAmp plasmid.

Two completely complementary primers were designed based on standard site-directed mutagenesis protocols. In addition to the target nucleotide (A to G), an additional control mutation was introduced such that the success of the mutagenesis can be verified without sequencing. This control came in the form of a silent mutation (C to G; ACC and ACG both code for Thr) that removes the NcoI recognition site (5' CCATGG 3') near the target nucleotide.

Table 2.3. Forward and reverse primers (FP and RP) for PCR-based site-directed mutagenesis of human nNOSΔ290 holoenzyme (pHnNOSΔ290hisAmp)with GC content and melting temperatures (T_m). Highlighted sequences correspond to the NcoI restriction site prior to the mutation. Bolded letters refer to the target mutations.

Primer	Sequence	GC	T_m[a]
NADPH FP	5′ CACATATACGTCTGT**G**GGGACGTCAC**G**ATGGCTGCTGATGTCC 3'	55.8%	76.3 ˚C
NADPH RP	5′ GGACATCAGCAGCCAT**C**GTGACGTCCC**C**ACAGACGTATATGTG 3′	55.8%	76.3 ˚C

[a] T_m values were calculated with the primer concentration at 0.5 µM, [NaCl] at 0 mM, [$MgCl_2$] at 2 mM and [dNTPs] at 200 µM using the IDT OligoAnalyzer®.

Completely complementary primers, especially ones as long and as GC-rich as NADPH FP and NADPH RP, present problems that could hinder PCR amplification and thus, the mutagenesis. To expedite the process, touchdown (TD) PCR experiments were performed using multiple combinations of reaction components. The amount of template used was varied from 10 to 100 ng, and the effect of primer concentration (0.5 µM versus 2.5 µM) was tested. Mg^{2+} content was investigated by varying $MgCl_2$ concentrations from 1.5 to 2.5 mM. Dimethyl sulfoxide (DMSO) was added to 3% and 5% to assess its effects on amplification. In some attempts, AccuTaq™ DNA polymerase (Sigma) was also used in lieu of Phusion®. All PCR experiments were performed in 50 µL volumes.

Table 2.4. Touchdown PCR program for site-directed mutagenesis of pHnNOSΔ290hisAmp.

PCR Step	Temperature	Duration, mm:ss	Cycles
Initial Denaturation	98 ˚C	03:00	1
Denaturation	98 ˚C	00:30	2[b]
Annealing	72 – 55.5 ˚C[a]	01:00	
Extension	72 ˚C	10:00	
Denaturation	98 ˚C	00:30	18
Annealing	68 ˚C	01:00	
Extension	72 ˚C	10:00	
Final Extension	72 ˚C	10:00	1
Hold	4 ˚C	Indefinite	-

[a] The annealing temperature was decreased from 72 to 55.5 ˚C in 1.5 ˚C increments.
[b] Two PCR cycles per annealing temperature.

Furthermore, parallel single-primer PCR experiments (with varying template and DMSO concentrations using the TD-PCR protocol) were performed to discourage primer-dimer

formation. In this case, only one primer (NADPH FP or NADPH RP) is added into the PCR mixture, which are combined after the amplification process and the DpnI digest. The single stranded complementary DNA were denatured at 98 ˚C and allowed to anneal completely by slow cooling to 37 ˚C. The combined forward- and reverse-primer PCR reactions were then used to transform competent DH5α cells, as described above.

Plasmid DNA were extracted from visible colonies and were subject to analytical digests with NcoI, EcoRI and NdeI. Potential mutants were sequenced to further confirm successful mutagenesis, as well as to check for spontaneous mutations.

2.2.2 Growth and expression of NOS holoenzymes

The transformation process for the expression of human and mammalian NOS proteins was similar to the procedures described in Section 2.2.1.1. However, the *E. coli* strain used was either BL21 (DE3) or BL21 (DE3) CodonPlus RP, instead of DH5α. The mammalian NOS (rat nNOS, bovine eNOS and murine iNOS) and the human iNOS holoenzymes have well-established expression systems that utilize the BL21 (DE3) strain. The rat nNOS (pRnNOShisAmp) and bovine eNOS (pBeNOShisAmp) were each co-expressed with GroES/EL proteins (pGroESLChlor) in BL21 (DE3). Meanwhile, the mouse iNOS (pMiNOSAmp) and the human iNOS (pHiNOSΔ70hisAmp) were both co-expressed with wild-type calmodulin (pCaMChlor), also in BL21 (DE3).

To assess the compatibility of *E. coli* strains in heterologous NOS expression, human nNOS and eNOS holoenzymes (pHnNOSΔ290hisAmp and pHeNOSΔ66hisAmp, respectively) were expressed in both BL21 (DE3) and BL21 (DE3) CodonPlus RP. In the former, co-expression with GroES/EL was possible because this strain does not have innate chloramphenicol resistance. In contrast, the latter contains tetracycline and chloramphenicol resistance such that expression for the GroES/EL plasmid cannot be selected for using antibiotic pressure. The high-expression plasmids pHnNOShisKan and pHeNOShisKan were also expressed in a similar manner.

2.2.2.1 Small-scale growth for verification of expression

To confirm that pHnNOShisKan, pHeNOShisKan, pHnNOSΔ290hisAmp and pHeNOSΔ66hisAmp would be expressed upon induction with isopropyl β-D-1-thiogalactopyranoside (IPTG), small-scale growth experiments were performed. 2 mL of TB with appropriate antibiotics was inoculated with a single colony of human nNOS- or human eNOS-expressing BL21 (DE3) or BL21 (DE3) CodonPlus RP. (Where possible, these NOS holoenzymes

were co-expressed with pGroESLChlor.) These cultures were left to grow for 16 hours at 37 ˚C at 250 rpm. Then, 1 mL of these starter cultures were used to inoculate 100 mL of TB with antibiotics. The OD_{600} of the media were monitored regularly until it reaches 1.0–1.2, at which point 500 µM IPTG was added to induce protein expression. The incubation temperature was decreased to 25 ˚C upon induction.

Culture samples (1 mL) were collected right before and 40 hours after induction. The OD_{600} of these samples recorded. Samples were centrifuged at 10000 rpm; the supernatant was decanted and the cell pellets were frozen and stored at –20 ˚C until use.

To determine if the human nNOS and eNOS holoenzymes can be expressed, the cell pellets were resuspended in MQW, given by the following equation:

$$\text{volume of water} = (OD_{600})(100\ \mu L)$$

The samples were boiled prior to sodium dodecyl sulfate polyacrylamide gel electrophoresis (SDS-PAGE). The protein expression was visually assessed from the change in the intensity of the bands at the expected protein size.

Because the human nNOSΔ290 and eNOSΔ66 holoenzymes have poly-histidine tags, His SpinTrap™ (GE Life Sciences) was used to purify the NOS proteins in the small scale. The cell pellets were lysed through freeze/thaw cycles. The samples were flash frozen in liquid nitrogen and thawed in an ice-water bath for 10 minutes; this process was repeated four times. The lysate was centrifuged at 10000 g for 10 minutes at 4 ˚C. The supernatant was loaded into the His SpinTrap™ column and the purification process proceeded as per the kit manual. Samples were taken from each wash step, and SDS-PAGE was performed to confirm protein expression and isolation.

2.2.2.2 Large-scale growth for expression and purification

Once the appropriate *E. coli* strain was determined from the small-scale growth, 6 x 25 mL TB with respective antibiotics, i.e. ampicillin and chloramphenicol or ampicillin, chloramphenicol and tetracycline, in 250 mL flasks were inoculated with a single colony from selective agar plates. These starter cultures were incubated at 37 ˚C for 16 hours at 225 rpm. Then, 6 x 1 L TB with antibiotics were inoculated with 15 mL of each of the starter cultures. As above, the OD_{600} was monitored until approximately 1.0–1.2 and the culture was induced with 500 µM IPTG, 400 µM δ-aminolevulinic acid (δ-ALA), 500 µM adenosine 5'-triphosphate (ATP), 9.6 µg/mL $FeSO_4 \cdot 7H_2O$, 2.4 µg/mL $AlCl_3 \cdot 6H_2O$, 2.4 µg/mL $MnCl_2 \cdot H_2O$, 1.0 µg/mL $CoCl_2 \cdot 6H_2O$, 0.5 µg/mL

$ZnSO_4 \cdot 7H_2O$, 2.4 µg/mL $NaMoO_4 \cdot 2H_2O$, 0.1 µg/mL $CuCl_2 \cdot H_2O$, 0.5 µg/mL H_3BO_3 and a pinch of riboflavin. The temperature was decreased to 25 ˚C and the cells were left to grow in the shaker for 40 hours at 225 rpm. After 40 hours, the cells were harvested via centrifugation at 6000 rpm for 10 minutes at 4 ˚C. The cell paste was flash froze in dry ice and stored at –80 ˚C until it was ready for purification.

The protocol detailed above was also applied to the large-scale growth of rat nNOS (pRnNOShisAmp) and bovine eNOS (pBeNOShisAmp) co-expressed with pGroESLChlor in BL21 (DE3) cells. Human iNOSΔ70 and mouse iNOS were both co-expressed with pCaMChlor in BL21 (DE3) cells.

2.2.2.3 NOS holoenzyme purification

Frozen cells expressing the NOS holoenzyme were thawed and resuspended in four volumes of cold NOS Lysis Buffer, which consists of 40 mM Tris-HCl (pH 7.5 at 4 ˚C), 10% glycerol, 1 mM L-arginine, 3 mM ascorbic acid, 150 mM NaCl and 10 µM H_4B and 1 mM phenylmethylsulfonyl fluoride (PMSF). The resuspended cells were lysed via homogenization using the Avestin EmulsiFlex-C5 homogenizer. One tablet of Roche cOmplete™ Mini EDTA-free was added per 50 mL of solution. The samples are centrifuged at 48000 g for 30 minutes at 4 ˚C. The supernatant were collected and the pellet was discarded. The supernatant was subjected to salt precipitation by adding $(NH_4)_2SO_4$ to 65% concentration. To ensure efficient precipitation, the mixture was shaken vigorously for one hour at 4 ˚C before centrifugation at 48000 g for 30 minutes at 4 ˚C. The supernatant was discarded and the pellets were resuspended in cold ADP Wash Buffer, which contains 50 mM Tris-HCl (pH 7.5 at 4 ˚C), 10% glycerol, 100 µM L-arginine, 100 mM NaCl, 1 mM DTT and 0.1 mM PMSF. One cOmplete protease inhibitor tablet was added per 50 mL of the resuspended pellet.

The resuspended pellet was further purified using the 2’ 5’ ADP Sepharose 4B column (Sigma), which is an affinity column that binds the NADPH binding site at the reductase domain of the NOS holoenzyme. Prior to loading the sample onto the column, it was regenerated by 3 cycles of alternate washes with 3 column volumes of ADP Regeneration Solution 1 (0.1 M Tris-HCl, pH 8.5 and 0.5 M NaCl) and 3 column volumes of ADP Regeneration Solution 2 (0.1 M NaOAc, pH 4.5 and 0.5 M NaCl). The ADP resin was equilibrated with at least 10 column volumes of the ADP Wash Buffer.

The resuspended pellet was transferred into a 250 mL centrifuge bottle, and the equilibrated ADP resin was poured into the same bottle. This mixture was incubated on the rotisserie at 4 ˚C for 1 hour to maximize protein binding into the affinity column. After incubation, the protein-resin mixture was poured into a 1 cm x 30 cm Glass Econo-Column® (Bio-Rad). With the column stopcock in the "off" position, the mixture was left to sit at 4 ˚C for another 30 minutes. The stopcock was opened and the sample was allowed to flow through the resin. The ADP resin was washed with 5 column volumes of ADP Wash Buffer, followed by 5 column volumes of ADP Salt Wash Buffer (same as the ADP Wash Buffer but with 500 mM NaCl). The bound NOS proteins were eluted with 10 mL of 5 mM 2' AMP dissolved in ADP Salt Wash Buffer. (Note that 2' AMP is hard to dissolve and, hence, was left in a 37 ˚C water bath to increase its solubility.) Eluted fractions were collected at 1 mL volumes.

In cases where there was no observed binding to the 2' 5' ADP column, the CaM Sepharose 4B resin was used. In this case, the precipitated pellet was resuspended in the CaM Wash Buffer (similar to the ADP Wash Buffer but contained 2 mM $CaCl_2$). The resin-sample incubation procedure was the same. The samples were then washed with 5 column volumes of CaM Wash Buffer and eluted with the CaM Elution Buffer (ADP Wash Buffer with 4 mM EDTA).

The most concentrated fractions, which are yellow in colour, were pooled and were transferred into cellulose dialysis tubing (6000–8000 MWCO, Spectra/Por™) to be dialyzed against NOS Dialysis Buffer 1 (50 mM Tris-HCl [pH 7.5 at 4 ˚C], 10% glycerol, 5 µM L-arginine, 3 mM ascorbic acid, 250 mM NaCl, 4 µM H_4B, 1 mM DTT and 0.1 mM PMSF) for at least 3 hours. Afterwards, the sample was dialyzed against NOS Dialysis Buffer 2 (same as NOS Dialysis Buffer 1 but with 100 mM NaCl) for at least 3 hours.

The protein yield was quantified via the UV-Vis spectra, taken at wavelengths from 300 to 700 nm with the Cary 5000 UV-Vis-NIR (Varian), using Beer's Law,

Equation 2.1.

$$[\mathrm{NOS}] = \frac{\mathrm{Abs}_{397}}{\varepsilon_{397}\, l}$$

where Abs_{397} is the absorbance at 397 nm, ε_{397} is the molar extinction coefficient at 397 nm (72 $cm^{-1}mM^{-1}$), and l is the path length (1 cm) (Ikuto et al. 1998). The absorbance at 450 nm (Abs_{450}) was recorded as well, as it corresponds to the flavin content, i.e. cofactors, of the sample.

7.5% SDS-PAGE was run to assess the purity of the sample, as well as to verify the size of the purified protein.

2.2.2.4 Active site analysis

The coordination status of the heme propionate at the substrate binding site, and thus the suitability of the enzyme for assays, is evaluated through ultraviolet (UV) visible spectra. The heme prosthetic group at the NOS active site has a characteristic UV absorbance at the Soret region that shifts either toward red or blue depending on the "oxidation, coordination and spin states of the heme iron," which are then dependent on ligand binding and the electrostatic environment at the binding site.(Rousseau, Li, Couture, & Yeh, 2005) The UV absorbance spectra of NOS enzymes have similar shapes across bacterial and mammalian isoforms.(Montgomery, Dupont, Leivo, & Guillemette, 2010; Rousseau et al., 2005)

The unbound heme iron in the presence of water absorbs at a maximum at 420 nm, where it exists at a six-coordinated low-spin (6C LS) state.(Rousseau et al., 2005) When L-arginine and H_4B are added, the heme iron moves into its preferred five-coordinated high spin (5C HS) state and the Soret peak shifts to 400 nm.(Rousseau et al., 2005) To confirm that the purified NOS is heme bound to the Cys ligand, addition of imidazole or carbon monoxide (CO) gas into the enzyme solution must cause a Soret peak shift at approximately 420 nm and 450 nm, respectively.(Rousseau et al., 2005)

UV-Vis spectroscopy was used, not only to quantify the purified protein, but also to verify that the heme at the NOS active site remains intact. Purified NOS holoenzymes were incubated with 10 mM H_4B, 1 mM L-arginine and 1 mM imidazole on ice for 10 minutes. As a negative control, an equivalent volume of 50 mM Tris-HCl (pH 7.5 @ 4 ˚C) was added into the sample. The absorbance spectra of these samples were read from 350–550 nm using Cary® 5000 UV-Vis-NIR (Varian). The absorbance values were normalized to the peak of the control sample.

2.2.2.5 Flavin content analysis

To determine the FAD and FMN content of the purified NOS holoenzyme samples. Faeder and Siegel's fluorimetric technique was performed with some modifications. In this method, excitation of FAD and FMN and 450 nm causes fluorescence at 535 nm. Standard curves were determined by measuring the fluorescence of FAD and FMN in concentrations varying from 10 to 75 nM. 10 μM FAD and FMN stock solutions were made by dissolving pure FAD and FMN in standard buffer (0.1 M potassium phosphate, pH 7.7; 0.1 mM EDTA). Further dilutions were made

using the standard buffer as well. The stock and standard solutions were stored in tubes wrapped in aluminum foil to protect them from the light.

The Bradford assay was used to quantify the protein content of the NOS protein samples. The samples were then diluted into 50 nM concentrations in standard buffer to a final volume of 1 mL. The diluted protein samples were boiled for 3 minutes and cooled rapidly on ice. To remove the proteins, the samples were centrifuged at 13000 rpm for 15 minutes. The supernatant was transferred into a fresh microfuge tube wrapped in aluminum foil.

Fluorescence measurements were performed using SpectraMax® Plus M5 Microplate Reader (Molecular Devices) at 27 ˚C. These experiments were performed using black (opaque) 96-well plates. Each fluorescence reading at pH 7.7 was performed in triplicates at 100 µL volumes. Afterwards, a 10 µL volume was removed from each well and 10 µL of 0.1 M HCl was added. This brings down the pH of the solution to 2.6. Fluorescence was measured once again.

The concentration of diluted material is related to the intensity of fluorescence by the equation F = k[c], i.e. fluorescence intensity F equals the product of fluorescence constant k and concentration c. For FAD and FMN, Faeder and Siegel state that

$$F = D\,[FAD] + N\,[FMN]$$

where D and N are fluorescence constants of FAD and FMN, respectively.(Faeder & Siegel, 1973) Furthermore, the pH of the solution affects the fluorescence of these flavins, and thus, their respective fluorescence constants. Hence,

$$F_{7.7} = D_{7.7}\,[FAD] + N_{7.7}\,[FMN]$$

$$F_{2.6} = D_{2.6}\,[FAD] + N_{2.6}\,[FMN]$$

Once these constants are determined from the FAD and FMN standard curves, the above equations can be used to calculate the FAD and FMN content of the protein samples.

2.2.3 Expression and purification of wild type CaM

Electrocompetent BL21 (DE3) cells were transformed with pCaMChlor as in Section 2.2.1.1. Starter cultures (25 mL LB broth with 45 µg/mL chloramphenicol) were inoculated with a single colony of CaM-expressing cells and were left to grow at 37 ˚C for 16 hours at 225 rpm. 6 x 1 L LB with chloramphenicol were inoculated with 15 mL of the starter culture. The cell cultures were kept under the same conditions until OD_{600} reaches 0.6-0.8. Afterwards, CaM expression was induced by the addition of 500 mM IPTG per culture flask. Cells were harvested four hours after

induction via centrifugation at 6000 x g for 10 minutes at 4 ˚C. The cell pellets were flash frozen and stored at -80 ˚C.

Cell pellets were resuspended in 4 volumes of CaM Buffer A (50 mM Tris-HCl, pH 7.5 @ 4 ˚C; 1 mM $CaCl_2$) with 100 mM NaCl and 1 mM DTT. The cells were lysed via homogenization. The samples were centrifuged at 48000 x g for 30 minutes at 4 ˚C. $CaCl_2$ was added into the clarified supernatant to raise the calcium concentration to 5 mM. Ca^{2+} exposes the hydrophobic patches of CaM. The sample is loaded onto a 5 mL phenyl sepharose column (GE Life Sciences) via FPLC. Note that prior to loading the sample, this column was first equilibrated with Buffer A.

After adding the sample, the column was washed by 5 column volumes of Buffer A. This was followed by 4 column volumes of CaM Buffer B (50 mM Tris-HCl, pH 7.5 @ 4˚C; 1 mM $CaCl_2$; 500 mM NaCl). Then, the column was once again washed with Buffer A (2.5 column volumes). Afterwards, the bound CaM protein was eluted with CaM Buffer C (10 mM Tris-HCl, pH 7.5 @ 4˚C; 10 mM EDTA). 2 mL fractions were collected and the fractions with peaks at 2810 nm, 277 nm and 215 nm were pooled and dialyzed against 1 L of Buffer A in two steps.

The UV-Vis spectrum of the dialyzed sample was taken from 250-300 nm. The spectrum of purified CaM has a characteristic staircase shape that has a maximum at 277 nm. The absorbance at 277 nm was used to calculate the protein concentration using Beer's Law and ε_{277} = 3029 M^{-1} cm^{-1}. If the concentration was less than 180 µM, then the sample was concentrated using 3K MCWO Millipore centrifugal concentrators. Samples were stored in 500 µL aliquots at -80 ˚C. The purified protein was verified using electrospray ionization mass spectrometry (ESI-MS).

2.2.4 Oxyhemoglobin capture assay

To assess the enzymatic activity of NOS enzymes, and consequently, the inhibitory activity of the NOS inhibitors, the rate of product formation, i.e. L-citrulline and/or NO production must be measured. A straightforward method is to use radiolabelled substrate, e.g. [^{3}H]arginine, and then measure the amount of [^{3}H]citrulline formed in solution over time. However, this method is labour intensive and produces a lot of radioactive waste. Fortunately, NO can react with certain compounds that render allows the NOS enzyme kinetics to be quantified spectrophotometrically.

The oxyhemoglobin (oxyHb) capture assay exploits the reaction between NO and O_2 bound to hemoglobin (Hb) to form $ONOO^-$ and methemoglobin (metHb) as shown below:(Hevel & Marletta, 1994)

$$\cdot NO + \text{oxyHb} \longrightarrow ONOO^- + \text{metHb}$$

OxyHb reacts with NO faster than unbound O_2 and since one equivalent of NO reacts with one equivalent of oxyHb, NO production by the NOS enzyme can be monitored at initial rate conditions through a change in absorbance at 401 nm.(Hevel & Marletta, 1994) The difference in the absorbance of metHb and oxyHb at 401 nm ($\Delta Abs_{401} = Abs_{401(metHb)} - Abs_{401(oxyHb)}$) directly correlates to the rate of NO formation.(Hevel & Marletta, 1994; Perdicakis, Montgomery, Guillemette, & Jervis, 2004) Under initial rate conditions, i.e. at less than 10% product formation, this assay allows for the direct assessment of the inhibitory activity of the NOS inhibitor when the substrate concentration is greater than the Michaelis constant K_m.(Hevel & Marletta, 1994)

2.2.4.1 Oxyhemoglobin preparation and calibration

Approximately 5 mL of loosely packed lyophilized bovine hemoglobin (Hb) was dissolved in the minimal amount of 50 mM Tris-HCl (pH 7.5 @ RT). Approximately 10–20 mg of $Na_2S_2O_4$ was added into the saturated Hb solution. Non-oxygenated Hb is dark brown in colour, but the addition of $Na_2S_2O_4$ oxidizes it and turns the colour of the solution into "cherry" red. This oxidation can be verified through the absorbance spectra of the sample; the oxyHb spectrum shows a more pronounced local peaks at 530 and 576 nm compared to non-oxygenated Hb (Figure 2.1). The oxyHb solution was desalted using PD-10 Desalting Column (GE LifeSciences). The absorbance spectra of the purified oxyHb and the sample concentration was calculated, per the following equation:

Equation 2.2

$$[\text{oxyHb}] = [1.013(Abs_{576}) - 0.369(Abs_{630}) - 0.7353(Abs_{560})] \times 100 \times \text{dilution factor}$$

The coefficients in the equation are in units of $cm^{-1}M^{-1}$, as published by Benesch et al. 1973. The multiplier 100 is a conversion factor, such that [oxyHb] is expressed in μM. Dilution of the sample was necessary to be able to read the distinct peaks in the spectra due to the spectrophotomer's limit of detection.

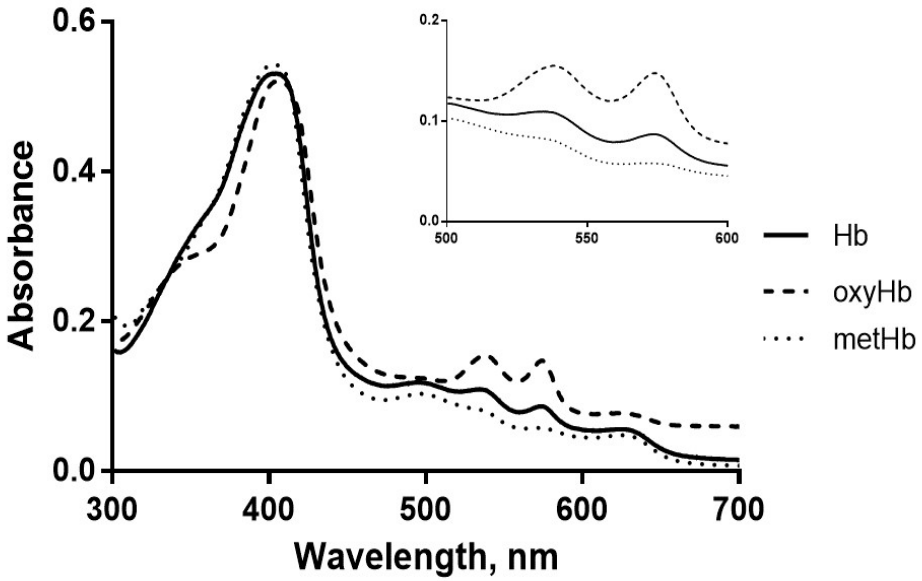

Figure 2.1. Absorbance spectra of oxyhemoglobin (oxyHb) and methemoglobin (metHb). The absorbance spectra of hemoglobin (Hb) shows the characteristic Soret peak for heme proteins at about 401 nm. Furthermore, the presence of two local maxima at 530 nm and 575 nm indicates that the formation of oxyHb. The oxidation of the horse heart Hb with sodium dithionite yields a bright red solution ("cherry red"). Reduced Hb formed via the addition of ferrous cyanide is a reddish-brown solution.

As mentioned above, ΔAbs_{401} can be used to calculate the rate of NO synthesis. Hevel and Marletta reported that the molar extinction coefficient of $\Delta\varepsilon_{401}$ is approximately 60000 $cm^{-1}M^{-1}$, suggesting that this assay is highly sensitive.(Hevel & Marletta, 1994) However, $\Delta\varepsilon_{401}$ tends to vary per oxyHb solution, especially at high concentrations. Hence, it is necessary to perform calibration experiments per oxyHb preparation.

To calculate $\Delta\varepsilon_{401}$, standard curves were generated for both oxyHb and metHb (Figure 2.2). The prepared oxyHb stock was diluted into 40 µM in 50 mM Tris-HCl (pH 7.5 @ RT). MetHb was generated by diluting 40 µM in 0.12 mM $K_3Fe(CN)_6$; this ferricyanide solution was made by dissolving the appropriate amount of solid $K_3Fe(CN)_6$ in 50 mM Tris-HCl (pH 7.5 @ RT). Using a 96-well plate reader, the oxyHb and metHb solutions were diluted two-fold from 40 µM to 0.625 µM in 100 µL-volume triplicates. 100 µL of 50 mM Tris-HCl (pH 7.5 @ RT) and 0.12 mM $K_3Fe(CN)_6$ were used as blanks for baseline measurements of oxyHb and metHb. The difference $\Delta Abs_{401} = Abs_{401(metHb)} - Abs_{401(oxyHb)}$ was plotted against [Hb], and the slope of this linear regression (times 10) corresponds to $\Delta\varepsilon_{401}$ per ng of Hb.

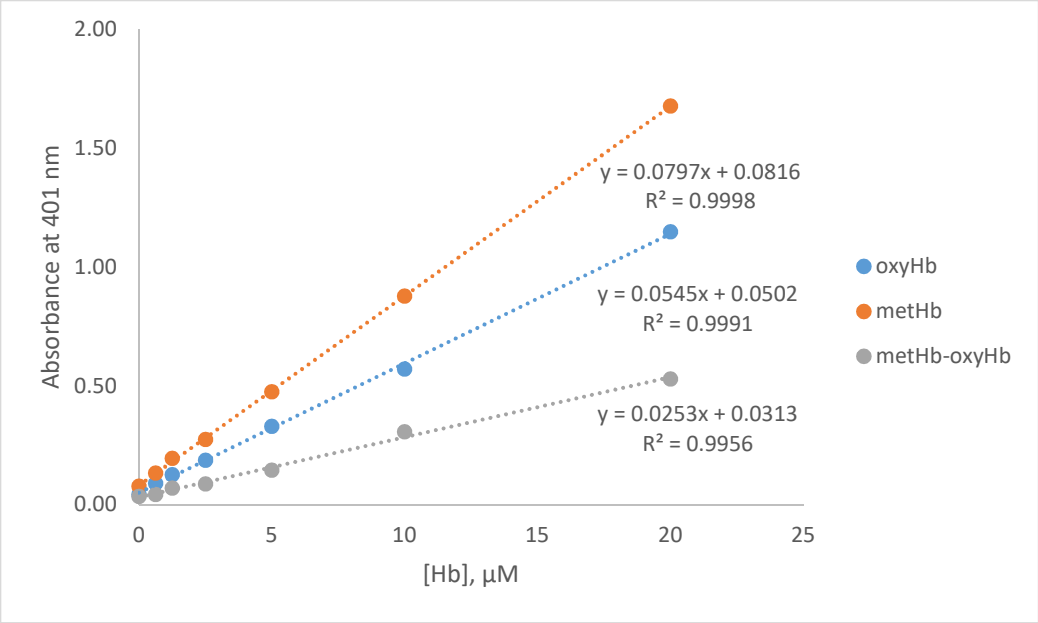

Figure 2.2. Sample oxyhemoglobin (oxyHb) calibration curve. The molar extinction coefficient of $Abs_{401(metHb)} - Abs_{401(oxyHb)}$ is given by the difference in slopes of the absorbance functions of oxyHb and metHb. This coefficient is used to convert the absorbance at 401 nm into moles of NO formed by the NOS enzyme from the L-arginine substrate.

2.2.4.2 Determination of enzymatic activity and K_m of NOS isozymes

The activity of NOS enzymes were quantitatively assessed via the oxyHb capture assay; the human NOS enzymes were compared to their mammalian counterparts. These experiments utilized 96-well plates and each reaction was performed in quadruplicates at 100 µL volumes.

For the activity assay, two different solutions were prepared prepared separately: the enzyme solution and the heme solution. The enzyme solution consists of 10 µM FAD, 10 µM FMN, 500 µM NADPH, 50 µM H_4B, 100 µM DTT, 50 U/mL catalase, 100 U/mL superoxide dismutase (SOD), 0.2 mg/mL bovine serum albumin (BSA), and 10% glycerol in 50 mM Tris-HCl (pH 7.5 @ RT). The amount of NOS added varied according to the isoform. The final concentration of nNOS, eNOS and iNOS were 30 nM, 70 nM and 28.5 nM, respectively; these values are the same for both human and mammalian NOS. CaM was diluted to 3 µM in 50 mM Tris-HCl (pH 7.5 @ RT) and 200 µM $CaCl_2$ or 250 µM EDTA. The complete enzyme solution contains the NOS isozyme of interest, its co-factors and in the case of nNOS and eNOS, CaM. This mixture was incubated at RT for 2 minutes before the reaction initiation to allow maximum interaction between CaM and the NOS holoenzymes.

Each well was filled with 10 µL complete enzyme solution and NOS synthesis was initiated by adding 90 µL heme solution into it. The heme solution contains the substrate, L-

arginine, and the NO-reporter, oxyHb. This solution was prepared such the final volume of 100 µL contained 5 µM oxyHb, 25 µM L-arginine, 500 µM NADPH, 0.18 mg/mL BSA, 50 U/mL catalase, 100 U/mL SOD, 10% glycerol and either 200 µM $CaCl_2$ or 250 µM EDTA in 50 mM Tris-HCl (pH 7.5 @ RT). Immediately after the addition of the heme solution, ΔAbs_{401} was obtained by measuring the Abs_{401} of reaction at RT over 5 minutes in 7-second intervals using SpectraMax® Plus 384 Microplate Reader (Molecular Devices). The ΔAbs_{401} was given in units of s^{-1}. Activity was then measured as follows:

Equation 2.3.

$$\text{Activity} = \frac{\Delta Abs_{401}\left(\frac{60\text{ s}}{1\text{ min}}\right)\left(\frac{1}{(\Delta\varepsilon_{401})}\right)}{\left[(\text{well volume})(\text{final NOS concentration})\left(\text{NOS molecular weight in}\frac{\text{g}}{\text{mol}}\right)\left(1000\frac{\text{mg}}{\text{g}}\right)\right]}$$

NOS activity is expressed in terms of NO formed in nmol per minute per mg of protein (nmol NO min^{-1} mgP^{-1}).

Kinetic parameters K_m and V_{max} for the L-arginine substrate were determined using the same protocol as above, only the final [L-arginine] was varied from 0.625 µM to 40 µM via two-fold serial dilutions. Baseline measurements were taken using a heme solution that did not contain any L-arginine in it. Calculated rate of reactions (per Equation 3.2) were plotted against substrate concentrations and were fitted to a Michaelis-Menten curve using GraphPad Prism.

2.3 Results and discussion

2.3.1 Human nNOS holoenzyme

2.3.1.1 pHnNOShisKan

As mentioned previously, the human nNOS holoenzyme has been successfully subcloned into a high-expression vector, PDS-78. pHnNOShisKan was expressed in both BL21 (DE3) and BL21 (DE3) CodonPlus RP and grown in the small-scale (Section 2.2.2.1).

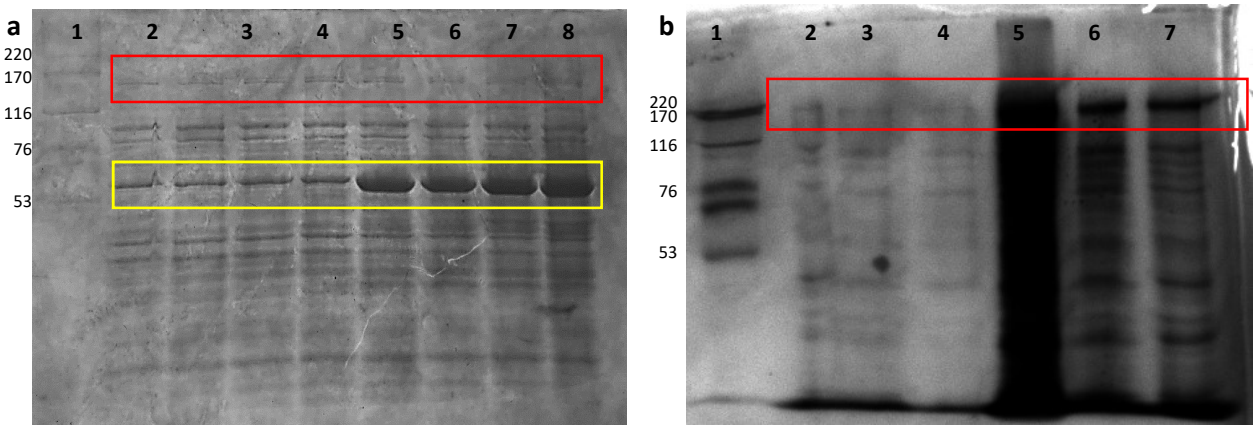

Figure 2.3. Small-scale expression of pHnNOShisKan in *E. coli* strains. (a) In BL21 (DE3) cells, there is no increase in intensity of bands corresponding to human nNOS holoenzyme (red box, 161 kDa) before and after induction (lanes 1-4 and lanes 5-8, respectively), especially relative to the GroEL bands (yellow box, 57 kDa). (b) There is an increase in human nNOS holoenzyme band intensity after induction (lanes 4-6) in BL21 (DE3) CodonPlus RP cells. GE High Molecular Weight Calibration Kit was used as ladders for both gels; weights are given in kDa.

In Figure 2.3a, the co-expression of GroES/EL serves as an internal control, so that the lack of change in band intensity for human nNOS holoenzyme indicates the lack of expression. This failure of expression could be due to either codon usage bias or the vector in use. However, since there was an observed change in band intensity in the BL21 (DE3) CodonPlus RP strain Figure 2.3b, this result can be attributed to the inability of the BL21 (DE3) strain to express the NOS protein. In this case, the NOS protein expression was induced via addition of IPTG. Indeed, the human nNOS holoenzyme sequence contains 61 instances of Arg rare codons (AGA, AGG, CGA and CGG) and 42 instances of Pro rare codon CCC. This mismatch could have hindered the human nNOS expression in the commonly used BL21 (DE3).

Since pHnNOShisKan can be expressed in BL21 (DE3) RP cells, large-scale growth and expression were commenced. The purification steps outlined were performed, but it did not yield any protein.

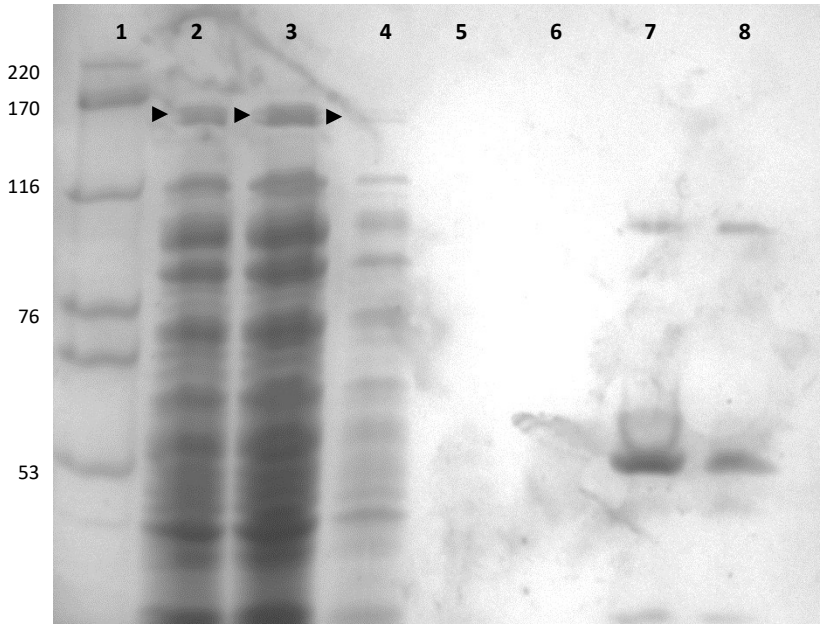

Figure 2.4. Purification of human nNOS holoenzyme from pHnNOShisKan expressed in BL21 (DE3) CodonPlus RP cells. Each lane represents stages of the purification process. From L-R: (1) Ladder, (2) Resuspended pellet, (3) ADP resin Flow-through, (4) ADP Wash, (5) ADP Salt Wash, (6) Eluted Fraction 1, (7) Eluted Fraction 2, and (8) Eluted Fraction 4. The human nNOS holoenzyme was present in the lysate, ADP Flow-through and ADP Wash.

NOS proteins usually elute from the 2' 5' ADP column starting from fractions 2–4. However, as seen on the gel in Figure 2.4, there were no bands that correspond to the size of human nNOS holoenzyme, though these were present in the lysate. The presence of the protein band in the column flow-through (and at roughly the same intensity as the lysate) suggests that the protein did not bind to the resin at all. This result was initially speculated to be due to possible protein aggregation from high expression, as well as the tendency of the nNOS PDZ domain to form inclusion bodies. However, the above results do not definitively lead to such conclusions.

2.3.1.2 pHnNOSΔ290hisAmp

The truncated human nNOS sequence (nNOSΔ290) was successfully subcloned into the pCWori vector through ligation; the resulting 8422-bp plasmid is called pHnNOSΔ290hisAmp (Figure 2.5). A double digest of the plasmid with EcoRI and NdeI separates the vector from the insert, which yields fragments of approximately 5.0 kbp and 3.4 kbp in size (Figure 2.6).

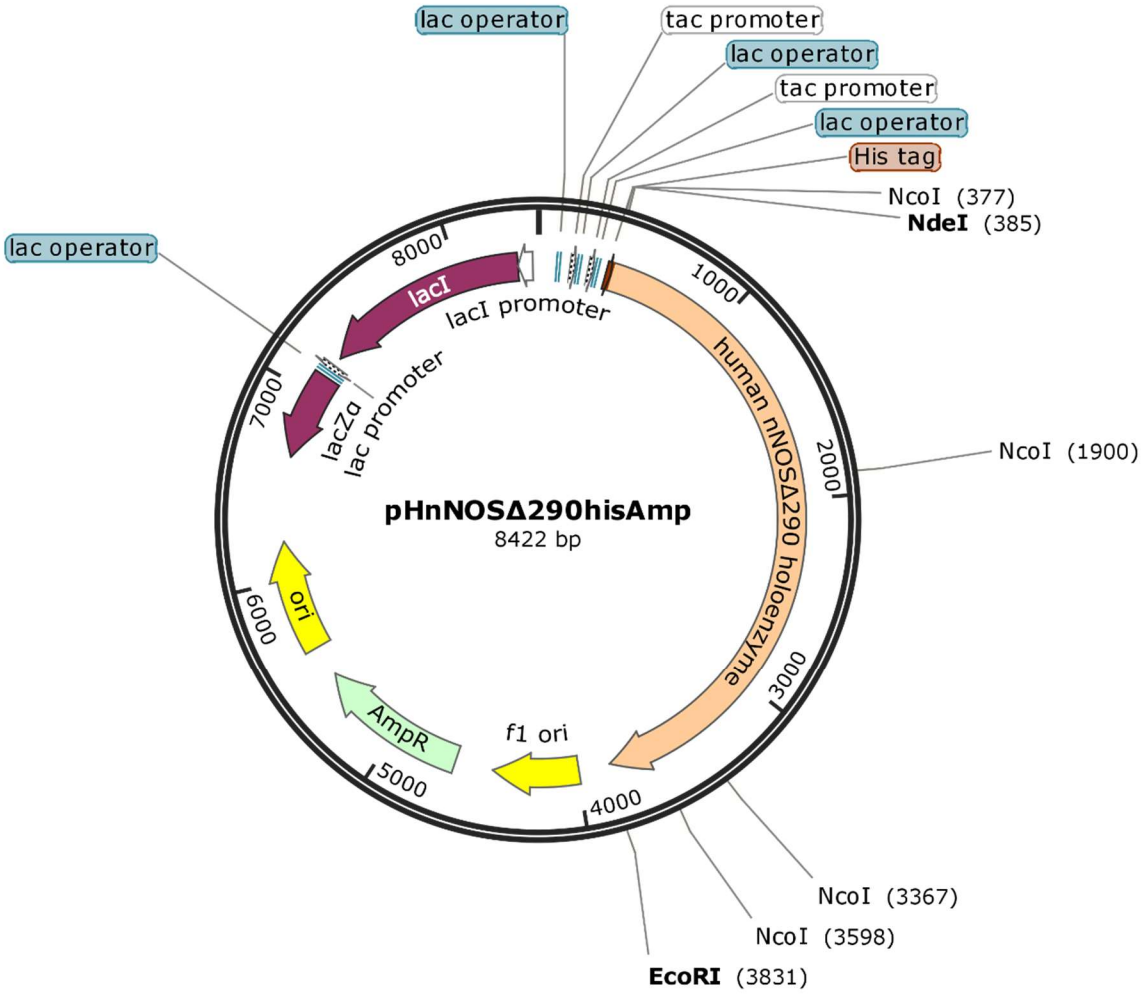

Figure 2.5. Plasmid map of pHnNOSΔ290hisAmp. This plasmid contains the truncated human nNOS holoenzyme subcloned into pCWori via ligation. It is ampicillin-resistant and uses the moderate-expression promoter tac. Restriction enzymes EcoRI, NcoI and NdeI (noted above) were used to validate subcloning success.

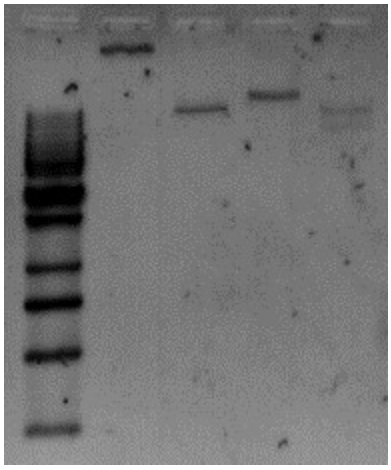

Figure 2.6. Analytical digests of the pHnNOSΔ290hisAmp construct. Single digest with either EcoRI (lane 2) or NdeI (lane 3) both yield fragments of approximately 8.4 kbp in length. Double digest with EcoRI and NdeI (lane 5)

results in 5.0 kbp and 3.4 kbp fragments, corresponding to the pCWori vector and nNOSΔ290 holoenzyme insert respectively.

Large-scale growth and expression followed for pHnNOSΔ290hisAmp in BL21 (DE3). Attempts to purify the protein using the 2' 5' ADP Sepharose 4B resin (Section 2.2.2.3) did not yield purified protein. However, when the CaM Sepharose 4B resin was used, purified protein was eluted.

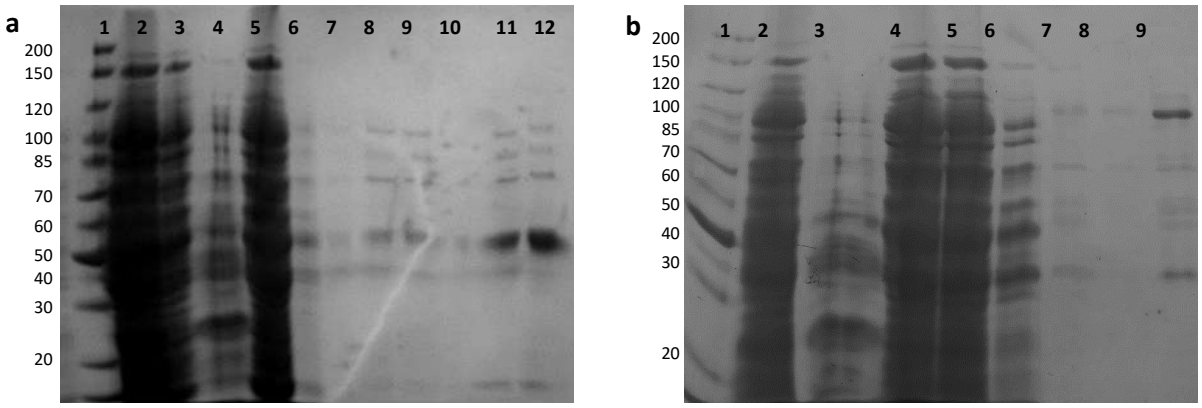

Figure 2.7. Purification of human nNOSΔ290 holoenzyme from pHnNOSΔ290hisAmp expressed in BL21 (DE3) CodonPlus RP using affinity columns. (a) 2' 5' ADP Sepharose resin, lanes: (1) ladder, (2) lysate, (3) resuspended pellet, (4) salt cut supernatant, (5) ADP column flow-through, (6) ADP wash, (7) ADP salt wash and (8-12) eluted fractions 1-5). (b) CaM Sepharose resin, lanes: (1) ladder, (2) lysate, (3) salt cut supernatant, (4) resuspended pellet, (5) CaM column flow-through, (6) CaM wash, (7) eluted fraction 4, (8) eluted fraction 8 and (9) pooled fractions.

Though Figure 2.7b shows that the protein is of size 120 kDa (10 Da less than expected), the UV-Vis spectra of the pooled fractions eluted from the CaM resin has the characteristic shape of NOS isozymes, which shows the Soret peak at approximately 397 nm (not shown, for details see Section 2.2.2.4). Hence, it was postulated that there must be a mutation in the NADPH binding site that prevents the human nNOS holoenzyme from binding to the ADP affinity resin. Recall that the unsuccessful purification of the human nNOS holoenzyme from pHnNOShisKan was previously attributed to aggregation. However, the results above, i.e. that the human nNOS holoenzyme can be purified using the CaM resin, suggests that the high-expression vector could still be worth trying. Perhaps, the CaM resin could be used to purify the human nNOS holoenzyme from pHnNOShisKan.

In any case, sequencing information show that pHnNOSΔ290hisAmp indeed contained mutations. These mutations were artifacts from the template used during the PCR amplification of the nNOSΔ290 insert sequence. Lee (2014) reported three single nucleotide mutations, all of which caused changes in the amino acid sequence.

Table 2.5. Mutations found in the nNOSΔ290 insert sequence carried over into the pHnNOSΔ290hisAmp plasmid. The nucleotide and amino acid numbers correspond to their positions in the truncated sequence.

Nucleotide change	Amino acid mutation
G → C (883)	Glu295Gln
G → T (1312)	Gly438Trp
G → A (3199)	Gly1067Arg

These mutations are absent in the original human nNOS holoenzyme (pHnNOS) plasmid obtained from Dr. Philip Marsden at the University of Toronto; these occurred spontaneously during the pHnNOShisKan subcloning process. The first two mutations were considered benign: Glu and Gln have similar structures, while the Gly438Trp mutation is a naturally occurring variant. There is no evidence shown that even though this mutation is within the CaM binding region, it does not interfere with the interaction between nNOS and CaM. Indeed, it was possible to purify the nNOSΔ290 holoenzyme using the CaM affinity resin, CaM Sepharose 4B.

However, the Gly1067Arg mutation proved to be problematic since it is within the NADPH binding region. As such, it decreased (or removed) the protein's affinity toward the 2' 5' ADP Sepharose resin that was used to purify NOS proteins. Furthermore, if it cannot bind NADPH, the enzymatic reaction cannot proceed because the electron transfer between the flavins cannot occur.

Two approaches were explored to reverse the Gly1607Arg mutation: (1) amplify the nNOS insert using the original plasmid pHnNOS as the template and ligate into pCWori, and (2) perform site-directed mutagenesis on the new plasmid pHnNOSΔ290hisAmp. Ultimately, the site-directed mutagenesis approach was the successful method. A full plasmid containing the correct phenotype Gly1607 was transformed into and extracted from DH5α *E. coli* cells. The PCR mixture components and program cycles were not optimized in the interest of time. A TD-PCR was used so that multiple combinations of PCR components could be assessed concurrently, since the ideal annealing temperature depends on factors such as salt content, and DNA and oligonucleotide concentrations.

The success of mutation was assessed using restriction enzyme digests with NcoI, EcoRI and NcoI, and EcoRI and NdeI. The removal of one NcoI site in the pHnNOSΔ290hisAmp meant that there would be one less band in the successful mutant (labelled as pHnNOSΔ290hisAmp').

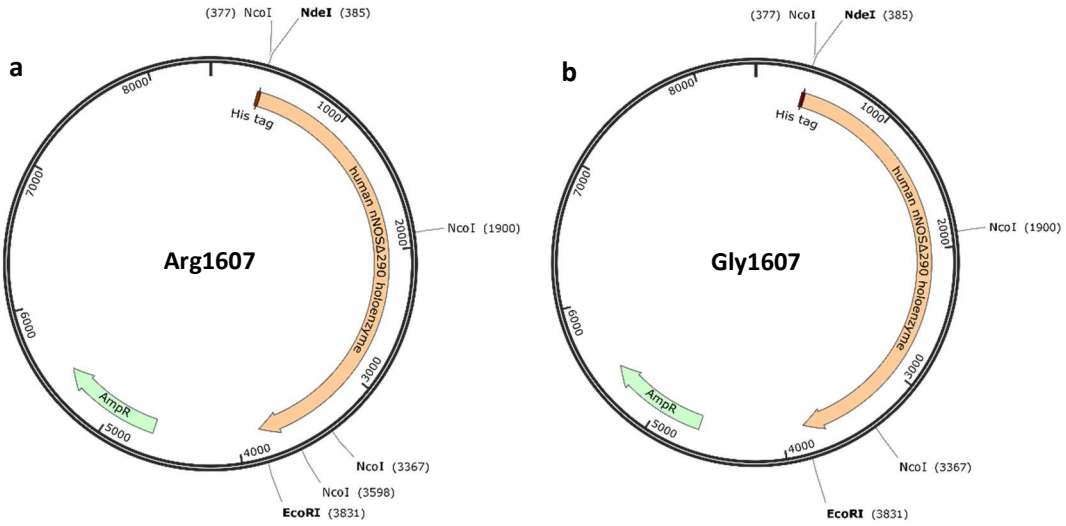

Figure 2.8. Simplified plasmid maps of pHnNOSΔ290hisAmp before (a) and after (b) site-directed mutagenesis. The successful mutant contains Gly1607 and lacks the NcoI cleavage site at position 3598.

Prior to site-directed mutagenesis, restriction digest by NcoI results in the formation of four fragments of lengths 5201 bp, 1523, 1467 bp and 231 bp. The removal of the NcoI restriction site downstream of the target mutation removes the smallest band, and the digest of pHnNOSΔ290hisAmp' yields 5432 bp, 1523 bp and 1467 bp fragments.

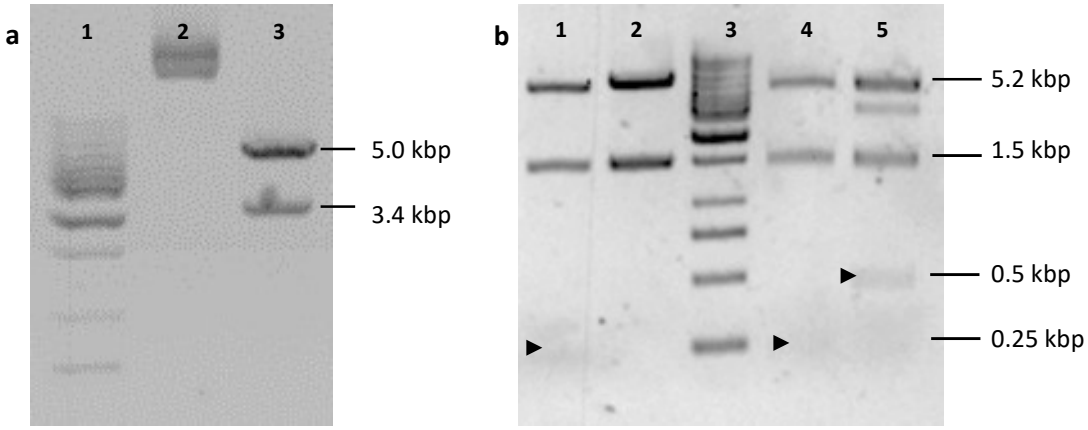

Figure 2.9. Analytical digests of successful pHnNOSΔ290hisAmp mutant, which lacks one NcoI restriction site. (a) Double digest with EcoRI and NdeI (lane 3) results in 5.0 kbp and 3.4 kbp fragments, corresponding to the pCWori vector and nNOSΔ290 holoenzyme insert respecitvely. (b) Single digest with NcoI shows that the ~250 bp band in the non-mutated plasmid (lane 1) is not present in the mutated plasmid (lane 2). Double digest with EcoRI and NcoI also shows that the ~250 band in the non-mutated plasmid (lane 4) was lost in the successful mutant, replaced by a ~500 bp band. 0.5 µg of GeneRuler 1kb DNA Ladders was used for both gels (lanes 1 and 3, respectively).

Sequencing data corroborated the findings from the analytical digests above: Arg1607 was successfully mutated back to Gly. Furthermore, Gln295 was reversed back into Glu at

random, suggesting that it was indeed a spontaneous mutation. No other mutations were found in the sequence.

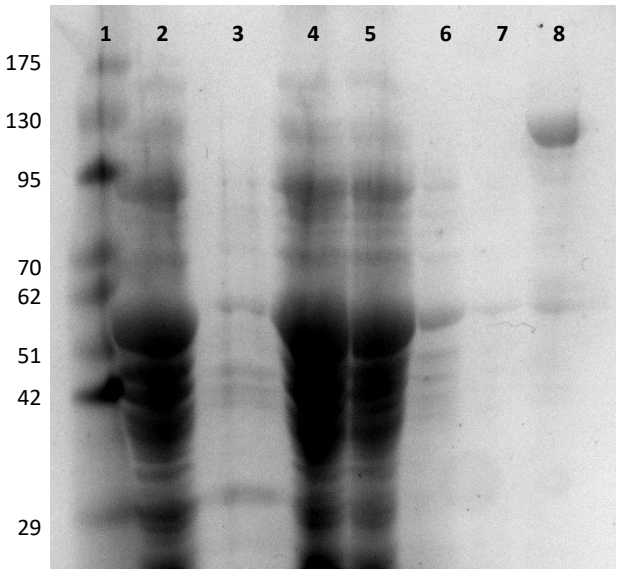

Figure 2.10. Purification of human nNOSΔ290 holoenzyme from pHnNOSΔ290hisAmp' in BL21 (DE3) CodonPlus RP using the ADP Sepharose 4B resin. Each lane represents stages of the purification process. From L-R: (1) Ladder, (2) Lysate, (3) Salt cut supernatant, (4) Resuspended pellet, (5) ADP resin flow-through, (6) ADP Wash, (7) ADP Salt Wash, (8) Pooled fractions.

Figure 2.14 shows that the purified protein is approximately 130 kDa in size. The absorbance spectra of the pooled fraction has the expected shape and Soret peak at approximately 397 nm (see Section 2.2.2.4 for more details). These results suggest that the correct truncated human nNOS holoenzyme was successfully expressed and purified.

2.3.2 Human eNOS holoenzyme

2.3.2.1 pHeNOShisKan

The human eNOS holoenzyme had been previously subcloned into the high-expression vector PDS-78. Hence, pHeNOShisKan was subject to small-scale growth and expression experiments to determine if the *E. coli* strain BL21 (DE3) was sufficient.

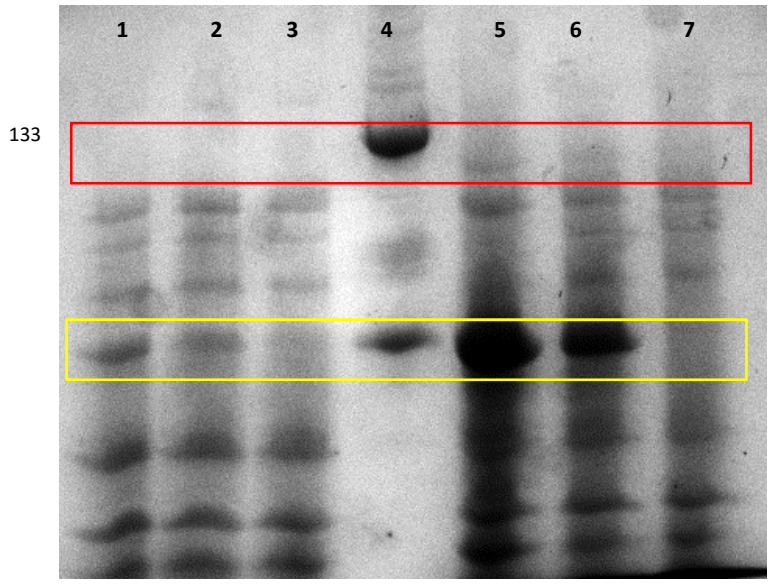

Figure 2.11. Small-scale expression of pHeNOShisKan in *E. coli* strains. Lanes 1–3 corr+espond to samples before induction, while lanes 5–7 refer to samples after induction. Lanes 1 and 5 are BL21 (DE3) cells that express GroES/EL; lanes 2 and 5 are BL21 (DE3) cells that express both GroES/EL and pHeNOShisKan; lanes 3 and 7 are BL21 (DE3) CodonPlus RP cells that express pHeNOShisKan. There are no visually discernible differences in the band intensities that correspond to human eNOS holoenzyme among all three samples, before and after induction. In lieu of a molecular weight ladder, purified bovine eNOS (133 kDa) was used to estimate band sizes (lane 4). Red box = human eNOS holoenzyme; yellow = GroEL.

From the gel on Figure 2.11, it appears that the human eNOS holoenzyme was not expressed at all in either BL21 (DE3) or BL21 (DE3) CodonPlus RP strains. None of the expected eNOS holoenzyme bands have an increase in intensity comparable to that of the GroES/EL internal control. The human eNOS holoenzyme exhibits codon bias; there are 60 instances of rare Arg codons AGA, AGG, CGA and CGG, and 54 instances of the Pro rare codon CCC, in the sequence. Given the above results, it is not clear whether the BL21 (DE3) CodonPlus RP strain was able to mitigate this codon usage bias and express the eNOS enzyme.

Such results may also indicate that the addition of IPTG could not induce NOS expression via the T7 promoter, at least in the case of pHeNOShisKan (since it was shown in pHnNOShisKan). If the problem lies with the PDS-78 vector, then the human eNOS holoenzyme must be expressed using a different vector, perhaps pCWori.

2.3.2.2 pHeNOSΔ66hisAmp

The truncated human eNOS sequences (eNOSΔ66) was also subcloned into the pCWori vector to produce the 8398-bp long plasmid pHeNOSΔ66hisAmp. The double digest reaction with EcoRI and NdeI yielded two fragments: 5.0 kbp and 3.4 kbp (Figure 2.13).

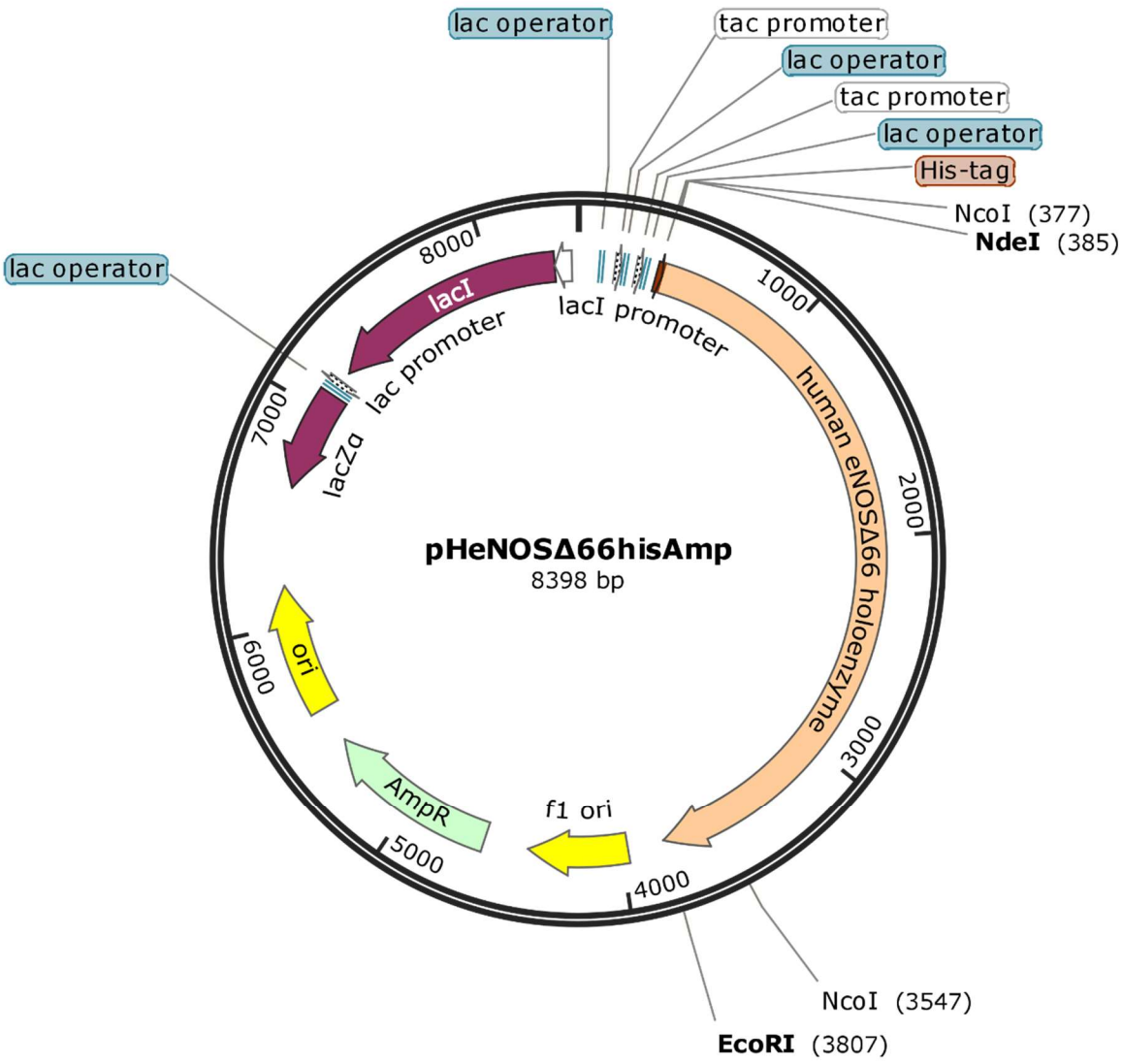

Figure 2.12. Plasmid map of pHeNOSΔ66hisAmp. This plasmid contains the truncated human eNOS holoenzyme subcloned into pCWori via ligation. It is ampicillin-resistant and uses the moderate-expression promoter tac. Restriction enzymes EcoRI, NcoI and NdeI (noted above) were used to validate subcloning success.

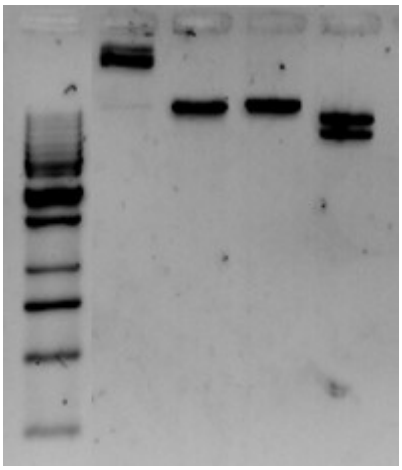

Figure 2.13. Analytical digests of the pHeNOSΔ66hisAmp construct. Single digest with either EcoRI (lane 2) or NdeI (lane 3) both yield fragments of approximately 8.4 kbp in length. Double digest with EcoRI and NdeI (lane 5) results in 5.0 kbp and 3.4 kbp fragments, corresponding to the pCWori vector and eNOSΔ66 holoenzyme insert respectively.

There were no reported mutations in the heNOS template that was used to amplify the heNOSΔ66 holoenzyme insert. Sequencing data showed that no spontaneous mutations occurred during the subcloning process of pHeNOSΔ66hisAmp. Hence, no further genetic manipulations were applied to the plasmid.

BL21 (DE3) CodonPlus RP cells that express pHeNOSΔ66hisAmp were grown in the small scale and purified using the His SpinTrap™ (2.2.2.1). The human eNOS holoenzyme can be expressed and purified, spurring on a large-scale expression and purification using the ADP affinity column.

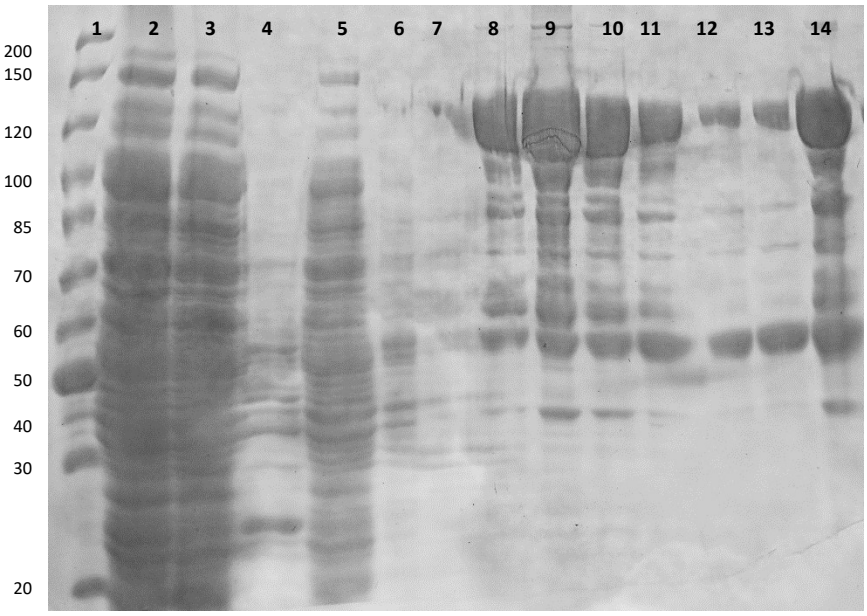

Figure 2.14. Purification of human eNOSΔ66 holoenzyme from pHeNOSΔ66hisAmp in BL21 (DE3) CodonPlus RP using ADP Sepharose 4B. Each lane represents stages of the purification process. From L-R: (1) Ladder, (2) Lysate, (3) Resuspended pellet, (4) Salt cut supernatant, (5) ADP resin flow-through, (6) ADP Wash, (7) ADP Salt Wash, (8-13) Collected fractions 2-7, (14) Pooled fractions.

The purified protein is approximately 130 kDa in size (Figure 2.14), which is the expected size for human eNOSΔ66 holoenzyme. The absorbance spectra of the pooled fractions showed a characteristic shape for NOS enzymes, including the Soret peak at about 397 nm. As such, it can be concluded that the expression and purification of the human eNOSΔ66 holoenzyme was a success.

2.3.3 NOS protein yields and purity

As mentioned above, this project aims to develop human constitutive NOS expression systems with yields comparable to that of well-established NOS expression systems. Table 2.6 lists the highest recorded yields for all nNOS and eNOS purifications that were performed to obtain all NOS isozymes to be used for the duration of this project. The values are expressed in terms of nmol of protein per L of culture grown for 40 hours.

Table 2.6. NOS holoenzyme yields calculated as moles per litre of culture.

Isoform	**Organism**	***E. coli* strain**	**nmol protein per L culture**
nNOS	rat	BL21 (DE3)	67 ± 14
	human	BL21 (DE3) CodonPlus RP	7.7 ± 4.0
eNOS	bovine	BL21 (DE3)	21 ± 1.4
	human	BL21 (DE3) CodonPlus RP	12 ± 3.0

The above values suggest that both human nNOS and eNOS holoenzyme have apparently lower yields than their mammalian counterparts. This discrepancy can be explained by the fact that the human NOS enzymes were expressed in BL21 (DE3) CodonPlus RP, which require three different antibiotics to maintain the selective pressure. Thus, these cells tend to grow more slowly than the BL21 (DE3) cells, which only needs one antibiotic (or two, if co-expressed with GroES/EL). Furthermore, the mammalian NOS were all co-expressed with GroES/EL, which stabilize the proteins' native fold during growth and purification and thus, increasing protein yield.

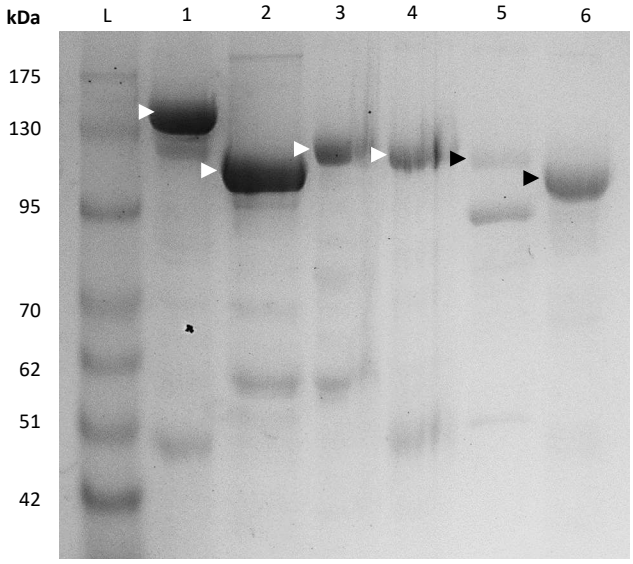

Figure 2.15. Purified human and non-human NOS holoenzymes in 7.5% SDS-PAGE. From L-R: (L) ladder, (1) rat nNOS, (2) human nNOS, (3) bovine eNOS, (4) human eNOS, (5) murine iNOS, (6) human iNOS.

As shown in Figure 2.15, the purified proteins vary in purity. This can be remedied by the addition of size exclusion chromatography in the purification process. However, this step requires the concentration of the eluted fractions into very small volumes, which then increases the risk of aggregation. Additionally, NOS is a highly unstable protein, such that further agitation may lead to protein misfolding and/or degradation. Though the presence of other proteins have negligible effects on kinetic assays, pure NOS proteins are still desired so that they can be used for other projects, especially those that involve structure determination such as X-ray crystallography. Further, a more pure sample can be used to study substrate and inhibitor binding kinetics using techniques such as isothermal calorimetry.

2.3.4 Active site heme analysis

The absorbance spectra of the purified human nNOS and eNOS holoenzymes have shapes similar to that of NOS isozymes with intact heme ligands (Figure 2.1). The spectra of NOS samples incubated with saturated imidazole show a distinct shift from about 397 nm to 420 nm. This change indicates that the heme ligand moved from the favourable five-coordinated high spin state to a six-coordinate low spin state. Hence, the heme propionate remained bound to the active site Cys residue of the NOS holoenzymes and the purified samples were fit for enzymatic studies. Although these results are conclusive, it can be further verified by bubbling the sample with CO, which would cause the peak to shift towards 450 nm. CO bubbling was not performed, however.

Note that the addition of control and L-arginine treatments have mostly overlapping NOS Soret peaks at about 397 nm. This observation is due to the fact that the buffers used for NOS purification and storage contain L-arginine. Indeed, the samples all contain 5 μM L-arginine,which has been found to aid in the stabilization of NOS holoenzymes. However, the present results show that the addition of excess L-arginine (1 mM of substrate is orders of magnitude more than required for most assays) does not affect the NOS absorbance spectra in any significant way. Furthermore, the substrate-free NOS samples have been shown to have the Soret peak at around 400 nm instead of the expected 420 nm because the sample buffers contain different salts that could interfere with the heme. The 420 nm Soret peak could theoretically be observed in samples that are dissolved in pure water, but this would compromise the native fold of the protein.

Finally, 10 μM H_4B was added to the samples as well and it caused protein aggregation, as evidenced by the increase in the turbidity of the sample. The spectra of these samples showed seemingly infinite increase in absorbance towards 300 nm (not shown). Recall that the pterin co-factor binds NOS at the dimer interface and promote the dimer stability by enhancing hydrophobic interactions. While H_4B is soluble in water at 10 μM, it can precipitate out of a solution that contains salts, such as the buffer in which NOS is stored. This could have driven the exposure of hydrophobic patches on NOS, leading to denaturation.

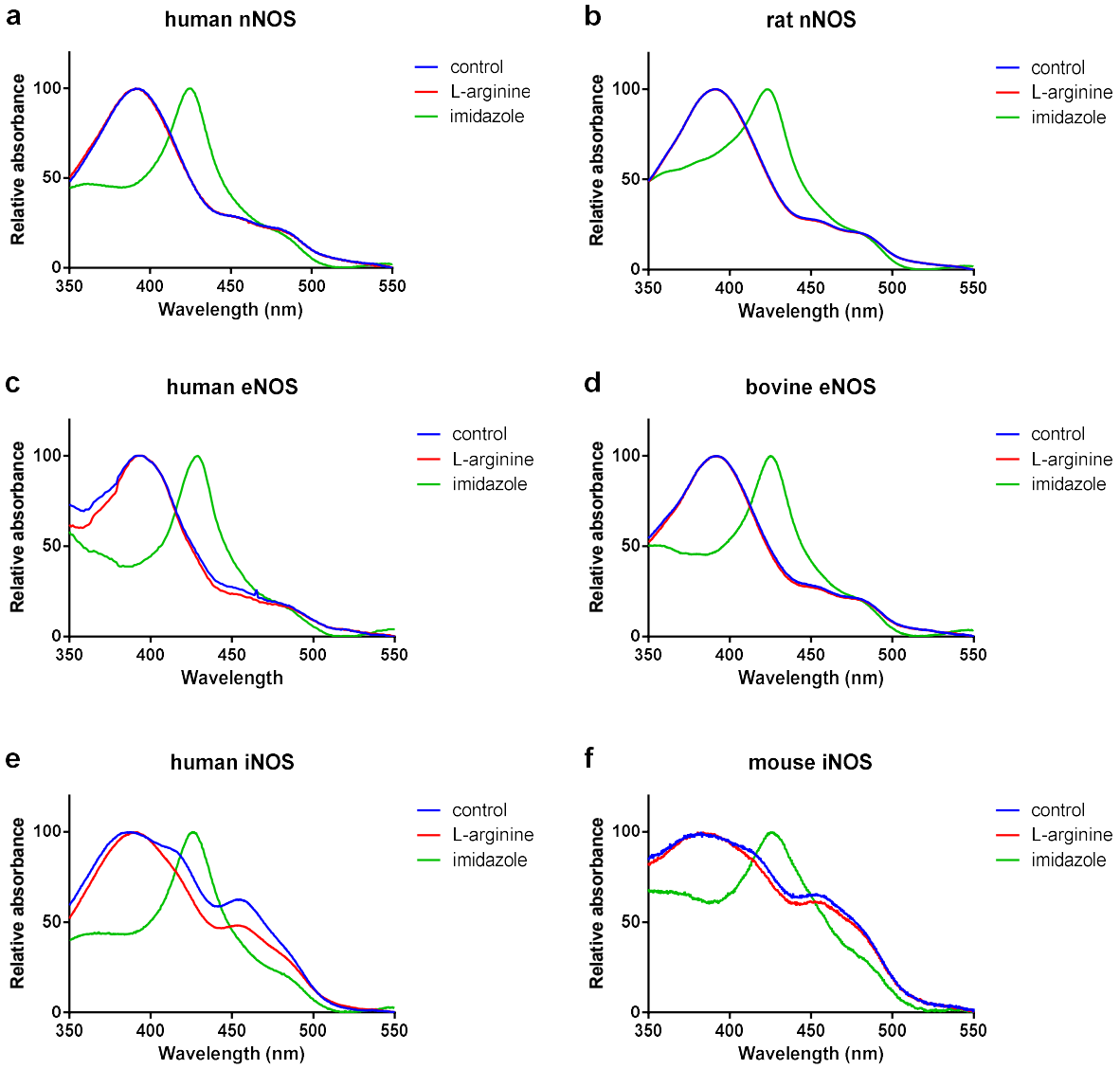

Figure 2.16. Absorbance spectra of purified NOS holoenzymes used in this project. The curves are normalized to the Soret peak of the control samples. Both human and mammalian NOS exhibit red-shifted Soret peaks from about 400 nm to 425 nm upon incubation with imidazole.

2.3.5 Flavin content analysis

Table 2.7 lists how much flavin cofactors are present in the purified NOS proteins. In general, NOS protein samples showed a higher concentration of FMN than FAD. These values are similar for both human and non-human isoforms, with the exception of the human nNOS, which contains 2.5-fold higher concentrations of both FAD and FMN. This result could be a consequence of concentrating the sample using a centrifugal concentrator. The human nNOS sample was concentrated because the concentration after elution from the ADP column was less than 2 µM.

This low concentration was not observed in the other purified NOS, so those samples were not concentrated before storage. However, using the centrifugal concentrators causes the denaturation and/or degradation of NOS proteins. The bound flavins FAD and FMN are likely to be released back into solution, such that the NOS sample now has higher mole of heme to mole of flavin ratios.

Table 2.7 .Heme to flavin content ratio of purified samples determined via fluorescence. The values are expressed in terms of mole of flavin per mole of heme.

Isoform	Organism	heme/FMN	heme/FAD
nNOS	human	2.60	2.60
	rat	0.56	0.43
eNOS	human	0.46	0.44
	bovine	0.52	0.47
iNOS	human	0.55	0.51
	mouse	0.37	0.61

2.3.6 Determining the kinetic parameters of human and non-human NOS holoenzymes

The L-arginine concentration of 25 μM was chosen as an appropriate concentration for steady-state activity assays. It is larger than the average K_m value for human and non-human NOS by a factor of at least 10, at which point the V_{max} would be reached. For these experiments, the measured activity in units of nmol NO min^{-1} mgP^{-1} were normalized against the activity of the non-human NOS with Ca^{2+} treatments. The relative activities are reported in the following figures.

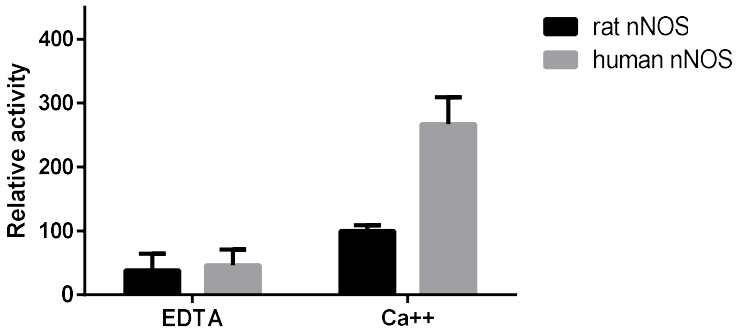

Figure 2.17. Relative activity of human and rat nNOS holoenzymes at 25 μM L-arginine. These values were normalized using the activity of rat nNOS with or Ca^{2+} (27 ± 5.1 nmol NO min^{-1} mgP^{-1}) as 100%. Non-parametric Mann-Whitney U Test for independent samples show that there is no significant difference in activity between rat and human nNOS ($p = 0.281$), as well as the difference in activity of eNOS in the presence and absence of Ca^{2+} ($p = 0.121$).

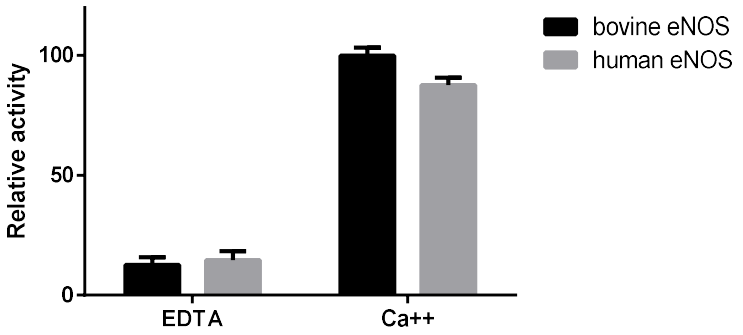

Figure 2.18. Relative activity of bovine and human eNOS holoenzymes at 25 μM L-arginine. These values were normalized using the activity of bovine eNOS with or Ca^{2+} (76 ± 2.5 nmol NO min^{-1} mgP^{-1}) as 100%. Non-parametric Mann-Whitney U Test for independent samples show that there is no significant difference in activity between bovine and human eNOS ($p = 0.551$), but the difference in activity of eNOS in the presence and absence of Ca^{2+} is statistically significant ($p < 0.001$)

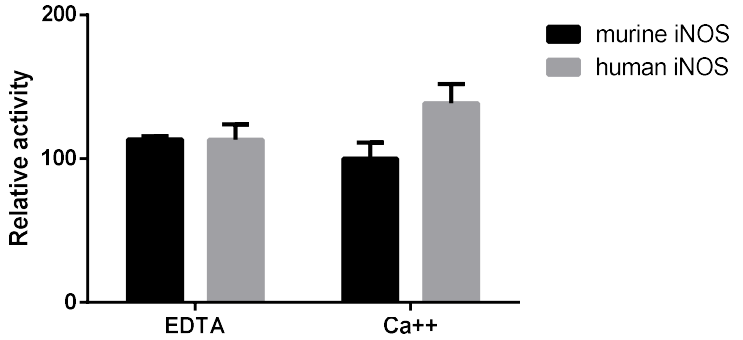

Figure 2.19. Relative activity of murine and human iNOS holoenzymes at 25 μM L-arginine. These values were normalized using the activity of murine iNOS with or Ca^{2+} (170 ± 46 nmol NO min^{-1} mgP^{-1}) as 100%. Non-parametric Mann-Whitney U Test for independent samples show that there is no significant difference in activity between murine and human iNOS ($p = 0.328$), as well as the difference in activity of iNOS in the presence and absence of Ca^{2+} ($p = 0.645$).

Statistical analyses were performed using a sample size of 6 for each treatment. A non-parametric test, Mann-Whitney U Test, was used because normality tests (from GraphPad) state that the samples do not have a normal distribution. As shown in the figures above, the both human and non-human cNOS have significantly low activity when EDTA is added to remove Ca^{2+} ions. This mechanism confirms the calcium-dependent CaM activation of cNOS. In the presence of Ca^{2+}, the human nNOS showed a significantly higher activity than the rat nNOS, at an approximately 300% increase. On the other hand, there is no significant difference observed between human and bovine eNOS. Meanwhile, the presence or absence of Ca^{2+} does not significantly affect both human and murine iNOS; the measured activities for both EDTA and Ca^{2+}

treatments are all apparently equivalent. This result agrees with the fact that iNOS activity is independent of calcium concentration.

Following the above results, NO production rates for each NOS isoform were used to obtain Michaelis-Menten curves, K_m and V_{max} values (Figure 2.20). In particular, V_{max} values are consistent with the steady-state activity assay results above. K_m and V_{max} values were calculated such that the Michaelis-Menten model fit gives R^2 values of greater than 0.90. These are compared against literature values (Table 2.8). Note, however, that the literature values were the kinetic parameters reported by different groups studying NOS enzymes. As mentioned previously, these values were not obtained using a standardized protein expression methods. For instance, Gross et al. performed NOS activity assays using crude lysates, which may have contain elements that could have interfered with the activity measurements. Indeed, there exist multiple entries for the same NOS isoform from the same organism, as listed on BRENDA.

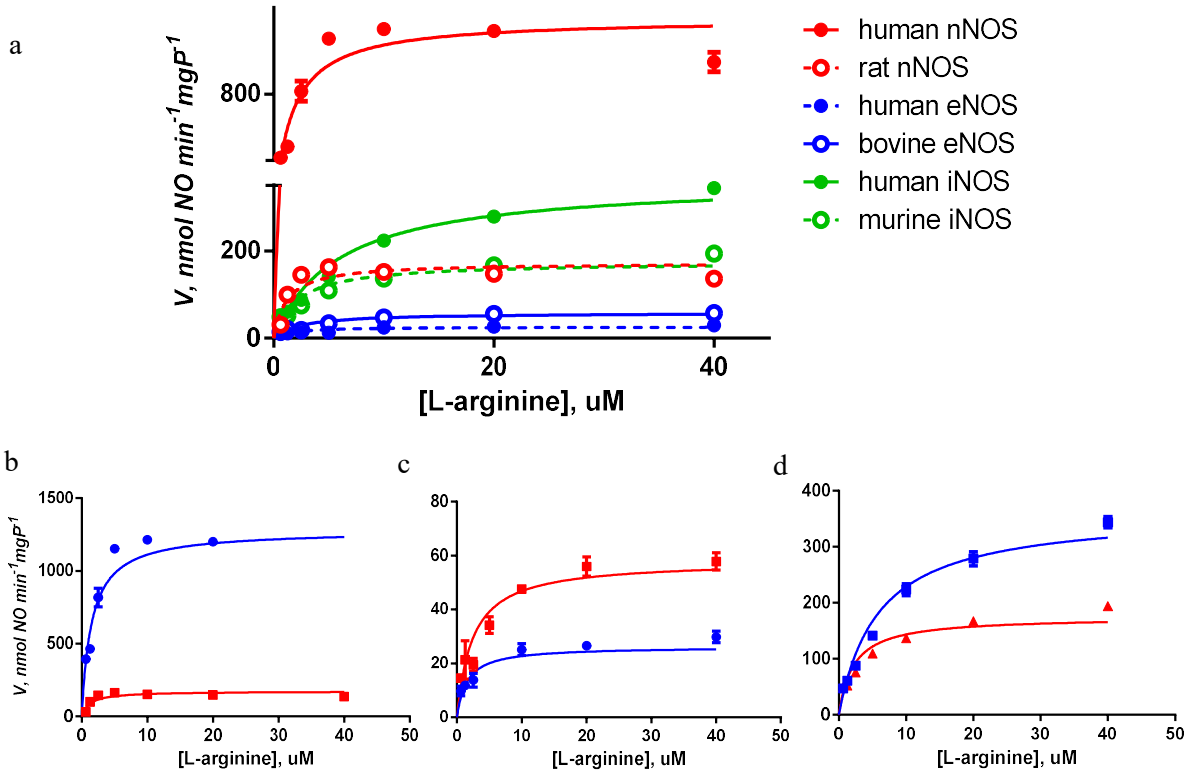

Figure 2.20. Michaelis-Menten plots of human and non-human NOS holoenzymes for the substrate L-arginine. (a) Combined plot of all NOS isoforms used in this study shows how the Michaelis-Menten curves look relative to each other. Separate plots with human (blue) and non-human (red) NOS are shown for (b) nNOS, (c) eNOS and (d) iNOS. The calculated K_m and V_{max} values are summarized in Table 2.8.

Table 2.8. K_m and V_{max} values for human and non-human NOS holoenzymes.

Isoform	Organism	Observed		Literature values	
		V_{max}, nmol min^{-1} mg^{-1}	**K_m (L-arginine), µM**	**V_{max}, nmol min^{-1} mg^{-1}**	**K_m (L-arginine), µM**
nNOS	**human**	1300 ± 61	1.5 ± 0.20	90[a], 400[b], 1000[c]	1.6[a,r]
	rat	170 ± 12	1.2 ± 0.28	9.8[d], 120-170[e], 284[b], 940-960[f]	1.3[r], 2-2.8[e], 14-18[d]
eNOS	**human**	26 ± 2.4	1.5 ± 0.41	0.90[a], 19[g], 142[h]	0.9[a], 3.9[g], 4.4[h]
	bovine	58 ± 4.3	2.4 ± 0.47	31[i], 143[j], 340-350[k]	1.7[r], 2.1[j]
iNOS	**human**	360 ± 31	5.9 ± 0.90	22[l], 290[a]	2.2[a], 16[s], 22[t]
	murine	170 ± 11	2.2 ± 0.33	170-815[m], 1006[n], 1100[o,p], 1620[q]	2.8[n], 14-18[q]

The above listed literature values for V_{max} and K_m were determined using purified proteins from either tissue extracts or heterologous expression in yeast or bacteria.
[a] Garvey, Furfine, & Sherman, 1996. [b]Fang et al., 2009. [c]Demady, Jianmongkol, Vuletich, Bender, & Osawa, 2001. [d]Hiki, Hattori, Kawai, & Yui, 1992. [e]Schmidt, Smith, Nakane, & Murad, 1992. [f]Bredt & Snyder, 1990 [g]Leber et al., 1999. [h]Golser, Gorren, Mayer, & Schmidt, 2003. [i]Nam et al., 1998. [j]Presta, Liu, Sessa, & Stuehr, 1997. [k]Ohshima et al., 1992. [l]Gerber, Nishida, & de Montellano, 1997. [m]Rusche, Spiering, & Marletta, 1998. [n]Stuehr, Cho, Kwon, Weise, & Nathan, 1991. [o]Baek, Thiel, Lucas, & Stuehr, 1993. [p]Ghosh & Stuehr, 1995. [q]Hevel & Marletta, 1992. [r]Cinelli et al., 2015. [s]Bretscher, Li, Poulos, & Griffith, 2003. [t]Gerber et al., 1997.

In a comprehensive review of NOS mechanism, Santolini summarized the global kinetic model of NOS catalysis. Computer simulations showed that the final product of NOS activity is not radical NO per se, but rather, the Fe(III)-NO complex.(Santolini, 2011; Stuehr et al., 2004) According to the model, NO synthesis is governed by three main kinetic parameters: k_r (reduction of Fe(III) at the heme), k_{ox} (oxidation of Fe(II)-NO to form peroxynitrite) and k_d (dissociation of NO from Fe(III) heme). The balance between k_r, k_{ox} and k_d determine whether NO will be released into solution (productive cycle) or remain bound to the heme (futile cycle). Set points for these parameters have been determined experimentally, which were then used to develop the global catalytic model. Furthermore, k_r has been shown to depend on the NOS reductase, while k_{ox} and k_d are determined by the NOS oxygenase. These values are specific to the NOS isoform and as such, account for the differences in their catalytic activities and kinetic parameters. Using NOS chimeras, Wang et al. determined that k_r values must have evolved optimally relative to k_d, which is determined by the distal heme pocket residues. Bulky residues such as Ile blocks NO release more effectively than small residues like Val. Indeed, they have shown that increasing k_r resulted in a decrease in k_d without further manipulating the distal heme pocket. From fastest to slowest, k_r values are ranked as nNOS > iNOS > eNOS; k_{ox}, iNOS > eNOS > nNOS; and k_d, nNOS > eNOS > iNOS. Taken together, these values determine the rank for the NOS synthesis rates: iNOS > nNOS >> eNOS. This ranking is consistent with the expected and observed V_{max} values for non-

human NOS but not for human NOS: nNOS > iNOS >> eNOS (Table 2.8). Given these results, it is worth noting that the kinetic parameter rankings were obtained using rat nNOS instead of human nNOS (Wang et al. 2016). Hence, it appears that k_r, k_{ox} and k_d values do not only vary between isoforms but across organisms as well.

Fang et al. (2009) attribute the discrepancies in V_{max} values between isoforms to the difficulty in quantifying exact NOS enzyme concentrations, such that the activity were miscalculated. However, it is clear in their study and multiple others (including this one) that human nNOS tend to have higher activity than rat nNOS. On the other hand, both published and observed data show that bovine eNOS exhibit higher activity than human eNOS. While literature values suggest that murine iNOS has higher activity than human iNOS, our experimental values show the opposite.

The observed Michaelis-Menten constants agree with the expected values, as well as the relative affinities of non-human NOS isoforms with their human counterparts. However, the observed K_m for human eNOS was higher than the observed K_m for bovine eNOS; this is the opposite of literature K_m values. This observation emphasizes the need for a standardized expression and assay systems for determining the kinetic parameters of NOS isoforms. Additionally, because these K_m values are to be used further in the inhibition assays (for calculating K_i), this discrepancy may affect the observed isoform-selectivity of NOS inhibitors. These deviations are especially important with regard to the active site inhibitors because the affinity of L-arginine to NOS determines how well they can displace the substrate and inhibit catalysis.

2.4 Conclusions

As discussed in Chapter 1, this project aims to develop expression systems for human cNOS holoenzymes. The process involves the verification of the published enzymatic activity and kinetic parameters associated with these proteins. The human nNOS and eNOS holoenzyme gene sequences were successfully cloned into pCWori, which is a commonly used vector for heterologously expressed heme-based oxygenases. The active site heme of these proteins were verified via UV-Vis and the full-length human NOS exhibited the expected Soret peak shifts characteristic of NOS.

The human NOS were further characterized using oxyhemoglobin capture assays. Although the steady-state NO synthesis activity of human eNOS and human iNOS are comparable to their non-human counterparts, human nNOS exhibited a significantly higher activity relative to

the rat nNOS. The maximum rates of reaction V_{max} reflect this prior result. However, the relative NOS activities vary between human and non-human NOS. The human NOS ranking (fast to slow) is nNOS > iNOS >> eNOS, whereas for the non-human NOS, it is iNOS > nNOS >> eNOS. In term of K_m, the relative affinities of the human NOS to L-arginine match up with those of the non-human NOS. However, the human eNOS was observed to have a lower K_m, i.e. higher affinity, than the bovine eNOS; this was the opposite of what was expected per published values. As previously mentioned, before this project, there is no published study using a standardized assay to determine the kinetic parameters for NOS activity. Our results provide a valid argument for the re-examination of first generation NOS inhibitors using human NOS because the kinetic differences may translate to differences on the isoform selectivity of NOS inhibitors.

Chapter 3

3. Inhibition of human and non-human NOS holoenzymes

3.1 Introduction

Maintenance of eNOS activity while blocking the target NOS isoform (either nNOS and iNOS) is paramount to the development of NOS inhibitors. However, NOS isoforms are highly conserved; the high homology among the isoforms hinders the development of isoform-selective drugs. Furthermore, structure-based drug design was not possible until recently, such that high-throughput screening of lead compounds is very difficult. As mentioned above, high resolution crystal structures of the human NOS isozymes were not available until recently, owing to the highly unstable and highly dynamic nature of the full-length holoenzymes. Hence, drug development studies were performed using the more readily available non-human isoforms: rat nNOS and bovine eNOS.

As discussed in Chapter 1, there exist slight structural differences between human NOS and their non-human counterparts. As shown in Chapter 2, these differences affect NOS activity and its affinity towards the substrate L-arginine. This chapter discusses the effects of the differences between human and non-human isoforms on the inhibitory activity of early generation active site and CaM-binding inhibitors.

3.1.1 Active site inhibitors

Since the active site inhibitors examined in this project are first generation compounds, they are not as complex as the most recently developed compounds. However, some have exhibited isoform selectivity by exploiting not only the differences in isoform structure, but also the differences in the active site binding kinetics.

3.1.1.1 L-arginine analogues: L-NMMA, L-ALA and L-NNA

The earliest compounds tested for NOS inhibition are L-arginine analogues, usually with a functional group substitution at a guanidino nitrogen. Two of these compounds (L-NMMA and L-ALA) contain hydrocarbon groups attached to a terminal guanidino nitrogen (
Figure 3.1). These compounds are all able to competitively displace L-arginine at the NOS active site but do not exhibit selectivity for any of the NOS isoforms. These small molecules share a similar mechanism of action. They inactivate NOS by modifying the heme at the active site. Using stopped-flow spectroscopy and UV-Vis, Zhang et al. show that when these compounds bind, the aromatic heme gets reduced.(Zhang et al., 1997) The loss of aromaticity corresponds to the

observed loss of the Soret peak at approximately 400 nm. The inhibitory effect of L-NMMA and L-ALA is time-dependent because the heme inactivation is preceded by enzyme mediated oxidation and hydroxylation of the inhibitors. In a mechanism reported by Zhang et al., an alkylic radical from either inhibitor forms an adduct with the heme.(Zhang et al., 1997) Furthermore, both L-NMMA and L-ALA undergo hydroxylation such that L-citrulline and NO are still formed; the guanidino group provides the proton for NO cleavage to proceed. However, the alkylated heme is now unable to coordinate Fe, rendering the NOS enzyme inactive (

Figure 3.2b).

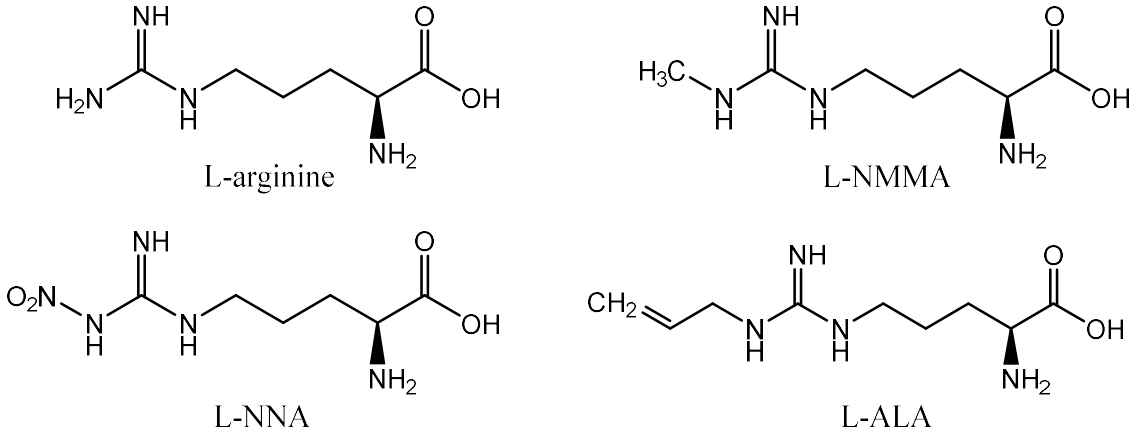

Figure 3.1. L-arginine and derivatives.

L-NMMA and L-ALA are anchored to the NOS active site with the same interactions as that of L-arginine. Additionally, the substituted alkyl group juts into binding pockets near the active site (Figure 3.3a). Apparently, these moieties do not quite extend towards the possible isoform-specific binding sites. Indeed, these compounds have been found to be non-selective.

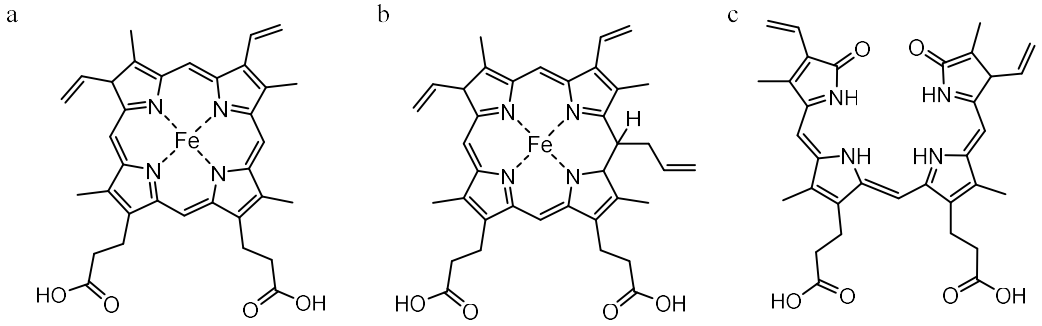

Figure 3.2. Structures of (a) intact heme, (b) inactivated heme via allylation from L-ALA and (c) biliverdin IX, a by-product of NOS inactivation by 1400W.

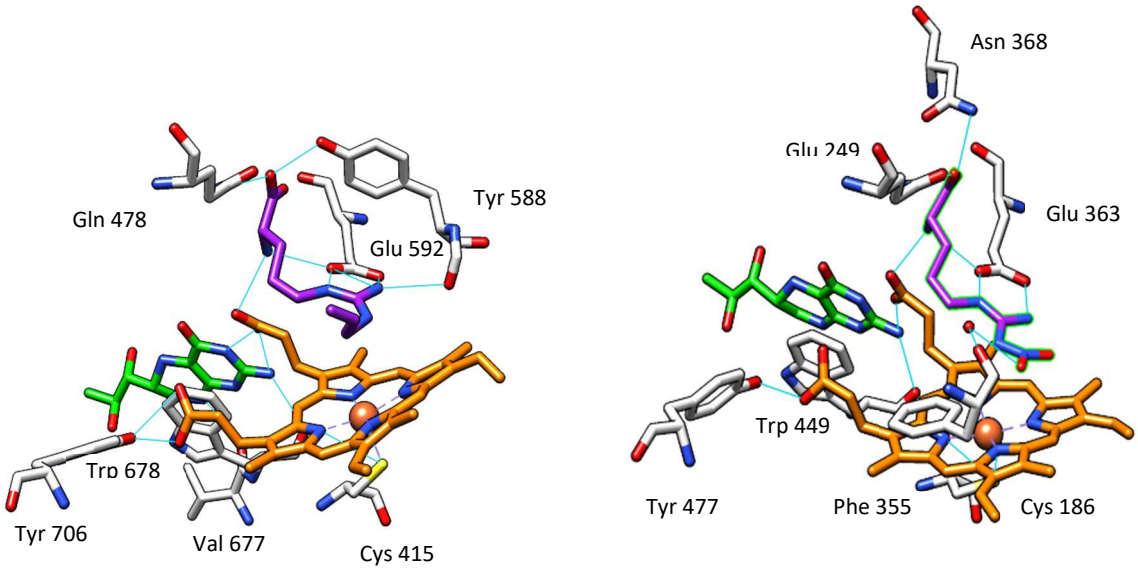

Figure 3.3. L-arginine analogues at the NOS active site. (a) L-ALA at the rat nNOS active site (PDB: 1K2S). (b) L-NNA at the bovine eNOS active site (PDB: 8NSE).

On the other hand, L-NNA does not inactivate the NOS heme. It binds NOS at a higher affinity than the substrate L-arginine (nM versus μM range, respectively). This increase in affinity is attributed to the additional H-bonds formed by the nitrate group with the active site backbones (Figure 3.3b). Unlike L-NMMA and L-ALA, L-NNA exhibits selectivity toward nNOS and eNOS over iNOS. This isoform-selectivity is due to the fast turnover at the iNOS active site. L-NNA has slow off-rates for cNOS. Consequently, L-NNA is considered a time-dependent inhibitor. NOS pre-incubated with L-NNA showed lower NO synthesis rates than NOS that were not pre-incubated.(Furfine, Harmon, Faith, & Garvey, 1993)

3.1.1.2 Cyclic aromatic inhibitors: 3-bromo-7-nitroindazole and 1400W

Since simply modifying L-arginine does not promote isoform selectivity, cyclic bulky compounds like 3-bromo-7-nitroindazole and 1400W were developed. The bulkiness allow these compounds to access binding sites that may be unique to one isoform. Like the L-arginine analogues, these compounds contain moieties that mimic the guanidino group of the substrate and interact with the heme via π-stacking.

3-bromo-7-nitroindazole (3Br7NI) was the most potent nitroindazole derivative developed as a NOS inhibitor. It is a competitive reversible NOS inhibitor that was originally thought to be nNOS selective, as shown in *in vivo* studies.(Poulos & Li, 2012) However, *in vitro* results showed

that 3Br7NI only has modest selectivity towards nNOS over eNOS. 3Br7NI was found to be unable to enter endothelial cells to affect eNOS. The selectivity of this compound is determined by the tissue distribution of NOS isoforms.(Rosenfeld et al., 2002)

The nitro group draws electron density away from the indazole. Hence, in addition to stacking interactions, 3Br7NI is anchored to the active site via electrostatic interactions. Unlike the L-arginine analogues, however, 3BrNI does not form H-bonds with the invariant Glu residue at the active site.(Raman et al., 2001) Crystal structures reveal that 3Br7NI bind differently between cNOS and iNOS; 3Br7NI was found to bind cNOS at the H_4B binding site in addition to the active site. Futhermore, it can displace previously bound H_4B, where it has partial π-stacking with Trp447.(Raman et al., 2001)

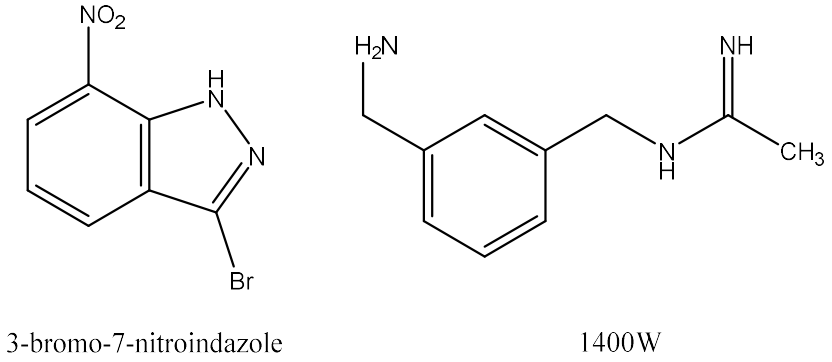

3-bromo-7-nitroindazole 1400W

Figure 3.4. Selective NOS inhibitors 3-bromo-7-nitroindazole and 1400W.

Lastly, 1400W is an irreversible inhibitor of iNOS. This isoform selectivity can be attributed to the conformational changes at the active site upon binding as well as the kinetics of NOS catalysis. The crystal structure of murine iNOS complexed with 1400W reveals that 1400W has two binding modes for iNOS. This conformational flexibility of the iNOS active site, compared to cNOS, partly explains the isoform selectivity.(Fedorov, Hartmann, Ghosh, Schlichting, & Carolina, 2003) The aromatic ring of 1400W has π-stacking interactions with the heme. Meanwhile, the aminomethyl group forms H-bonds with the conserved Tyr485 and H_4B. Further, the amidine forms H-bonds with the invariant Glu371. These interactions, particularly the latter, cause a helical shift driven by hydrophobic interactions that is not possible in nNOS due to the presence of the Tyr hydroxyl (equivalent to Phe in iNOS, Leu in eNOS). With 1400W oriented as such, the heme inactivation mechanism proceeds very rapidly in iNOS.

The heme inactivation mechanism of 1400Wis different from that of L-NMMA and L-NNA, as there is no formation of an inhibitor-heme adduct.(Li, Raman, Marta, Masters, & Poulos,

2001) 1400W cannot act as a substrate like L-NMMA and L-ALA because it lacks a proton to donate to the heme-bound peroxide (See the mechanism on Figure 1.5b). Consequently, there is no L-citrulline and NO produced.(Li et al., 2001) The resulting peroxide-heme complex gets degraded into biliverdin IX, in an irreversible reaction (Figure 3.2c). The fast rate of kinetic turnover of iNOS allows this reaction to proceed much faster in iNOS compared to nNOS and cNOS, the difference in enzyme kinetics and structural differences make 1400W an effective iNOS-selective inhibitor.

3.1.2 CaM-binding inhibitors

As mentioned before, CaM binds and activates approximately 300 other proteins. Hence, using CaM-binding inhibitors poses the risk of off-target inhibition, not only of eNOS but also of other unrelated proteins. Despite this, compounds such as mastoparan and monobutylin trichloride have been reported to block nNOS activity.(Curtin et al., 2015) The calmodulin binding sequences of human NOS have 100% homology with their non-human counterparts. As such, one would expect that the treatment of, say, human eNOS and bovine eNOS with a CaM-binding inhibitor would yield similar IC50s. CaM-binding inhibitors have been studied in the last 20 years, alongside active site NOS inhibitors. The compounds target either CaM itself or the CaM-binding sequences within the NOS proteins. In this chapter, inhibitors of the first kind trifluoperazine (TFP) and melatonin are examined (Figure 3.5). Inhibition studies with TFP and melatonin may provide insight on NOS activation by CaM, and if there are differences in human and non-human NOS.

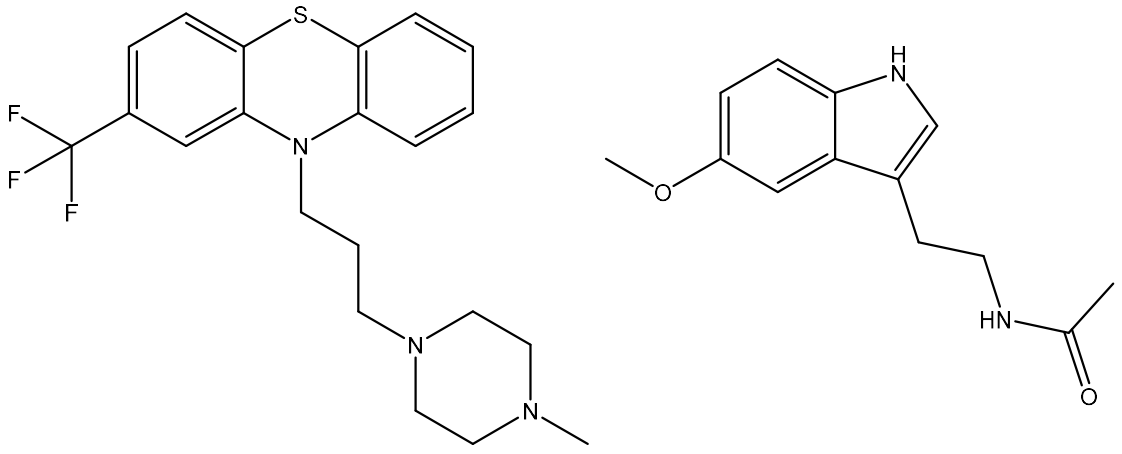

Figure 3.5. CaM-binding inhibitors trifluoperazine and melatonin.

3.1.2.1 Trifluoperazine

TFP is a phenothiazine-based antipsychotic compound that has been used to treat schizophrenia.(Vandonselaar, Hickie, Quail, & Delbaere, 1994) Its pharmacological effects include blocking adrenaline and dopamine receptors in brain neurons. Additionally, TFP also acts as a CaM inhibitor.(Mata et al., 2015) TFP binding to CaM gas been shown to have a negative effect on the activation of other CaM-dependent proteins such as troponin. Lee and Stull reported that TFP completely inhibits NOS activity at concentrations ranging from 200 μM – 1 mM.(S. Lee & Stull, 1998)

TFP binding to CaM requires at least three occupied Ca^{2+}-binding sites.(Vandonselaar et al., 1994) As discussed earlier, Ca^{2+}-binding exposes hydrophobic patches that bind NOS. TFP binds at these very sites, thereby preventing NOS binding and activation. The CaM linker helix that separates the C and N-lobes is further split into two smaller helices upon TFP binding, such that CaM is unable to bind NOS.(Koevesi, Menyhard, Laberge, & Fidy, 2008) Despite multiple published crystal structures, the correct binding stoichiometry is yet to be solved; previous studies reported that 2-7 TFP molecules bind per CaM. In any case, it was reported that TFP exhibits anti-cooperative binding, i.e. binding of more TFP molecules diminishes its affinity. Its binding constant K_d was observed to be between 1-8 μM.(Vandonselaar et al., 1994)

3.1.2.2 Melatonin

Melatonin is a ubiquitous signalling molecule in mammals and other organisms that is responsible for the regulation of circadian and seasonal rhythms. Endogenous melatonin is synthesized at the pineal gland, although experiments using anti-melatonin antibodies have shown that there are extrapineal melatonin sources.(Acuña et al., 2014) In particular, melatonin-synthesizing enzyme have been found in immune cells and endothelial cells. Interestingly, the concentrations of melatonin at night were sufficient to significantly inhibit nNOS, especially since they exceed the K_d of approximately 10 μM (Mukherjee et al., 2014; Turjanski et al., 2004)

Like TFP, melatonin also requires CaM to be Ca^{2+} before it can bind the protein.(Benitez-King, Huerto-Delgadillo, & Anton-Tay, 1993; Turjanski et al., 2004) Consequently, it also interacts with the hydrophobic patches in CaM. Furthermore, the structures obtained from NMR and molecular docking experiments show that melatonin-bound CaM resembles TFP-bound CaM. It follows, then, that the two compounds would be expected to inhibit NOS activity in a similar manner.

3.2 Methods

3.2.1 K_i determination assays

For the active site inhibitors, the inhibition assays were performed using the oxyhemoglobin capture assay as described in Section 2.2.4 with a few modifications. Prior to the addition of the heme solution to initiate the reactions (with 5 μM L-arginine), 10 μL of enzyme solution containing NOS and CaM were incubated with the appropriate inhibitor concentration for 10 minutes at room temperature. The concentration of inhibitors were varied from 10^{-5} to 1 mM. In general, the inhibitors were dissolved in water; however, 3-bromo-7-nitroindazole is insoluble in water and was thus dissolved in DMSO. For each inhibitor concentration, NOS response was measured as the rate of reaction as a percentage of the maximum rate when there is no inhibitor present. NOS response was plotted against the log concentration of inhibitors; the inhibition response curves were fitted and IC50s were obtained using GraphPad. The K_i values for each isoform and inhibitor pair were calculated using the Cheng-Prusoff equation:

$$K_i = \frac{IC50}{1 + \frac{[S]}{K_m}}$$

where [S] is the concentration of L-arginine added in solution. For CaM-binding inhibitors, the concentration of CaM was also varied (750 nM to 3 μM). To calculate the K_i values of TFP and melatonin, the same equation is used but [S] is the concentration of CaM and K_m is the dissociation constant K_d values from NOS peptide binding studies: 5.6 nM for nNOS, 1.6 for eNOS and 3.3 for iNOS (Wu, Berta, & Tsai, 2011). These NOS peptides correspond to the CaM binding peptides (Figure 1.2). Note that the human CaM binding sequences are 100% homologous with their non-human counterparts, so the same values are used for each isoform.

3.3 Results and discussion

3.3.1 Active site inhibitors

As discussed above, the L-arginine analogues L-NMMA and L-ALA do not exhibit isoform selectivity over eNOS, though previous studies have shown that they have a lower affinity towards murine iNOS.(Olken & Marletta, 1992; Reif & McCreedy, 1995; Zhang et al., 1997) Indeed, a similar trend was observed in L-NMMA inhibition studies (Figure 3.6). Furthermore, the relative affinities of human NOS towards L-NMMA agree with that of the non-human NOS: (highest to lowest affinity) eNOS > nNOS >> iNOS. However, it is worth noting that the K_i values

for human nNOS and eNOS were an order of magnitude less than rat nNOS and bovine eNOS, respectively. Meanwhile, the inhibition assays for L-ALA showed a larger difference in the order of magnitude of the K_i values for human NOS compared to non-human NOS (Figure 3.7). Such differences translate to a change in the relative affinity ranking: eNOS > nNOS >> iNOS for non-human NOS and eNOS > iNOS > nNOS for human NOS. Given that both L-NMMA and L-ALA exhibit the highest affinity towards eNOS over nNOS and iNOS, these inhibition assays agree with previous research that both compounds cannot be used clinically as NOS inhibitors.

Recall that L-NNA has been shown to be non-selective *in vitro*, though K_i values suggest that it has modest selectivity over iNOS.(Nam et al., 1998; Reif & McCreedy, 1995) The relative affinity for the non-human NOS is nNOS > eNOS ~ iNOS; human NOS, nNOS ~ eNOS > iNOS (Figure 3.8). As with L-ALA, the ranking for L-NNA is not preserved between human and non-human NOS. Of particular interest are the K_i values for human nNOS and eNOS, which are very similar within two significant digits. As such, it is an unsuitable candidate for clinical use, as previous research would suggest.

The dose-inhibition curves for 3Br7NI are very tight, which corresponds to K_i values that are not only in the same order of magnitude but are very similar (Figure 3.9). Consequently, the relative affinity for both human and non-human NOS are similar as well: nNOS ~ eNOS ~ iNOS. This suggests that 3Br7NI is not at all selective *in vitro*, agreeing with the current consensus. To verify if the tissue-dependent nNOS selectivity observed for L-NNA using mice, further tests (*in vivo* or *ex vivo*) must be performed.

As shown in Figure 3.10, 1400W shows considerable selectivity towards iNOS for both human and non-human NOS. Furthermore, the K_i values for eNOS are several orders of magnitude larger than nNOS and iNOS. As well, the relative affinity ranking for both human and non-human NOS agree with each other: iNOS >> nNOS >> eNOS, which is consistent with previously published data.(Garvey et al., 1997) However, it is worth noting that the observed values were a result of one assay run with quadruplicate samples. Hence, standard errors were not obtained and statistical analyses cannot be performed as of yet.

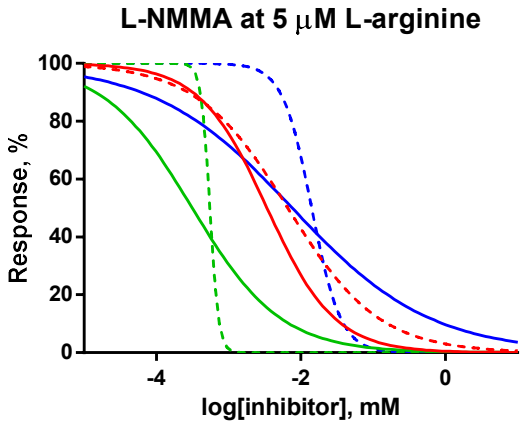

Isoform	Obs. K_i, μM	Lit. K_i, μM
HnNOS	0.79 ± 0.74	nd
RnNOS	1.3 ± 0.24	0.65[a]
HeNOS	0.074 ± 016	0.70[a]
BeNOS	0.18 ± 0.089	nd
HiNOS	4.11 ± 0.19	nd
MiNOS	4.28 ± 0.12	3.9[a]

Figure 3.6. Dose-inhibition curves for L-NMMA in the presence of 5 μM L-arginine after 10 mins of pre-incubation. Calculated K_i values for each isoform are listed on the right. [a]K_i values obtained from (Reif & McCreedy, 1995). nd stands for no data.

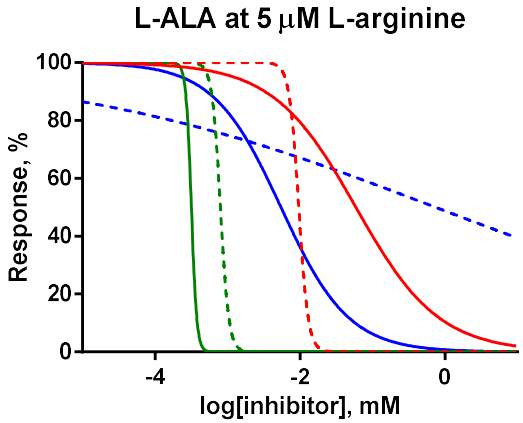

Isoform	Obs. K_i, μM	Lit. K_i, μM
HnNOS	13 ± 0.11	nd
RnNOS	1.9 ± 0.025	0.47[a]
HeNOS	0.075 ± 0.19	nd
BeNOS	0.26 ± 0.013	nd
HiNOS	3.0 ± 0.10	nd
MiNOS	240 ± 0.14	3.4[b]

Figure 3.7. Dose-inhibition curves for L-ALA in the presence of 5 μM L-arginine after 10 mins of pre-incubation. Calculated K_i values for each isoform are listed on the right. [b]K_i from (Zhang et al., 1997). [c]K_i from (Olken & Marletta, 1992). nd stands for no data.

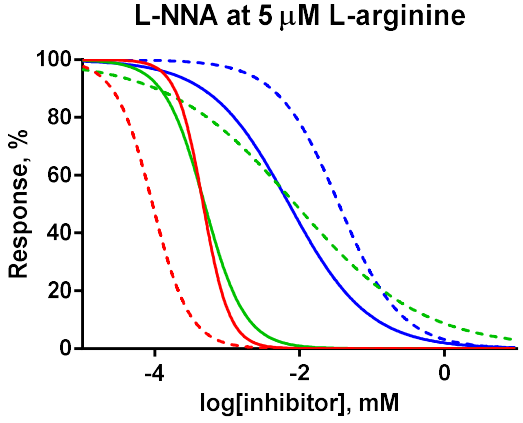

Isoform	Obs. K_i, μM	Lit. K_i, μM
HnNOS	0.11 ± 0.11	nd
RnNOS	0.018 ± 0.036	0.09[a]
HeNOS	0.11 ± 0.14	0.02[a]
BeNOS	2.9 ± 0.21	1.5[b]
HiNOS	3.9 ± 0.17	nd
MiNOS	11 ± 0.12	8.1[a]

Figure 3.8. Dose-inhibition curves for L-NNA in the presence of 5 μM L-arginine after 10 mins of pre-incubation. Calculated K_i values for each isoform are listed on the right. [a]K_i values from Reif and

McCreedy (1995).(Reif & McCreedy, 1995) [b]K_i values from Nam et al. (1998).(Nam et al., 1998) nd stands for no data.

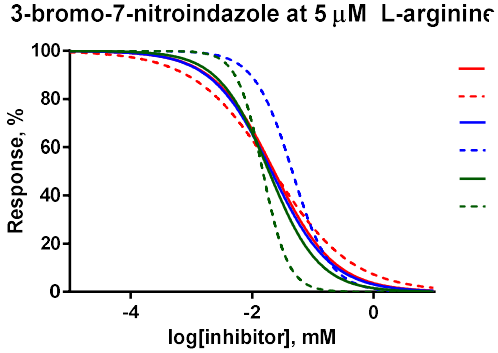

Isoform	Obs. K_i, µM	Obs. IC50, µM	Lit. IC50, µM
HnNOS	5.4 ± 0.23	0.023	nd
RnNOS	4.4 ± 0.10	0.022	0.17[a]
HeNOS	4.9 ± 0.14	0.021	nd
BeNOS	15 ± 0.13	0.046	0.86[a]
HiNOS	10 ± 0.31	0.019	nd
MiNOS	4.6 ± 031	0.015	0.29[a]

Figure 3.9. Dose-inhbition curves for 3-bromo-7-nitroindazole in the presence of 5 µM L-arginine after 10 mins of pre-incubation. Calculated K_i and IC50 values for each isoform are listed on the right.[a]K_i values are not available so IC50s from (Bland-Ward & Moore, 1995) are listed. nd stands for no data.

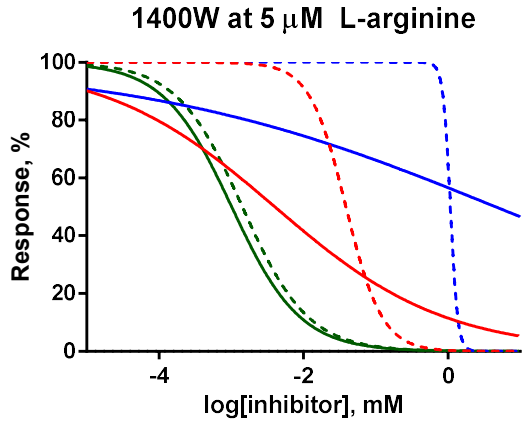

Isoform	Obs. K_i, µM	Lit. K_i, µM
HnNOS	13 ± 0.49	2.0[a]
RnNOS	7.6 ± 0.26	nd
HeNOS	1100 ± 0.017	50[a]
BeNOS	350 ± 0.27	nd
HiNOS	0.55 ± 0.15	0.5[a]
MiNOS	0.43 ± 0.44	nd

Figure 3.10. Dose-inhibition curves for 1400W in the presence of 5 µM L-arginine after 10 mins of pre-incubation. Calculated K_i values for each isoform are listed on the right. [a]K_i values from (Garvey et al., 1997). nd stands for no data.

3.3.2 CaM-binding inhibitors

The CaM-binding inhibitors require Ca^{2+}-occupied EF hands; the inhibition assays were performed under saturated Ca^{2+} concentrations, while varying the concentration of the inhibitors. Figure 3.11 shows the dose-inhibition curves for TFP at a constant L-arginine concentration of 5 µM. Because the curves exhibit a sigmoidal decay characteristic of inhibitors and because it is known that TFP does not bind the NOS active site, it can be said that TFP acts as an allosteric inhibitor of NOS. The calculated IC50 values are all within the same order of magnitude for both human and non-human NOS. For all NOS, the inhibition effect can only be observed at higher concentrations of TFP. Recall that Lee and Stull reported that it takes 200 µM to 1 mM of TFP to

inhibit NOS activity. Furthermore, there is no observed isoform selectivity.(S. Lee & Stull, 1998) Indeed, iNOS are also inhibited at similar concentrations, albeit at the higher end of the range.This result is expected since TFP binds the CaM molecule itself and not the NOS isoform. It is worth noting, however, that these experiments were performed in excess CaM and Ca^{2+} so the effect of TFP may be masked.

To further assess NOS inhibition by TFP, CaM concentrations were varied for nNOS and eNOS. (Recall that iNOS are co-expressed with CaM and so varying [CaM] is not possible for this isoform.) Figure 3.12a shows the dose-inhibition curves of human and non-human nNOS at varying CaM concentrations. In general, the inhibition curves at lower CaM concentrations are shifted to the right, implying an increase in IC50. Meanwhile, the inhibition curves for eNOS exhibit an opposite trend (Figure 3.12b). At lower CaM concentrations, the inhibition curves are shifted to the left, i.e. the IC50s decreased. At this point, however, the effect of CaM is not conclusive; inhibition curves at lower CaM concentrations need to be obtained as well. Further, the effect of Ca^{2+}, especially at physiological conditions (225 nM), will have to be assessed.

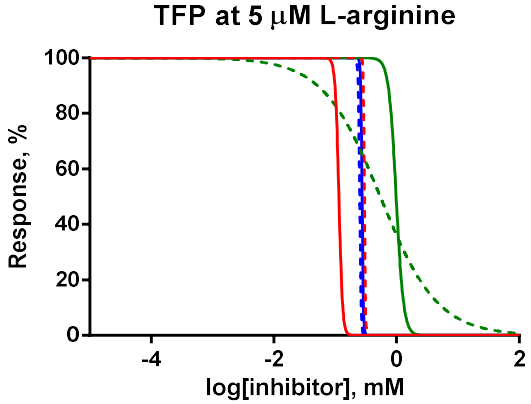

Isoform	Obs. IC50, μM	Obs. K_i, μM
HnNOS	0.12	0.075
RnNOS	0.30	0.19
HeNOS	0.27	0.095
BeNOS	0.25	0.087
HiNOS	0.98	0.52
MiNOS	0.54	0.28

Figure 3.11. Dose-inhibition curves for TFP in the presence of 5 μM L-arginine after 10 mins of pre-incubation. Calculated IC50s and K_i values for each isoform are listed on the right.

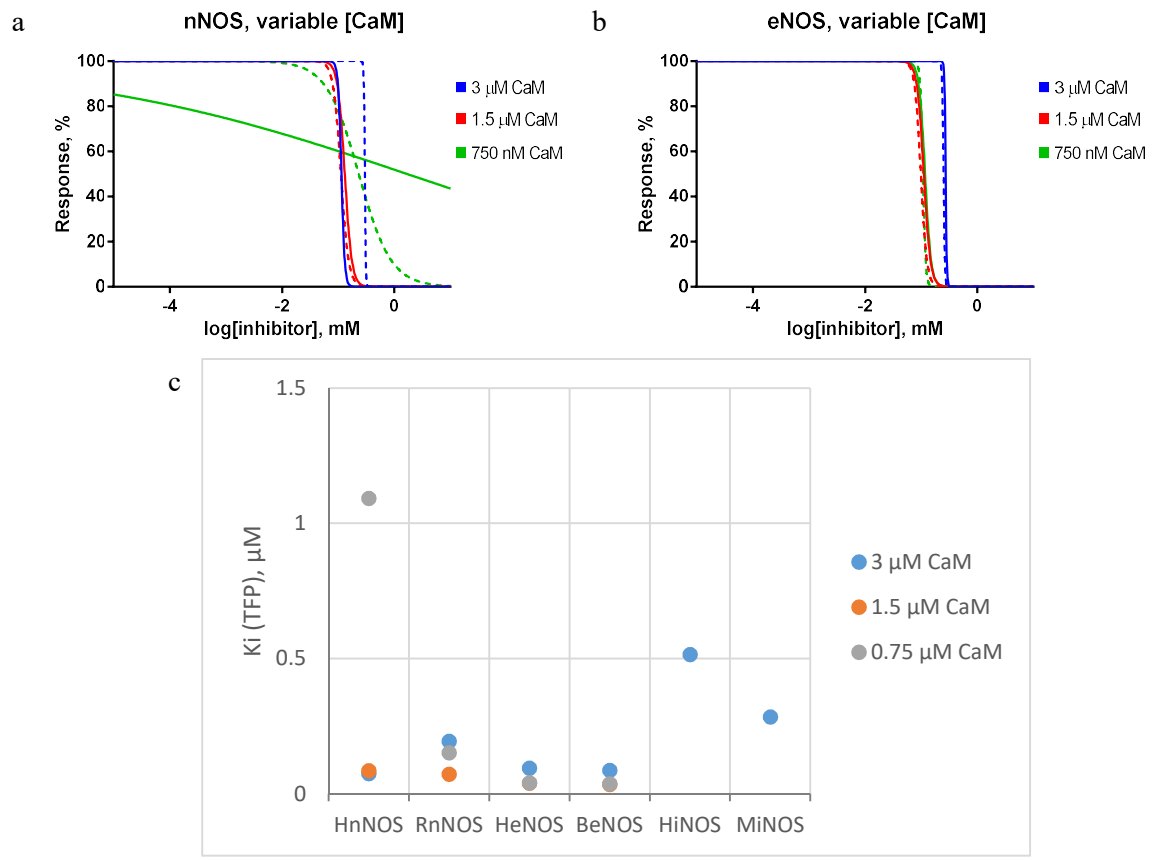

Figure 3.12. Dose-inhibition curves of (a) nNOS and (b) eNOS for TFP at varying CaM concentrations (750 nM to 3 µM CaM). Solid lines refer to human cNOS and dotted lines refer to non-human cNOS. (c) K_i values of TFP for each NOS isoform.

The effect of incubation time on TFP inhibition of NOS was also assessed, by adding TFP directly into the NOS enzyme solution before preincubation with CaM. (Note that the NOS enzyme solution needs to be preincubated with CaM to ensure that NOS is bound to CaM). It was observed that the addition of TFP in the absence of CaM causes precipitates to form; the clear yellow NOS enzyme solution, which contains the flavin cofactors, turned opaque when TFP was added. However, there was no NOS activity observed upon the addition of L-arginine to initiate the reaction. Attempts to optimize the incubation time assays are under way, including preincubating the TFP in the CaM solution instead of the NOS solution. The ratio of [NOS enzyme] to [CaM] and the ratio of [CaM] to [TFP] will also be assessed.

Meanwhile, the CaM-binding inhibitor melatonin showed no inhibitory effect under conditions used for active site inhibitors. Figure 3.13 shows that there is no apparent inhibition by melatonin for all NOS. However, it must be noted that here, melatonin was added after the incubation of NOS with CaM in the enzyme solution such that the NOS-CaM complex was already

formed when melatonin was added. The results shown here agree with the fact that melatonin can only bind Ca^{2+}-bound CaM but not apoCaM or CaM in complex with NOS. To circumvent this, melatonin was added to the NOS enzyme solution at the same time as CaM. However, as with TFP, precipitates formed and no NOS activity was observed.

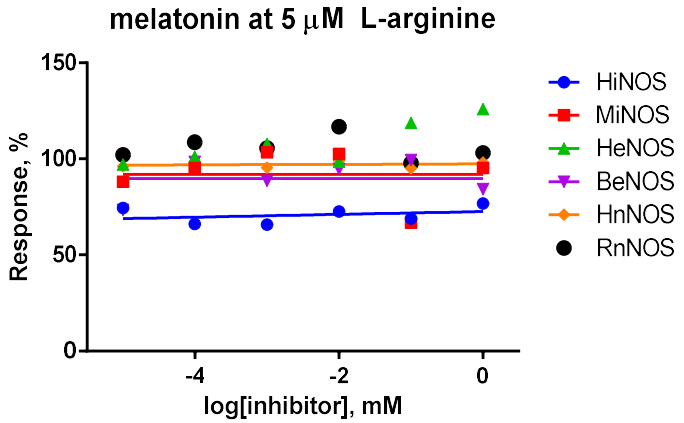

Figure 3.13. Dose-inhibition curves for melatonin in the presence of 5 μM L-arginine after 10 mins of preincubation.

3.4 Conclusions

As Boer et al. report, the selectivity of NOS inhibitors can be evaluated by taking the ratio of K_i values.(Boer et al., 2000) Table 3.1 summarizes the observed selectivity (or non-selectivity) for active site inhibitors discussed above. Since these ratios are calculated with eNOS K_i values as denominators, the most selective inhibitor must have small non-zero values. Indeed, as mentioned above, 1400W exhibits selectivity toward iNOS (and nNOS) over eNOS for both human and non-human NOS. In general, none of the other inhibitors (except L-NNA for non-human NOS) exhibited selectivity according to this metric. In fact, most ratios give large numbers, suggesting low K_i values or high affinity for eNOS. These results mean that these inhibitors cannot be used clinically due to off-target inhibition of eNOS. It is also worth noting that there exist differences in these ratios between human and non-human NOS, suggesting that the relative selectivity vary between them as well. Indeed, this was discussed previously with regard to the affinity rankings. These observations then lend validity to our earlier claim that the structural differences in human and non-human NOS lead to differences in the isoform selectivity of early active site inhibitors. However, these findings need to be further verified by performing more assay runs to obtain sample means for statistical analyses of these apparent differences in inhibitor selectivity.

Table 3.1. Ratio of observed Ki values for active site inhibitors.

	human		**non-human**	
	n/e	**i/e**	**n/e**	**i/e**
L-NMMA	11	56	7.2	24
L-ALA	180	40	7.2	870
L-NNA	0.95	34	0.006*	3.7
3Br7NI	1.1	2.1	0.29*	0.31*
1400W	0.012*	0.001*	0.022*	0.001*

*These values infer selectivity.

Meanwhile, the preliminary experiments with CaM-binding inhibitors TFP and melatonin show that these do not exhibit isoform-selectivity as expected. Further experiments featuring changes in CaM and Ca^{2+} concentrations, as well as variable incubation times, are to be performed to gain insight in the differences (if any) between human and non-human NOS.

Chapter 4

4. Summary and future work

Chapter 2 describes the development of heterologous expression systems for human constitutive NOS holoenzymes. Human nNOS and eNOS sequences were successfully cloned and expressed in *E. coli*. The purification of these human NOS were similar to that of non-human NOS in the lab. However, the yield was lower than that of non-human NOS. In any case, assessment of the active site heme via UV-Vis and activity assays via oxyhemoglobin capture have produced expected results. In particular, the Michaelis-Menten constants K_m that were determined for each NOS isoform is consistent with previously published values. However, it is worth noting that the purified NOS proteins are not "clean," i.e. the sample contains other unwanted proteins as evidenced by the extra bands in the SDS-PAGE gels. Consequently, other assays that could corroborate the calculated K_m values such as the binding assay isothermal calorimetry could not be performed using the aforementioned protein samples. Hence, it would be beneficial to improve expression and purification protocols to ensure qualitatively and quantitatively better yields for the human NOS holoenzymes. For example, assays to optimize the storage buffer components may be performed. Note that the proteins were purified and stored in a monovalent buffer Tris, but perhaps using HEPES and MOPS would be appropriate. Certainly a good expression system would encourage the use human NOS instead of the more convenient rat nNOS and bovine eNOS.

Chapter 3 describes whether there is a difference in the isoform selectivity of NOS inhibitors between human and non-human NOS. Preliminary experiments showed that the relative affinities of the active site inhibitors, as given by the ratios of K_i values per isoform, mostly differ between human and non-human NOS, with the exception of 1400W. Unlike the others, 1400W showed significant selectivity towards iNOS for both human and non-human NOS, as described in previously published studies. It is worth noting, of course, that these inhibition assays are merely the first step in determining the differences in the interactions of inhibitors with human NOS versus their non-human counterparts. Structural studies such as x-ray crystallography and molecular docking simulations are necessary in pinpointing which specific structural features differ between human and non-human NOS when bound to these inhibitors.

CaM-binding inhibitors were also examined to determine if there is a difference in human and non-human NOS. The results of these assays would provide insight in the activation of NOS by CaM. In addition to the planned assays where CaM and calcium concentrations are to be varied,

experiments where incubation time with these inhibitors could be performed to determine whether human and non-human NOS are affected by these factors similarly. Furthermore, assays that monitor the electron transfer activity within the NOS enzymes can be performed.

Letter of Copyright Permission

License Details

This Agreement between Miss. Danica Estavillo ("You") and John Wiley and Sons ("John Wiley and Sons") consists of your license details and the terms and conditions provided by John Wiley and Sons and Copyright Clearance Center.

License Number	4243701107892
License date	Dec 07, 2017
Licensed Content Publisher	John Wiley and Sons
Licensed Content Publication	FEBS Journal
Licensed Content Title	Towards the free energy landscape for catalysis in mammalian nitric oxide synthases
Licensed Content Author	Nicole G. H. Leferink,Sam Hay,Stephen E. J. Rigby,Nigel S. Scrutton
Licensed Content Date	Dec 26, 2014
Licensed Content Pages	14
Type of Use	Dissertation/Thesis
Requestor type	University/Academic
Format	Print and electronic
Portion	Figure/table
Number of figures/tables	1
Original Wiley figure/table number(s)	Figure 6
Will you be translating?	No
Title of your thesis / dissertation	In vitro studies of enzymatic activities of human nitric oxide synthase isoforms
Expected completion date	Dec 2017
Expected size (number of pages)	100
Requestor Location	Miss. Danica Estavillo 50 Rosewood Avenue Guelph, ON N1H 6A1 Canada Attn: Miss. Danica Estavillo
Publisher Tax ID	EU826007151
Billing Type	Invoice
Billing address	Miss. Danica Estavillo 50 Rosewood Avenue Guelph, ON N1H 6A1 Canada Attn: Miss. Danica Estavillo
Total	**0.00 CAD**

License Details

This Agreement between Miss. Danica Estavillo ("You") and Nature Publishing Group ("Nature Publishing Group") consists of your license details and the terms and conditions provided by Nature Publishing Group and Copyright Clearance Center.

License Number	4184020529360
License date	Sep 08, 2017
Licensed Content Publisher	Nature Publishing Group
Licensed Content Publication	Nature Chemical Biology
Licensed Content Title	Anchored plasticity opens doors for selective inhibitor design in nitric oxide synthase
Licensed Content Author	Elsa D Garcin, Andrew S Arvai, Robin J Rosenfeld, Matt D Kroeger, Brian R Crane et al.
Licensed Content Date	Oct 12, 2008
Licensed Content Volume	4
Licensed Content Issue	11
Type of Use	reuse in a dissertation / thesis
Requestor type	academic/educational
Format	print and electronic
Portion	figures/tables/illustrations
Number of figures/tables/illustrations	1
High-res required	no
Figures	Supplementary Figure 4
Author of this NPG article	no
Your reference number	
Title of your thesis / dissertation	In vitro studies of enzymatic activities of human nitric oxide synthase isoforms
Expected completion date	Dec 2017
Estimated size (number of pages)	100
Requestor Location	Miss. Danica Estavillo 50 Rosewood Avenue Guelph, ON N1H 6A1 Canada Attn: Miss. Danica Estavillo
Billing Type	Invoice
Billing address	Miss. Danica Estavillo 50 Rosewood Avenue Guelph, ON N1H 6A1 Canada Attn: Miss. Danica Estavillo
Total	**0.00 CAD**

License Details

This Agreement between Miss. Danica Estavillo ("You") and Elsevier ("Elsevier") consists of your license details and the terms and conditions provided by Elsevier and Copyright Clearance Center.

License Number	4182551113278
License date	Sep 05, 2017
Licensed Content Publisher	Elsevier
Licensed Content Publication	Nitric Oxide
Licensed Content Title	NO synthase: Structures and mechanisms
Licensed Content Author	Simon Daff
Licensed Content Date	Aug 1, 2010
Licensed Content Volume	23
Licensed Content Issue	1
Licensed Content Pages	11
Type of Use	reuse in a thesis/dissertation
Portion	figures/tables/illustrations
Number of figures/tables/illustrations	1
Format	both print and electronic
Are you the author of this Elsevier article?	No
Will you be translating?	No
Original figure numbers	Figure 2
Title of your thesis/dissertation	In vitro studies of enzymatic activities of human nitric oxide synthase isoforms
Expected completion date	Dec 2017
Estimated size (number of pages)	100
Requestor Location	Miss. Danica Estavillo 50 Rosewood Avenue Guelph, ON N1H 6A1 Canada Attn: Miss. Danica Estavillo
Total	**0.00 CAD**

References

Acuña, D., Germaine, C., Carmen, E., Díaz, M. E., Elena, C., Cabello, L., … Reiter, R. J. (2014). Extrapineal melatonin: sources, regulation, and potential functions. *Cellular and Molecular Life Sciences*, *71*, 2997–3025. http://doi.org/10.1007/s00018-014-1579-2

Alderton, W. K., Cooper, C. E., & Knowles, R. G. (2001). Nitric oxide synthases : structure , function and inhibition. *Biochemistry Journal*, *615*, 593–615.

Baek, K. J., Thiel, B. A., Lucas, S., & Stuehr, D. J. (1993). Macrophage nitric oxide synthase subunits. Purification, characterization, and role of prosthetic groups and substrate in regulating their association into a dimeric enzyme. *Journal of Biological Chemistry*, *268*, 21120–21129.

Benitez-King, G., Huerto-Delgadillo, L., & Anton-Tay, F. (1993). Binding of [3]H-melatonin to calmodulin. *Life Sciences*, *53*(101), 201–207.

Bland-Ward, P. A., & Moore, P. K. (1995). 7-Nitro Indazole Derivatives are Potent Inhibitors of Brain, Endothelium and Inducible Isoforms of Nitric Oxide Synthase. *Life Sciences*, *57*(11), 131–135.

Boer, R., Udiger, W., Klein, T., Mirau, B., Haas, S., & Baur, I. (2000). The Inhibitory Potency and Selectivity of Arginine Substrate Site Nitric-Oxide Synthase Inhibitors Is Solely Determined by Their Affinity toward the Different Isoenzymes. *Molecular Pharmacology*, *58*(5), 1026–1034.

Bredt, D. S., & Snyder, S. H. (1990). Isolation of nitric oxide synthetase, a calmodulin-requiring enzyme. *Proceedings of the National Academy of Sciences of the United States of America*, *87*, 682–685.

Bretscher, L. E., Li, H., Poulos, T. L., & Griffith, O. W. (2003). Structural Characterization and Kinetics of Nitric-oxide Synthase Inhibition by Novel N5-(Iminoalkyl)- and N5-(Iminoalkenyl)-ornithines. *Journal of Biological Chemistry*, *278*(47), 46789–46797. http://doi.org/10.1074/jbc.M306787200

Brunel, A., Lang, J., Couture, M., Boucher, J., Dorlet, P., & Santolini, J. (2016). Oxygen activation in NO synthases : evidence for a direct role of the substrate. *FEBS Open Bio*, *6*, 386–397. http://doi.org/10.1002/2211-5463.12036

Campbell, M. G., Smith, B. C., Potter, C. S., Carragher, B., & Marletta, M. A. (2014). Molecular architecture of mammalian nitric oxide synthases. *Proceedings of the National Academy of Sciences*, E3614–E3623. http://doi.org/10.1073/pnas.1413763111

Cinelli, M. A., Li, H., Pensa, A. V., Kang, S., Roman, L. J., Martásek, P., … Silverman, R. B. (2015). Phenyl Ether- and Aniline-Containing 2-Aminoquinolines as Potent and Selective Inhibitors of Neuronal Nitric Oxide Synthase. *Journal of Medicinal Chemistry*, *58*(21), 8694–8712. http://doi.org/10.1021/acs.jmedchem.5b01330

Cinelli, M. a, Li, H., Chreifi, G., Martásek, P., Roman, L. J., Poulos, T. L., & Silverman, R. B. (2014). Simplified 2-Aminoquinoline-Based Scaffold for Potent and Selective Neuronal Nitric Oxide Synthase Inhibition. *Journal of Medicinal Chemistry*, *57*(4), 1513–1530. http://doi.org/10.1021/jm401838x

Curtin, A. M., Kinsella, G. K., & Stephens, J. C. (2015). Computational Development of Selective nNOS Inhibitors: Binding Modes and Pharmacokinetic Considerations. *CURRENT MEDICINAL CHEMISTRY*, *22*(21), 2558–2579.

Demady, D. R., Jianmongkol, S., Vuletich, J. L., Bender, A. T., & Osawa, Y. (2001). Agmatine enhances the NADPH oxidase activity of neuronal NO synthase and leads to oxidative inactivation of the enzyme. *Molecular Pharmacology*, *59*, 24–29.

Eliasson, M. J., Blackshaw, S., Schell, M. J., & Snyder, S. H. (1997). Neuronal nitric oxide synthase alternatively spliced forms: prominent functional localizations in the brain. *Proceedings of the National Academy of Sciences of the United States of America*, *94*(7), 3396–401. http://doi.org/10.1073/pnas.94.7.3396

Faeder, E. J., & Siegel, L. M. (1973). A Rapid Micromethod for Determination of FMN and FAD in Mixtures. *Analytical*, *53*, 332–336.

Fan, B., Stuehr, D. J., & Rousseau, D. L. (2009). Role of substrate functional groups in binding to nitric oxide synthase. *Biochemical and Biophysical Research Communications*, *382*(1), 21–25. http://doi.org/10.1016/j.bbrc.2009.02.084

Fang, J., Haitao, J., Lawton, G. R., Xue, F., Roman, L. J., & Silverman, R. B. (2009). L337H Mutant of Rat Neuronal Nitric Oxide Synthase Resembles Human Neuronal Nitric Oxide Synthase toward Inhibitors. *Journal of Medicinal Chemistry2*, *54*(14), 4533–4537.

Fedorov, R., Hartmann, E., Ghosh, D. K., Schlichting, I., & Carolina, N. (2003). Structural Basis for the Specificity of the Nitric-oxide Synthase Inhibitors W1400 and N(G)-Propyl-L-Arg for the Inducible and Neuronal Isoforms. *The Journal of Biological Chemistry*, *278*(46), 45818–45825. http://doi.org/10.1074/jbc.M306030200

Fischmann, T. O., Hruza, a, Niu, X. D., Fossetta, J. D., Lunn, C. a, Dolphin, E., … Weber, P. C. (1999). Structural characterization of nitric oxide synthase isoforms reveals striking active-site conservation. *Nature Structural Biology*, *6*(3), 233–242. http://doi.org/10.1038/6675

Fleming, I., & Busse, R. (2003). Molecular mechanisms involved in the regulation of the endothelial nitric oxide synthase. *Am. J. Physiol. Regul. Integr Comp Physiol*, *284*, R1–R12.

Furfine, E. S., Harmon, M. F., Faith, J. E., & Garvey, E. P. (1993). Selective Inhibition of Constitutive Nitric Oxide Synthase by L-N(G)-Nitroarginine. *Biochemistry*, *32*, 8512–8517. http://doi.org/10.1021/bi00084a017

Garcin, E. D., Arvai, A. S., Rosenfeld, R. J., Kroeger, M. D., Brian, R., Andersson, G., … Getzoff, E. D. (2008). Anchored plasticity opens doors for selective inhibitor design in nitric oxide synthase. *Nat Chem Biol.*, *4*(11), 700–707. http://doi.org/10.1038/nchembio.115.Anchored

Garvey, E. P., Furfine, E. S., & Sherman, P. A. (1996). Purification and Inhibitor Screening of Human Nitric Oxide Synthase Isozymes. *Methods in Enzymology*, *268*, 339–349.

Garvey, E. P., Oplinger, J. A., Furfine, E. S., Kiff, R. J., Laszlo, F., Whittle, B. J. R., & Knowles, R. G. (1997). 1400W Is a Slow, Tight Binding, and Highly Selective Inhibitor of Inducible Nitric-oxide Synthase in Vitro and in Vivo. *The Journal of Biological Chemistry*, *272*(8), 4959–4963.

Gerber, N. C., Nishida, C. R., & de Montellano, P. R. O. (1997). Characterization of human liver inducible nitric oxide synthase expressed in Escherichia coli. *Archives of Biochemistry and Biophysics*, *343*, 249–253.

Ghosh, D. K., & Stuehr, D. J. (1995). Macrophage NO synthase: characterization of isolated oxygenase and reductase domains reveals a head-to-head subunit interaction. *Biochemistry*, *34*, 801–807.

Golser, R., Gorren, A. C., Mayer, B., & Schmidt, K. (2003). Functional characterization of Glu298Asp mutant human endothelial nitric oxide synthase purified from a yeast expression system. *Nitric Oxide*, *8*, 7–14.

Green, S. J., Scheller, L. F., Marletta, M. A., Seguin, M. C., Klotz, F. W., Slayter, M., … Nacy, C. A. (1994). Nitric oxide: Cytokine-regulation of nitric oxide in host resistance to intracellular pathogens. *Immunology Letters*, *43*(1–2), 87–94. http://doi.org/10.1016/0165-2478(94)00158-8

Gross, S. S., Stuehrt, D. J., Jaffet, E. A., & Griffitho, O. W. (1990). Macrophage and Endothelial Cell Nitric Oxide Synthesis: Cell-Type Selective Inhibition by N(G)-aminoarginine, N(G)-nitroarginine and N(G)-methylarginine. *Biochemical and Biophysical Research Communications*, *170*(1), 96–103.

Haque, M. M., Ray, S. S., & Stuehr, D. J. (2016). Phosphorylation Controls Endothelial Nitric-oxide Synthase by Regulating Its Conformational Dynamics. *The Journal of Biological Chemistry*, *291*(44), 23047–23057. http://doi.org/10.1074/jbc.M116.737361

Hevel, J. M., & Marletta, M. A. (1992). Macrophage nitric oxide synthase: relationship between enzyme-bound tetrahydrobiopterin and synthase activity. *Biochemistry*, *31*, 7160–7165.

Hevel, J. M., & Marletta, M. A. (1994). [25] Nitric-oxide synthase assays. In *Methods in Enzymology* (Vol. 233, pp. 250–258). Elsevier. http://doi.org/10.1016/S0076-6879(94)33028-X

Hiki, K., Hattori, R., Kawai, C., & Yui, Y. (1992). Purification of insoluble nitric oxide synthase from rat cerebellum. *Journal of Biochemistry*, *111*, 556–558.

Hopper, R. A., & Garthwaite, J. (2006). Tonic and Phasic Nitric Oxide Signals in Hippocampal Long-Term Potentiation. *Journal of Neuroscience*, *26*(45), 11513–11521. http://doi.org/10.1523/JNEUROSCI.2259-06.2006

Huang, H., Ji, H., Li, H., Jing, Q., Labby, K. J., Martasek, P., … Silverman, R. B. (2012). Selective monocationic inhibitors of neuronal nitric oxide synthase. Binding mode insights from molecular dynamics simulations. *J Am Chem Soc*, *134*(28), 11559–11572. http://doi.org/10.1021/ja302269r

Joubert, J., & Malan, S. F. (2011). Novel nitric oxide synthase inhibitors: a patent review. *Expert Opinion on Therapeutic Patents*, *21*(4), 537–60. http://doi.org/10.1517/13543776.2011.556619

Kellogg, D., Zhao, J., Coey, U., & Green, J. (2005). Acetylcholine-induced vasodilation is mediated by nitric oxide and prostaglandins in human skin. *J. Appl. Physiol.*, *78229*, 629–632.

Koevesi, I., Menyhard, D. K., Laberge, M., & Fidy, J. (2008). Interaction of Antagonists with Calmodulin: Insights from Molecular Dynamics Simulations. *Journal of Med*, *51*, 3081–3093.

Lang, J., Santolini, J., & Couture, M. (2011). The Conserved Trp − Cys Hydrogen Bond Dampens the "Push Effect" of the Heme Cysteinate Proximal Ligand during the First Catalytic Cycle of Nitric Oxide Synthase. *Biochemistry*, *50*, 10069–10081.

Leber, A., Hemmens, B., Klosch, B., Goessler, W., Raber, G., & Schmidt, K. (1999). Characterization of recombinant human endothelial nitric-oxide synthase purified from the yeast Pichia pastoris. *Journal of Biological Chemistry*, *274*, 37658–37664.

Lee, C. (Erica). (2015). *Development of Expression Systems for Various Forms of Human Nitric Oxide Synthase Isozymes*.

Lee, S., & Stull, J. T. (1998). Calmodulin-dependent Regulation of Inducible and Neuronal Nitric-oxide Synthase. *The Journal of Biological Chemistry*, *273*(42), 27430–27437.

Leferink, N. G. H., Hay, S., Rigby, S. E. J., & Scrutton, N. S. (2014). Towards the free energy landscape for catalysis in mammalian nitric oxide synthases. *FEBS Journal*, *282*, 3016–3029. http://doi.org/10.1111/febs.13171

Li, H., Jamal, J., Plaza, C., Hai Pineda, S., Chreifi, G., Jing, Q., … Poulos, T. L. (2014). Structures of human constitutive nitric oxide synthases. *Acta Crystallographica Section D*, *D70*, 2667–2674. http://doi.org/10.1107/S1399004714017064

Li, H., Raman, C. S., Marta, P., Masters, B. S. S., & Poulos, T. L. (2001). Crystallographic Studies on Endothelial Nitric Oxide Synthase Complexed with Nitric Oxide and Mechanism-Based Inhibitors. *Biochemistry*, *40*(1), 5399–5406. http://doi.org/10.1021/bi002658v

Maddaford, S. P. (2012). A Medicinal Chemistry Perspective on Structure-Bases Drug Design and Development. In L. W. Tari (Ed.), *Methods in Molecular Biology* (pp. 351–381).

Mata, R., Figueroa, M., Gonzalez-Andrade, M., Rivera-Chavez, J. A., Abraham, M.-M., & Del Valle, P. (2015). Calmodulin Inhibitors from Natural Sources: An Update. *Journal of Natural Products*, *78*, 576–586. http://doi.org/10.1021/np500954x

Montgomery, H. J., Dupont, A. L., Leivo, H. E., & Guillemette, J. G. (2010). Cloning, Expression, and Purification of a Nitric Oxide Synthase-Like Protein from Bacillus cereus. *Biochemistry Research International*, *2010*, 489892. http://doi.org/10.1155/2010/489892

Montgomery, H. J., Romanov, V., & Guillemette, J. G. (2000). Removal of a Putative Inhibitory Element Reduces the Calcium-dependent Calmodulin Activation of Neuronal Nitric-oxide Synthase *. *The Journal of Biological Chemistry*, *275*(7), 5052–5058.

Mukherjee, P., Cinelli, M. A., Kang, S., & Silverman, R. B. (2014). Development of nitric oxide synthase inhibitors for neurodegeneration and neuropathic pain. *Chemical Society Reviews*, *43*(19), 6814–38. http://doi.org/10.1039/c3cs60467e

Nam, S. W., Seo, D. W., Sung, D. S., Han, J. W., I, S. Y. H., & Lee, H. W. (1998). Nitric Oxide Synthase from Bovine Pancreas: Purification and Characterization. *Archives of*

Pharmacological Research, *21*(2), 128–134.

Ohshima, H., Oguchi, S., Adachi, H., Iida, S., Suzuki, H., Sugimura, T., & Esumi, H. (1992). Purification of nitric oxide synthase from bovine brain: immunological characterization and tissue distribution. *Biochemical and Biophysical Research Communications*, *183*, 238–244.

Okamoto, T., Khan, S., Oyama, K., Fujii, S., Sawa, T., & Akaike, T. (2010). A new paradigm for antimicrobial host defense mediated by a nitrated cyclic nucleotide. *J Clin Biochem Nutr*, *46*(1), 14–19. http://doi.org/10.3164/jcbn.SR09-70

Olken, N., & Marletta, M. A. (1992). NG-Allyl- and NG-Cyclopropyl-L-arginine: Two Novel Inhibitors of Macrophage Nitric Oxide Synthase. *Journal of Medicinal Chemistry*, *35*(6), 1137–1144. http://doi.org/10.1021/jm00084a020

Palmer, R. M. J., Ashton, D. S., & Moncada, S. (1988). Vascular endothelial cells synthesize nitric oxide from L-arginine. *Nature*, *333*, 664–666.

Perdicakis, B., Montgomery, H. J., Guillemette, J. G., & Jervis, E. (2004). Validation and characterization of uninhibited enzyme kinetics performed in multiwell plates. *Analytical Biochemistry*, *332*(1), 122–136. http://doi.org/10.1016/j.ab.2004.04.023

Piazza, M., Guillemette, J. G., & Dieckmann, T. (2015). Dynamics of Nitric Oxide Synthase − Calmodulin Interactions at Physiological Calcium Concentrations. *Biochemistry*, *54*(1989–2000). http://doi.org/10.1021/bi501353s

Poulos, T. L., & Li, H. (2012). Structural Basis for Isoform-Selective Inhibition in Nitric Oxide Synthase. *Accounts of Chemical Research*, *XXX*(Xx). http://doi.org/10.1021/ar300175n

Presta, A., Liu, J., Sessa, W. C., & Stuehr, D. J. (1997). Substrate binding and calmodulin binding to endothelial nitric oxide synthase coregulate its enzymic activity. *Nitric Oxide*, *1*, 74–87.

Raman, C. S., Li, H., Marta, P., Southan, G., Masters, B. S. S., & Poulos, T. L. (2001). Crystal Structure of Nitric Oxide Synthase Bound to Nitro Indazole Reveals a Novel Inactivation Mechanism. *Biochemistry*, *40*, 13448–13455. http://doi.org/10.1021/bi010957u

Ramasamy, S., Haque, M. M., & Gangoda, M. (2016). Tetrahydrobiopterin redox cycling in nitric oxide synthase : evidence supports a through-heme electron delivery. *FEBS Journal*, *283*, 4491–4501. http://doi.org/10.1111/febs.13933

Reif, D. W., & McCreedy, S. A. (1995). N-Nitro-L-arginine and N-Monomethyl-L-arginine Exhibit a Different Pattern of Inactivation toward the Three Nitric Oxide Synthases. *Archives of Biochemistry and Biophysics*, *320*(1), 170–176.

Roman, L. J., Marta, P., Sue, B., Masters, S., & Domain, B. A. (2002). Intrinsic and Extrinsic Modulation of Nitric Oxide Synthase Activity. *Chem. Rev.*, *102*, 1179–1189. http://doi.org/10.1021/cr000661e

Roman, L. J., Sheta, E. A., Martasek, P., Gross, S. S., Liu, Q., & Masters, B. S. S. (1995). High-level expression of functional rat neuronal nitric oxide synthase in Escherichia coli. *Proceedings of the National Academy of Sciences*, *92*(August), 8428–8432. http://doi.org/10.1073/pnas.92.18.8428

Rosenfeld, R. J., Garcin, E. D., Panda, K., Andersson, G., Åberg, A., Wallace, A. V, … Getzoff, E. D. (2002). Conformational Changes in Nitric Oxide Synthases Induced by Chlorzoxazone and Nitroindazoles: Crystallographic and Computational Analyses of Inhibitor Potency. *Biochemistry*, *41*, 13915–13925. http://doi.org/10.1021/bi026313j

Rousseau, D. L., Li, D., Couture, M., & Yeh, S. R. (2005). Ligand-protein interactions in nitric oxide synthase. *Journal of Inorganic Biochemistry*, *99*(1), 306–332. http://doi.org/10.1016/j.jinorgbio.2004.11.007

Rusche, K. M., Spiering, M. M., & Marletta, M. A. (1998). Reactions catalyzed by tetrahydrobiopterin-free nitric oxide synthase. *Biochemistry*, *37*, 15503–15512.

Santolini, J. (2011). The molecular mechanism of mammalian NO-synthases: A story of electrons and protons. *Journal of Inorganic Biochemistry*, *105*(2), 127–141. http://doi.org/10.1016/j.jinorgbio.2010.10.011

Schmidt, H. H. H. W., Smith, R. M., Nakane, M., & Murad, F. (1992). Ca2+/calmodulin-dependent NO synthase type I: a biopteroflavoprotein with Ca2+/calmodulin-independent diaphorase and reductase activities. *Biochemistry*, *31*, 3243–3249.

Stuehr, D. J., Cho, H. J., Kwon, N. S., Weise, M. F., & Nathan, C. F. (1991). Purification and characterization of the cytokine-induced macrophage nitric oxide synthase: an FAD- and FMN-containing flavoprotein. *Proceedings of the National Academy of Sciences of the United States of America*, *88*, 7773–7777.

Stuehr, D. J., Santolini, J., Wang, Z.-Q., Wei, C.-C., & Adak, S. (2004). Update on Mechanism and Catalytic Regulation in the NO Synthases. *Journal of Biological Chemistry*, *279*(35), 36167–36170. http://doi.org/10.1074/jbc.R400017200

Taqatqeh, F., Mergia, E., Neitz, A., Eysel, U. T., Koesling, D., & Mittmann, T. (2009). More than a Retrograde Messenger: Nitric Oxide Needs Two cGMP Pathways to Induce Hippocampal Long-Term Potentiation. *Journal of Neuroscience*, *29*(29), 9344–9350. http://doi.org/10.1523/JNEUROSCI.1902-09.2009

Tejero, J., & Stuehr, D. (2013). Critical Review Tetrahydrobiopterin in Nitric Oxide Synthase. *International Union of Biochemistry and Molecular Biology*, *65*(4), 358–365. http://doi.org/10.1002/iub.1136

Tiso, M., Konas, D. W., Panda, K., Garcin, E. D., Sharma, M., Getzoff, E. D., & Stuehr, D. J. (2005). C-terminal Tail Residue Arg 1400 Enables NADPH to Regulate Electron Transfer in Neuronal Nitric-oxide Synthase. *The Journal of Biological Chemistry*, *280*(47), 39208–39219. http://doi.org/10.1074/jbc.M507775200

Turjanski, A. G., Estrin, D. A., Rosenstein, R. E., McCormick, J. E., Martin, S. R., Pastore, A., … Martorana, V. (2004). NMR and molecular dynamics studies of the interaction of melatonin with calmodulin. *Protein Science*, *13*, 2925–2938. http://doi.org/10.1110/ps.04611404.Calmodulin

Vandonselaar, M., Hickie, R. A., Quail, J. W., & Delbaere, L. T. (1994). Trifluoperazine-induced conformational change in calcium-calmodulin. *Structural Biology*, *1*(11), 795–801.

Víteček, J., Lojek, A., Valacchi, G., & Kubala, L. (2012). Arginine-Based Inhibitors of Nitric

Oxide Synthase: Therapeutic Potential and Challenges. *Mediators of Inflammation*, *2012*, 1–22. http://doi.org/10.1155/2012/318087

Volkmann, N., Martásek, P., Roman, L. J., Xu, X., Page, C., Swift, M., … Sue, B. (2014). Holoenzyme structures of endothelial nitric oxide synthase – An allosteric role for calmodulin in pivoting the FMN domain for electron transfer. *Journal of Structural Biology*, *188*(1), 46–54. http://doi.org/10.1016/j.jsb.2014.08.006

Weissman, B. A., Jones, C. L., Liu, Q., & Gross, S. S. (2002). Activation and inactivation of neuronal nitric oxide synthase : characterization of Ca 2 + -dependent [125 I] Calmodulin binding. *European Journal of Pharmacology*, *435*, 9–18.

Wu, G., Berta, V., & Tsai, A. (2011). Binding kinetics of calmodulin with target peptides of three nitric oxide synthase isozymes. *Journal of Inorganic Biochemistry*, *105*(9), 1226–1237.

Yamamoto, K., Kimura, S., Shiro, Y., & Iyanagi, T. (2005). Interflavin one-electron transfer in the inducible nitric oxide synthase reductase domain and NADPH-cytochrome P450 reductase. *Archives of Biochemistry and Biophysics*, *440*, 65–78. http://doi.org/10.1016/j.abb.2005.05.027

Yang, Y., Yu, T., Lian, Y., Ma, R., Yang, S., & Cho, J. Y. (2014). Nitric oxide synthase inhibitors: a review of patents from 2011 to the present. *Expert Opinion on Therapeutic Patents*, *3776*(September), 1–20. http://doi.org/10.1517/13543776.2014.979154

Zhang, H. Q., Dixon, R. P., Marletta, M. A., Nikolic, D., Breemen, R. Van, & Silverman, R. B. (1997a). Mechanism of Inactivation of Neuronal Nitric Oxide Synthase by N ω -Allyl- L -Arginine. *J Am Chem Soc*, *119*(45), 10888–10902. http://doi.org/10.1021/ja964160f

Appendix A – Truncated human NOS

The human nNOS and eNOS sequences were truncated at the C-terminal, such that the reductase domain only consists of the FMN binding site. Note that these sequences were also truncated at the N-terminal end to improve purification yields. The subcloning process was the same as the protocol detailed on Section 2.2.1. The oxyFMN sequences were generated via PCR using the following primers:

Table A1. Forward and reverse primers (FP and RP) for PCR amplification of truncated human nNOS and eNOS with GC content and melting temperatures (T_m). Highlighted sequences correspond to the restriction sites for NcoI (cyan), NdeI (yellow) and EcoRI (green).

Primer	Sequence	GC	T_m[a]
hnNOSΔ290FP	5′ CCACCATGGTCATATGGGAAAACAGTCCCCCACAAAGAATGGC 3'	51.2%	75.9 ˚C
hnNOSoxyFMNRP	5′ GCGGAATTCTTAATCTCCCACACAGAAGACATCACA 3′	44.4%	71.8 ˚C
heNOSΔ66FP	5′ CCACCATGGTCATATGCCCAAGTTCCCTCGTGTGAAGAACTGG 3′	53.5%	76.1 ˚C
heNOSoxyFMNRP	5′ GCGGAATTCTTAATCCTCTCCCACACAGAAGGTCTCACA 3′	48.7%	73.8 ˚C

[a] T_m values were calculated with the primer concentration at 0.5 µM, [NaCl] at 0 mM, [$MgCl_2$] at 2 mM and [dNTPs] at 200 µM using the IDT OligoAnalyzer®.

Analytical digests were performed to verify subcloning success. Results from restriction enzymes experiments were corroborated by nucleotide sequences aligned with corresponding entries on the GenBank database.

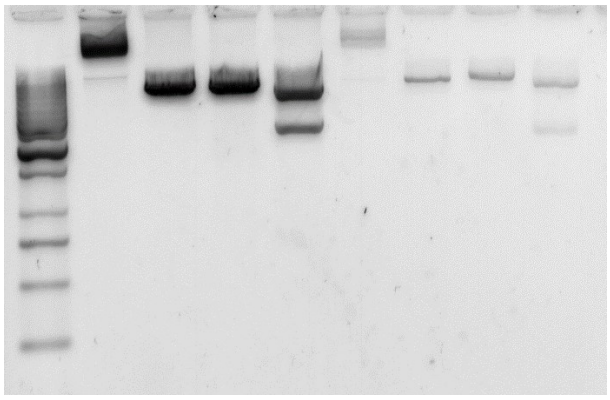

Figure A1. Analytical digests of successful pHnNOSoxyFMN (6973 bp) and pHeNOSoxyFMN (6934 bp) constructs. Lanes from L-R: (1) Ladder, (2) pHnNOSoxyFMN no enzyme control, (3) pHnNOSoxyFMN EcoRI single digest, (4) pHnNOSoxyFMN NdeI single digest, (5) pHnNOSoxyFMN EcoRI and NdeI double digest, (6) pHeNOSoxyFMN no enzyme control, (7) pHeNOSoxyFMN EcoRI single digest, (8) pHeNOSoxyFMN NdeI single digest, (9) pHeNOSoxyFMN EcoRI and NdeI double digest. Because the plasmid lengths are approximately the same size, the fragment lengths appear similar on the gel. Single digests yield fragments of 7.0 kbp; double digests, 5.0 and 2.0 kbp.0.5 µg of GeneRuler 1kb DNA Ladder was used.

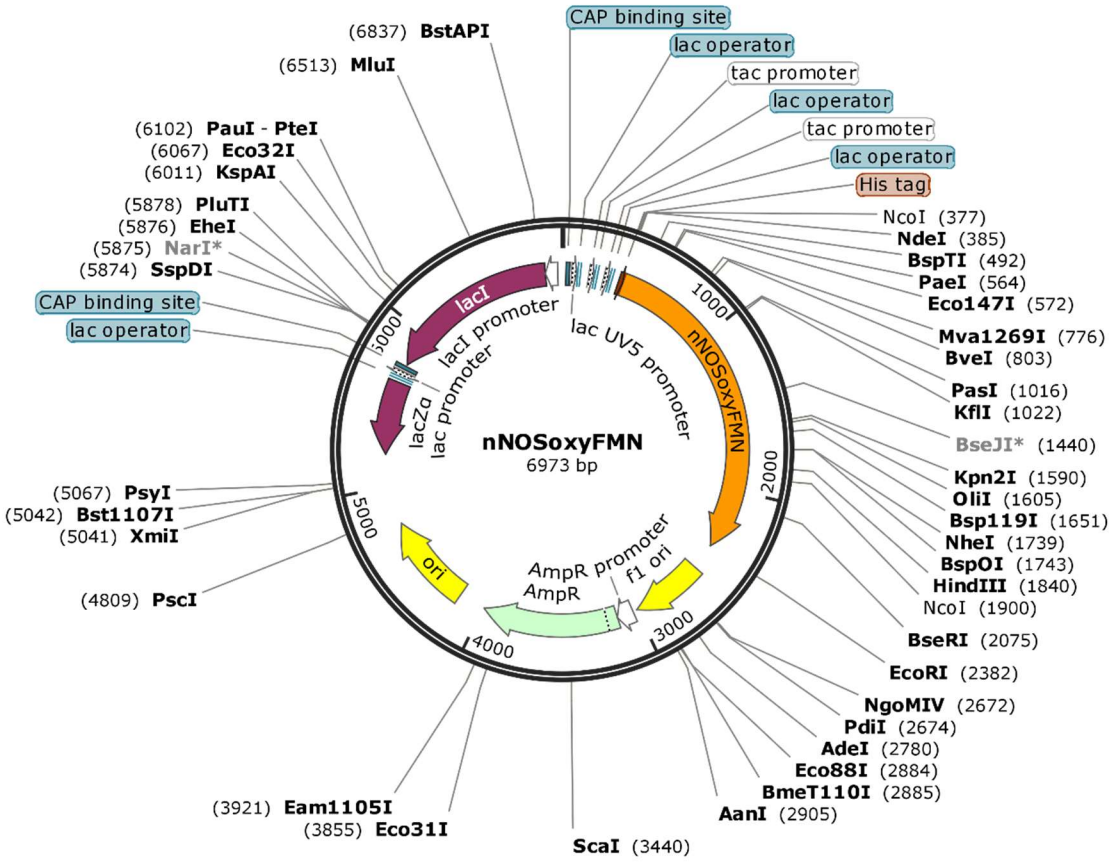

Figure A2. Plasmid map of pHnNOSoxyFMN. This plasmid contains the truncated human nNOS oxyFMN sequence subcloned into pCWori via ligation. It is ampicillin-resistant and uses the moderate-expression promoter tac. Restriction enzymes EcoRI and NdeI were used to validate subcloning success.

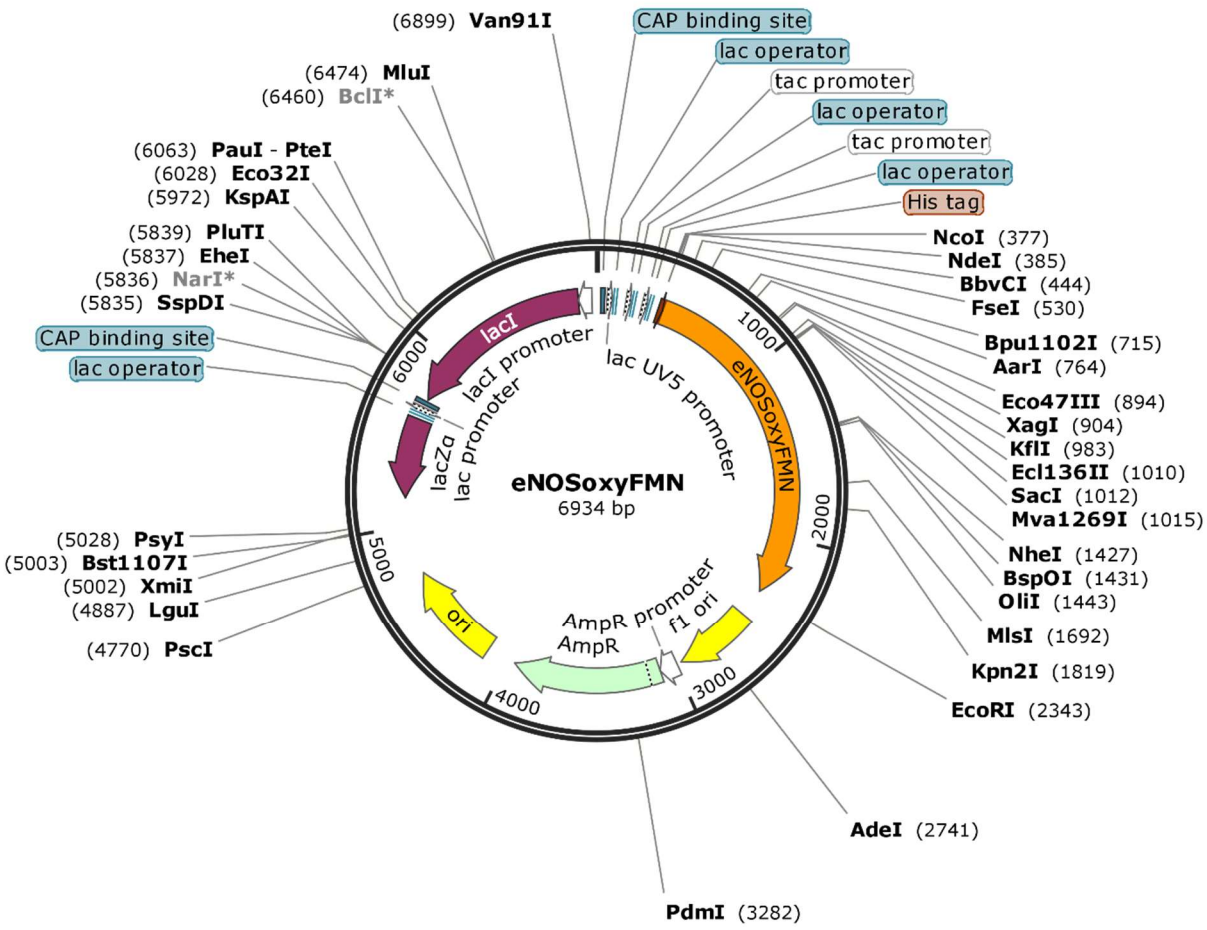

Figure A3. Plasmid map of pHeNOSoxyFMN. This plasmid contains the truncated human eNOS oxyFMN sequence subcloned into pCWori via ligation. It is ampicillin-resistant and uses the moderate-expression promoter tac. Restriction enzymes EcoRI and NdeI were used to validate the subcloning process.

The nNOSoxyFMN and eNOSoxyFMN proteins are expressed in *E. coli* BL21 (DE3) cells under the same growth conditions as described in Section 2.2.2.2. However, since the chaperone proteins GroES and GroEL were not co-expressed, ATP was not added into the media upon induction.

The cell pellets expressing nNOSoxyFMN or eNOSoxyFMN were resuspended in four column volumes of NOS Lysis Buffer (40 mM Tris-HCl, pH 7.5 @ 4 ˚C, 10% glycerol, 150 mM NaCl, 1 mM L-arginine, 1 mM PMSF). One tablet of cOmplete EDTA-free protease inhibitor was added per 1 L growth worth of cell pellet. The cells were lysed via homogenization. The samples were then centrifuged at 48000 x g for 30 minutes at 4 ˚C.

While the samples were spinning, 20 mL of Ni^{2+}-NTA resin, which binds His-tagged proteins, was recharged with two column volumes of 100 mM $NiSO_4$. The resin was washed with

10 column volumes of Milli-Q® water, followed by 10 column volumes of His Binding Buffer (NOS Lysis Buffer with 5 mM imidazole). The packed resin was resuspended after equilibration and then poured directly into the clarified supernatant. The resin-protein mixture was mixed in the rotisserie for 1 hour at 4 ˚C for maximal protein binding. Afterwards, the mixture was poured into a 1 cm x 30 cm Glass Econo-Column® (Bio-Rad) and was left to incubate at 4 ˚C for 30 minutes with the stopcock closed. Once the sample has flowed through the resin, it was washed with 5 column volumes of the His Binding Buffer. Then, the resin was 5 column volumes of the His Wash Buffer (NOS Lysis Buffer with 20 mM imidazole) to remove non-specifically bound proteins. The bound proteins were eluted with His Elution Buffer (NOS Lysis Buffer with 200 mM imidazole); 1 mL fractions were collected.

The most concentrated fractions, which were yellow in colour, were concentrated into a final volume of approximately 2 mL using a 30K MWCO Vivaspin® 6 centrifugal concentrator. This concentrated sample was loaded onto the HiLoad 16/60 Sephadex 200 (GE Life Sciences) for size exclusion chromatography via FPLC. Gel Filtration Buffer (50 mM Tris-HCl, pH 7.5 @ 4 ˚C, 10% glycerol, 250 mM NaCl, 5 µM L-arginine, 1 mM DTT and 0.1 mM PMSF) was used as the running buffer. 1 mL fractions were collected. The absorbance at wavelengths 280 nm, 398 nm and 425 nm were monitored, and most concentrated fractions were pooled. Aliquots were flash frozen and stored at –80 ˚C.

To quantify the protein yield, the UV-Vis spectra of the pooled sample was read from 300 to 700 nm. The Soret peak absorbance was plugged into Equation 2.1 to calculate the protein concentration in mM. The purity of the protein sample was assessed via 7.5% SDS-PAGE. The active site heme was assessed as described in Section 2.2.2.4. The flavin content of the sample was measured as in Section 2.2.2.5

Appendix B – Calcium-deficient CaM mutant

The CaM sequence containing the aforementioned mutations was obtained from Invitrogen. This 452-bp sequence contains an upstream NcoI and a downstream BamHI restriction sites, allowing it to be cloned into pET9d (4308 bp) using the protocols outlined in Section 2.2.1. The successful construct, referred to as pCaM$_{1234}$DNKan were verified via restriction enzyme digest and DNA sequencing. The CaM$_{1234}$ plasmids were expressed in *E. coli* BL21 (DE3) as described in Section 2.2.2.

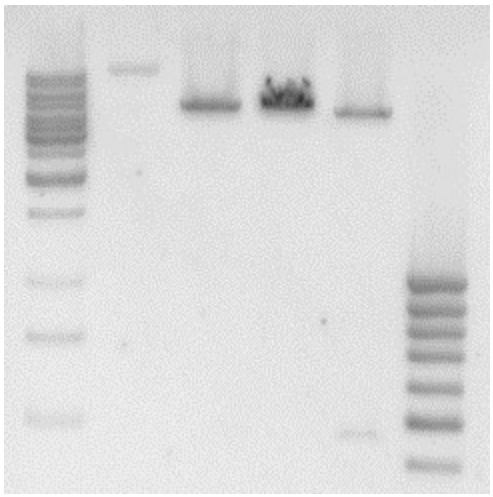

Table B1. Analytical digest of successful pCaM$_{1234}$DNKan construct (4754 bp). Lanes from L-R: (1) GeneRuler 1 kb DNA Ladder, (2) no enzyme control, (3) BamHI single digest, (4) NcoI single digest, (5) BamHI and NcoI double digest and (6) GeneRuler 100 bp DNA Ladder. Single digests yield fragments of about 5.0 kbp; double digests, 4.3 kbp and 452-bp.

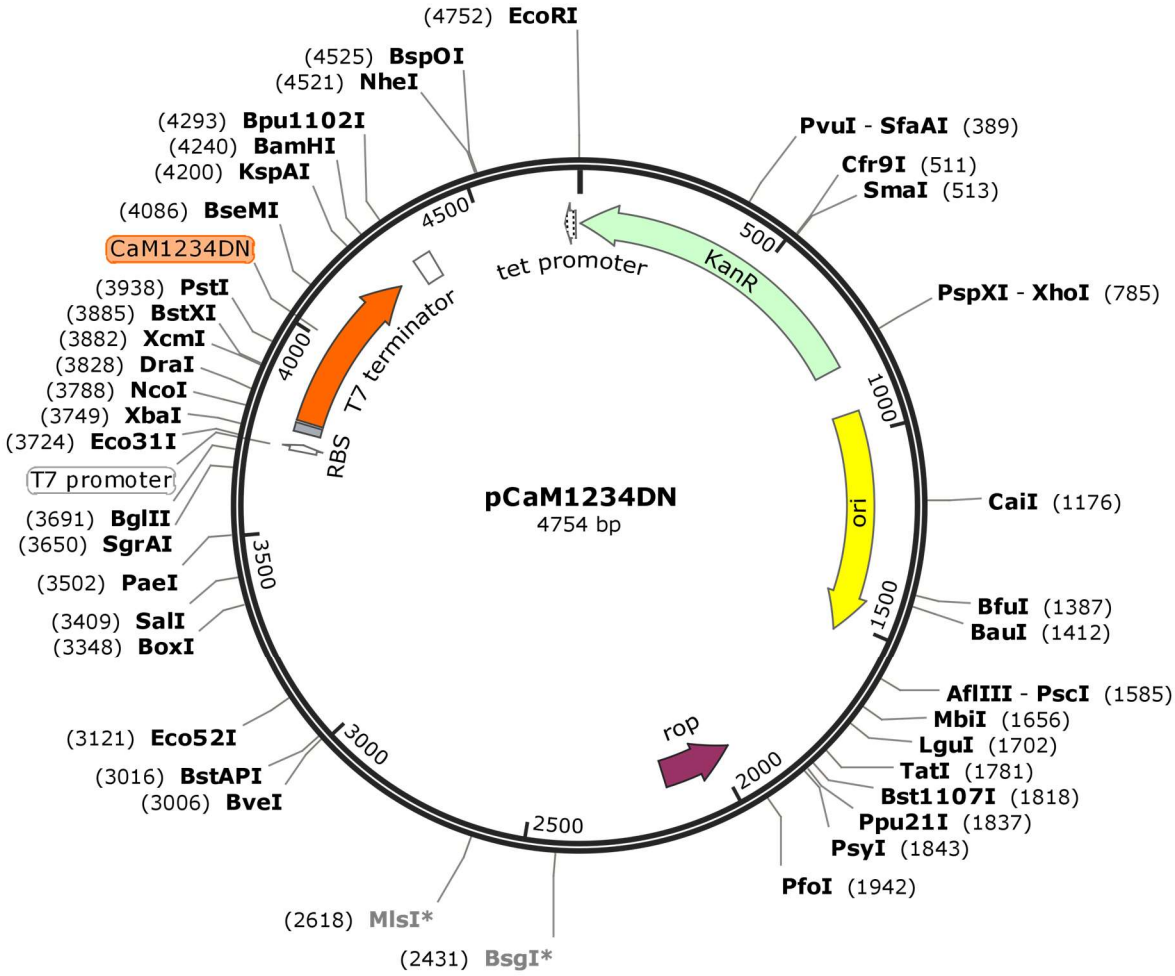

Table B2. . Plasmid map of pCaM$_{1234}$DNKan. This plasmid contains the truncated apoCaM mutant sequence subcloned into pET9d via ligation. It is kanamycin-resistant and uses the high-expression promoter T7. Restriction enzymes BamHI and NcoI were used to verify subcloning success.

Appendix C – NOS and CaM DNA sequences

pHnNOShisAmp (p537) – Human nNOSΔ290 holoenzyme with N-terminal polyhistidine tag in pCWori, cloned between NdeI and EcoRI. Mutation relative to PubMed sequence P29475.2: G438W.

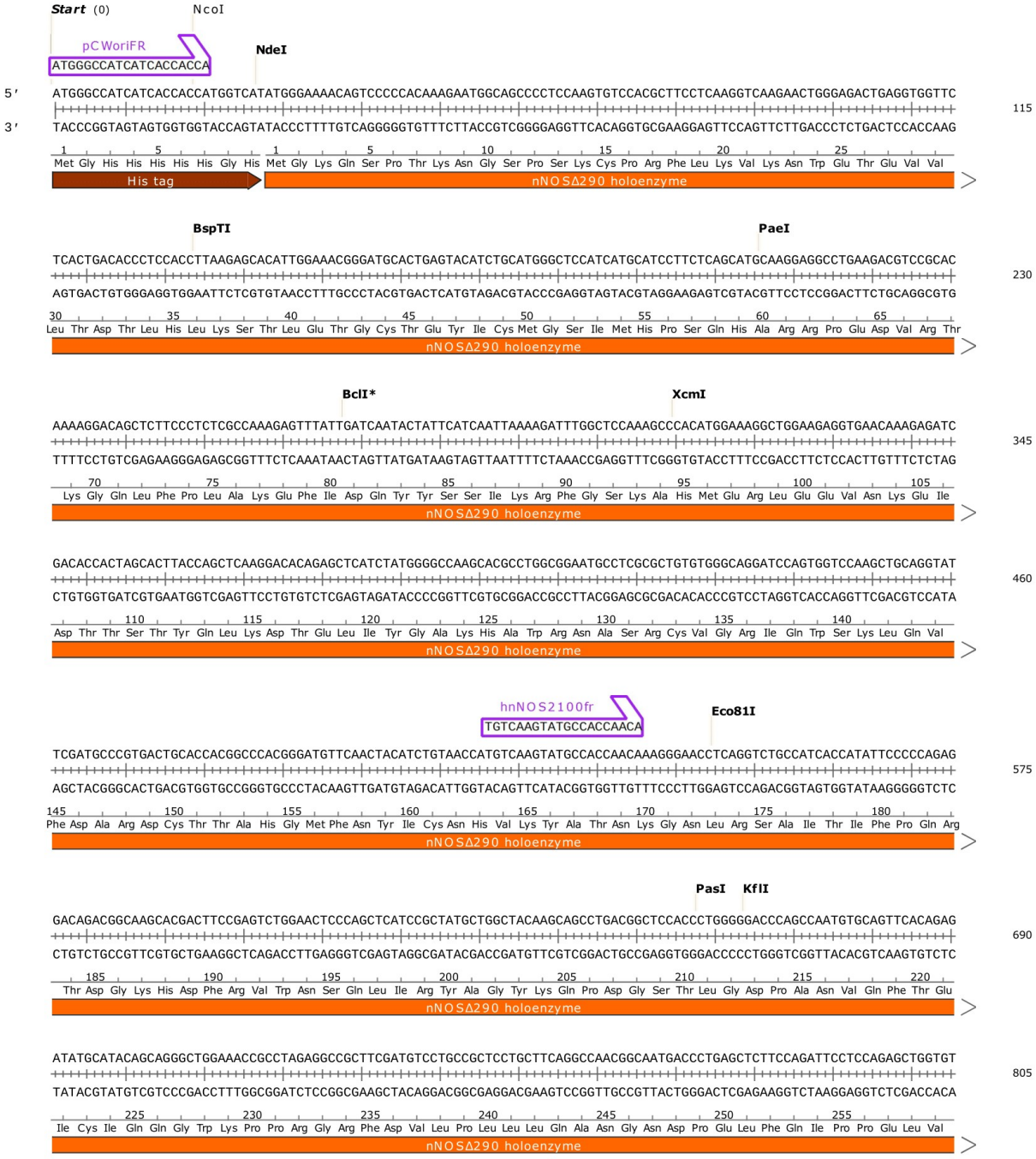

pHnNOShisAmp (cont'd – 2)

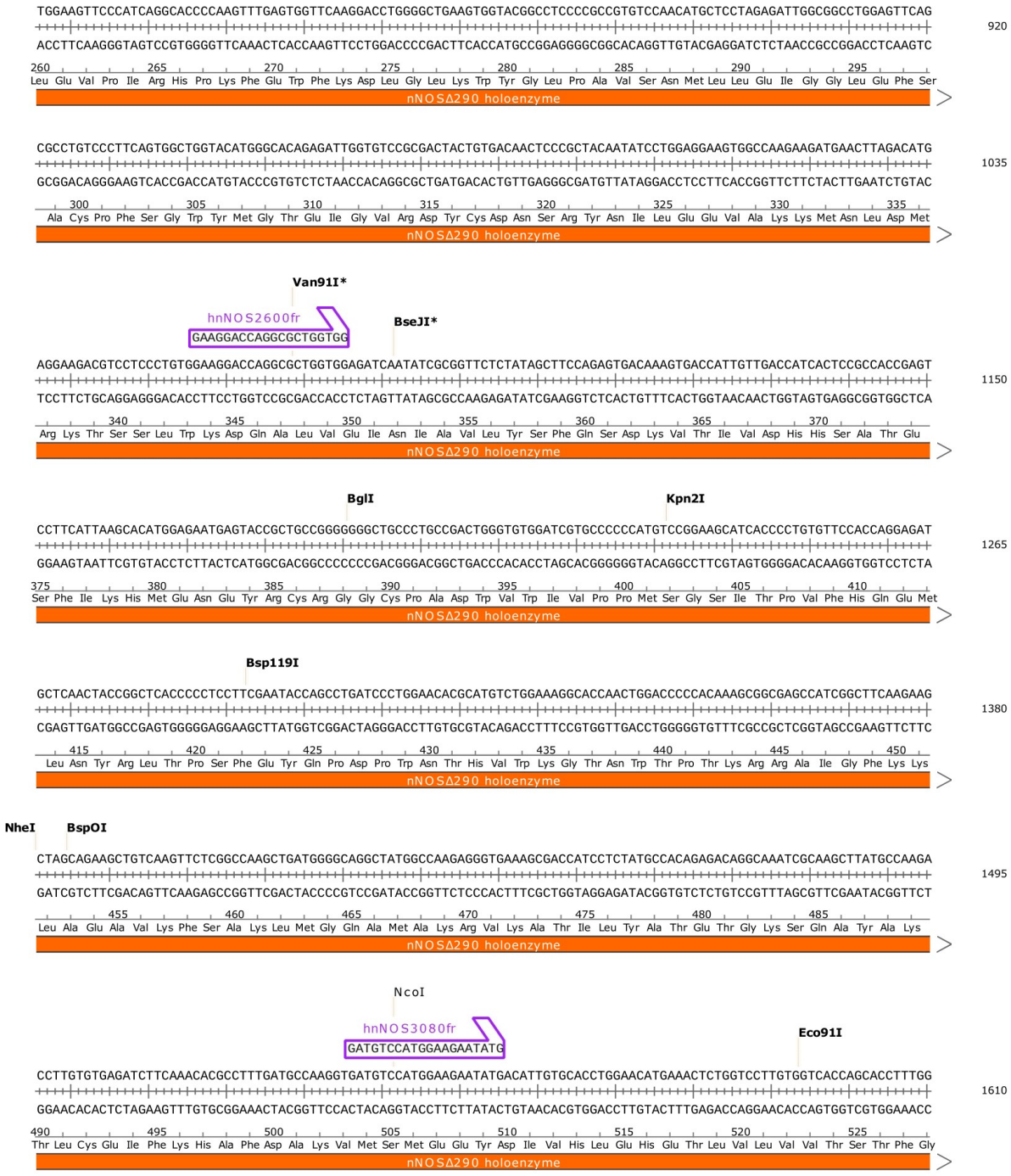

pHnNOShisAmp (cont'd – 3)

pHnNOShisAmp (cont'd – 4)

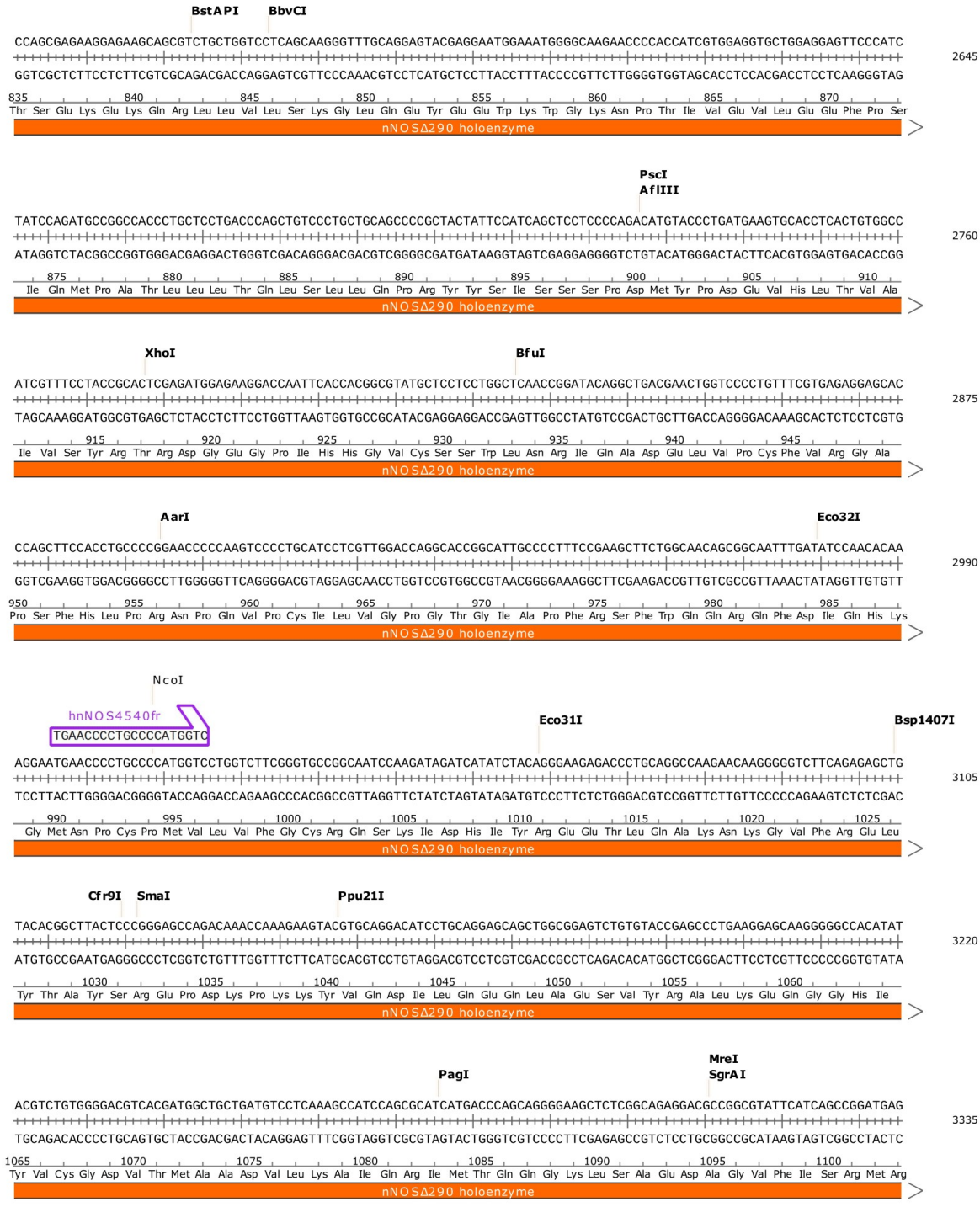

pHnNOShisAmp (cont'd – 5)

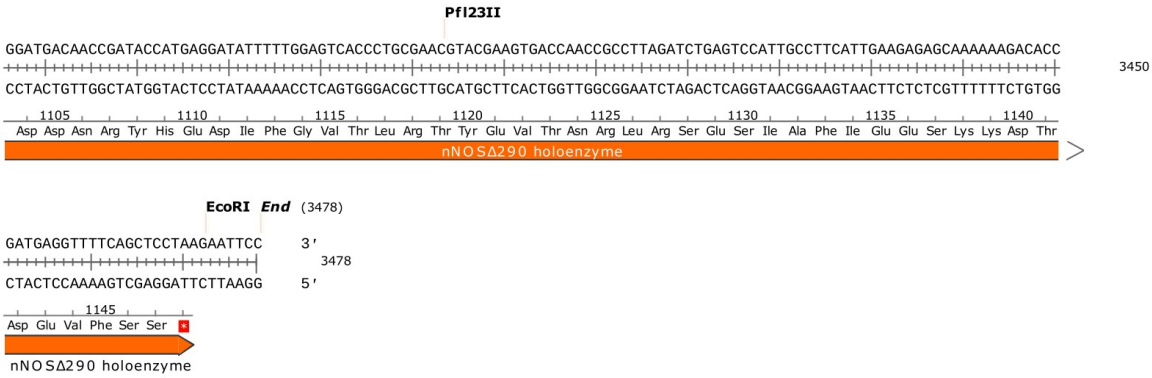

Protein sequence alignment of nNOS (GenPept: P29475.2; Query) and nNOS holoenzyme (Sbjct) aligned using NCBI BLAST.

```
Query  289  GKQSPTKNGSPSKCPRFLKVKNWETEVVLTDTLHLKSTLETGCTEYICMGSIMHPSQHAR  348
            GKQSPTKNGSPSKCPRFLKVKNWETEVVLTDTLHLKSTLETGCTEYICMGSIMHPSQHAR
Sbjct  1    GKQSPTKNGSPSKCPRFLKVKNWETEVVLTDTLHLKSTLETGCTEYICMGSIMHPSQHAR   60

Query  349  RPEDVRTKGQLFPLAKEFIDQYYSSIKRFGSKAHMERLEEVNKEIDTTSTYQLKDTELIY  408
            RPEDVRTKGQLFPLAKEFIDQYYSSIKRFGSKAHMERLEEVNKEIDTTSTYQLKDTELIY
Sbjct  61   RPEDVRTKGQLFPLAKEFIDQYYSSIKRFGSKAHMERLEEVNKEIDTTSTYQLKDTELIY  120

Query  409  GAKHAWRNASRCVGRIQWSKLQVFDARDCTTAHGMFNYICNHVKYATNKGNLRSAITIFP  468
            GAKHAWRNASRCVGRIQWSKLQVFDARDCTTAHGMFNYICNHVKYATNKGNLRSAITIFP
Sbjct  121  GAKHAWRNASRCVGRIQWSKLQVFDARDCTTAHGMFNYICNHVKYATNKGNLRSAITIFP  180

Query  469  QRTDGKHDFRVWNSQLIRYAGYKQPDGSTLGDPANVQFTEICIQQGWKPPRGRFDVLPLL  528
            QRTDGKHDFRVWNSQLIRYAGYKQPDGSTLGDPANVQFTEICIQQGWKPPRGRFDVLPLL
Sbjct  181  QRTDGKHDFRVWNSQLIRYAGYKQPDGSTLGDPANVQFTEICIQQGWKPPRGRFDVLPLL  240

Query  529  LQANGNDPELFQIPPELVLEVPIRHPKFEWFKDLGLKWYGLPAVSNMLLEIGGLEFSACP  588
            LQANGNDPELFQIPPELVLEVPIRHPKFEWFKDLGLKWYGLPAVSNMLLEIGGLEFSACP
Sbjct  241  LQANGNDPELFQIPPELVLEVPIRHPKFEWFKDLGLKWYGLPAVSNMLLEIGGLEFSACP  300

Query  589  FSGWYMGTEIGVRDYCDNSRYNILEEVAKKMNLDMRKTSSLWKDQALVEINIAVLYSFQS  648
            FSGWYMGTEIGVRDYCDNSRYNILEEVAKKMNLDMRKTSSLWKDQALVEINIAVLYSFQS
Sbjct  301  FSGWYMGTEIGVRDYCDNSRYNILEEVAKKMNLDMRKTSSLWKDQALVEINIAVLYSFQS  360

Query  649  DKVTIVDHHSATESFIKHMENEYRCRGGCPADWVWIVPPMSGSITPVFHQEMLNYRLTPS  708
            DKVTIVDHHSATESFIKHMENEYRCRGGCPADWVWIVPPMSGSITPVFHQEMLNYRLTPS
Sbjct  361  DKVTIVDHHSATESFIKHMENEYRCRGGCPADWVWIVPPMSGSITPVFHQEMLNYRLTPS  420

Query  709  FEYQPDPWNTHVWKGTNGTPTKRRAIGFKKLAEAVKFSAKLMGQAMAKRVKATILYATET  768
            FEYQPDPWNTHVWKGTN TPTKRRAIGFKKLAEAVKFSAKLMGQAMAKRVKATILYATET
Sbjct  421  FEYQPDPWNTHVWKGTNWTPTKRRAIGFKKLAEAVKFSAKLMGQAMAKRVKATILYATET  480

Query  769  GKSQAYAKTLCEIFKHAFDAKVMSMEEYDIVHLEHETLVLVVTSTFGNGDPPENGEKFGC  828
            GKSQAYAKTLCEIFKHAFDAKVMSMEEYDIVHLEHETLVLVVTSTFGNGDPPENGEKFGC
Sbjct  481  GKSQAYAKTLCEIFKHAFDAKVMSMEEYDIVHLEHETLVLVVTSTFGNGDPPENGEKFGC  540

Query  829  ALMEMRHPNSVQEERKSYKVRFNSVSSYSDSQKSSGDGPDLRDNFESAGPLANVRFSVFG  888
            ALMEMRHPNSVQEERKSYKVRFNSVSSYSDSQKSSGDGPDLRDNFESAGPLANVRFSVFG
Sbjct  541  ALMEMRHPNSVQEERKSYKVRFNSVSSYSDSQKSSGDGPDLRDNFESAGPLANVRFSVFG  600

Query  889  LGSRAYPHFCAFGHAVDTLLEELGGERILKMREGDELCGQEEAFRTWAKKVFKAACDVFC  948
            LGSRAYPHFCAFGHAVDTLLEELGGERILKMREGDELCGQEEAFRTWAKKVFKAACDVFC
Sbjct  601  LGSRAYPHFCAFGHAVDTLLEELGGERILKMREGDELCGQEEAFRTWAKKVFKAACDVFC  660

Query  949  VGDDVNIEKANNSLISNDRSWKRNKFRLTFVAEAPELTQGLSNVHKKRVSAARLLSRQNL 1008
            VGDDVNIEKANNSLISNDRSWKRNKFRLTFVAEAPELTQGLSNVHKKRVSAARLLSRQNL
Sbjct  661  VGDDVNIEKANNSLISNDRSWKRNKFRLTFVAEAPELTQGLSNVHKKRVSAARLLSRQNL  720

Query  1009 QSPKSSRSTIFVRLHTNGSQELQYQPGDHLGVFPGNHEDLVNALIERLEDAPPVNQMVKV 1068
            QSPKSSRSTIFVRLHTNGSQELQYQPGDHLGVFPGNHEDLVNALIERLEDAPPVNQMVKV
Sbjct  721  QSPKSSRSTIFVRLHTNGSQELQYQPGDHLGVFPGNHEDLVNALIERLEDAPPVNQMVKV  780
```

nNOS holoenzyme alignment (cont'd – 2)

```
Query  1069 ELLEERNTALGVISNWTDELRLPPCTIFQAFKYYLDITTPPTPLQLQQFASLATSEKEKQ 1128
            ELLEERNTALGVISNWTDELRLPPCTIFQAFKYYLDITTPPTPLQLQQFASLATSEKEKQ
Sbjct  781  ELLEERNTALGVISNWTDELRLPPCTIFQAFKYYLDITTPPTPLQLQQFASLATSEKEKQ 840

Query  1129 RLLVLSKGLQEYEEWKWGKNPTIVEVLEEFPSIQMPATLLLTQLSLLQPRYYSISSSPDM 1188
            RLLVLSKGLQEYEEWKWGKNPTIVEVLEEFPSIQMPATLLLTQLSLLQPRYYSISSSPDM
Sbjct  841  RLLVLSKGLQEYEEWKWGKNPTIVEVLEEFPSIQMPATLLLTQLSLLQPRYYSISSSPDM  900

Query  1189 YPDEVHLTVAIVSYRTRDGEGPIHHGVCSSWLNRIQADELVPCFVRGAPSFHLPRNPQVP 1248
            YPDEVHLTVAIVSYRTRDGEGPIHHGVCSSWLNRIQADELVPCFVRGAPSFHLPRNPQVP
Sbjct  901  YPDEVHLTVAIVSYRTRDGEGPIHHGVCSSWLNRIQADELVPCFVRGAPSFHLPRNPQVP  960

Query  1249 CILVGPGTGIAPFRSFWQQRQFDIQHKGMNPCPMVLVFGCRQSKIDHIYREETLQAKNKG 1308
            CILVGPGTGIAPFRSFWQQRQFDIQHKGMNPCPMVLVFGCRQSKIDHIYREETLQAKNKG
Sbjct  961  CILVGPGTGIAPFRSFWQQRQFDIQHKGMNPCPMVLVFGCRQSKIDHIYREETLQAKNKG 1020

Query  1309 VFRELYTAYSREPDKPKKYVQDILQEQLAESVYRALKEQGGHIYVCGDVTMAADVLKAIQ 1368
            VFRELYTAYSREPDKPKKYVQDILQEQLAESVYRALKEQGGHIYVCGDVTMAADVLKAIQ
Sbjct  1021 VFRELYTAYSREPDKPKKYVQDILQEQLAESVYRALKEQGGHIYVCGDVTMAADVLKAIQ 1080

Query  1369 RIMTQQGKLSAEDAGVFISRMRDDNRYHEDIFGVTLRTYEVTNRLRSESIAFIEESKKDT 1428
            RIMTQQGKLSAEDAGVFISRMRDDNRYHEDIFGVTLRTYEVTNRLRSESIAFIEESKKDT
Sbjct  1081 RIMTQQGKLSAEDAGVFISRMRDDNRYHEDIFGVTLRTYEVTNRLRSESIAFIEESKKDT 1140

Query  1429 DEVFSS 1434
            DEVFSS
Sbjct  1141 DEVFSS 1146
```

pHeNOShisAmp (p536) – Human eNOSΔ66 holoenzyme with N-terminal polyhistidine tag in pCWori, cloned between NdeI and EcoRI.

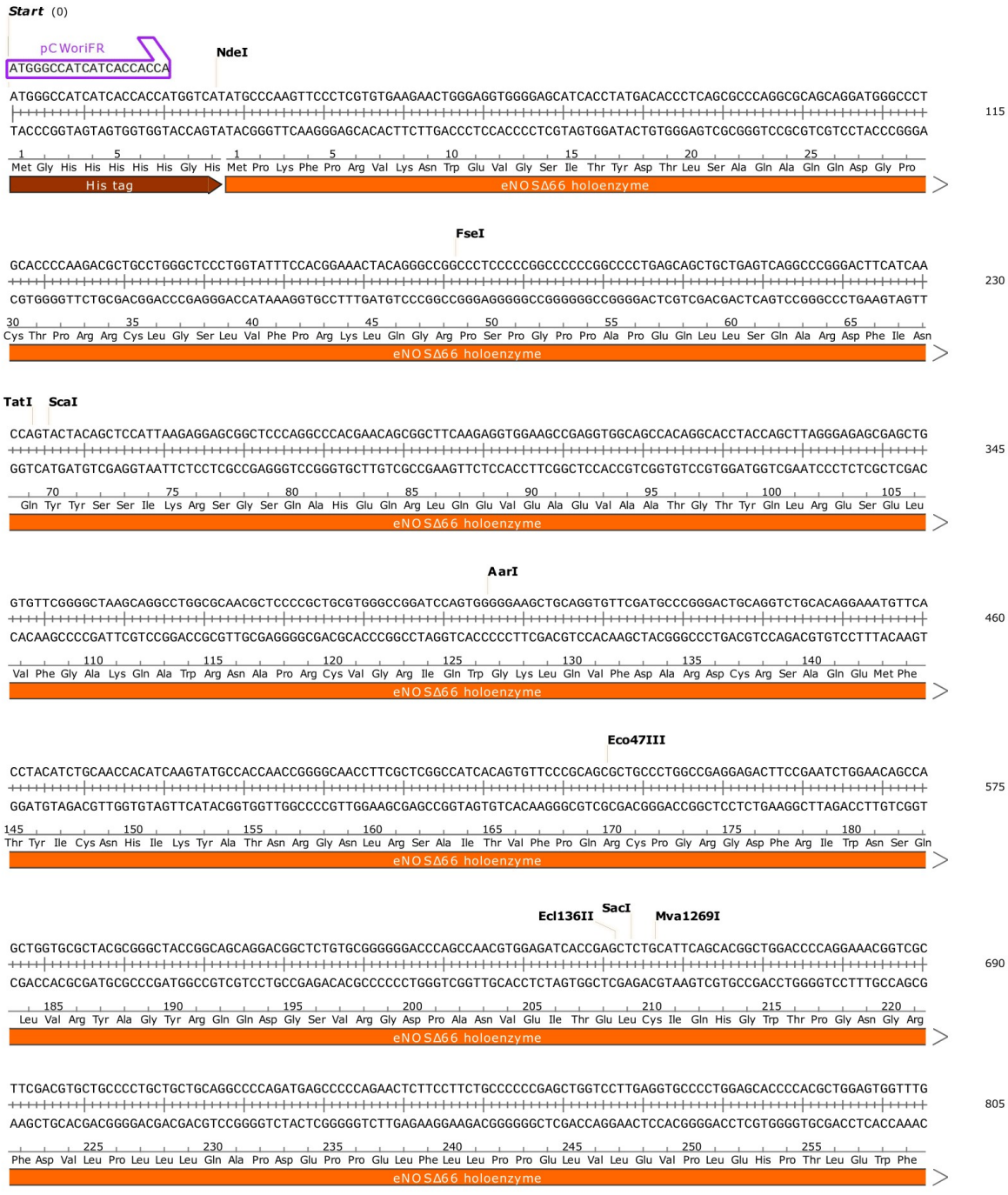

pHeNOShisAmp (cont'd – 2)

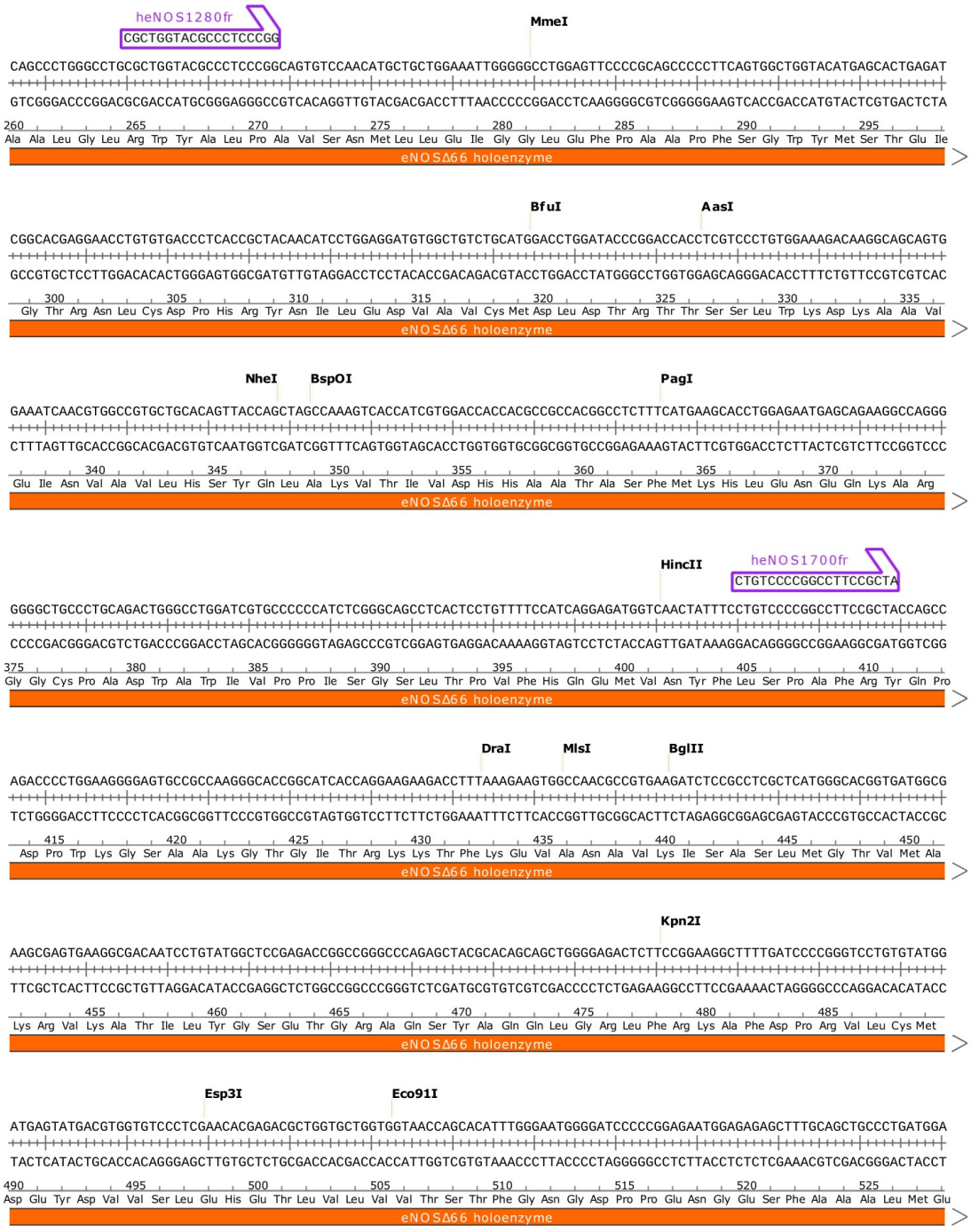

pHeNOShisAmp (cont'd – 3)

pHeNOShisAmp (cont'd – 4)

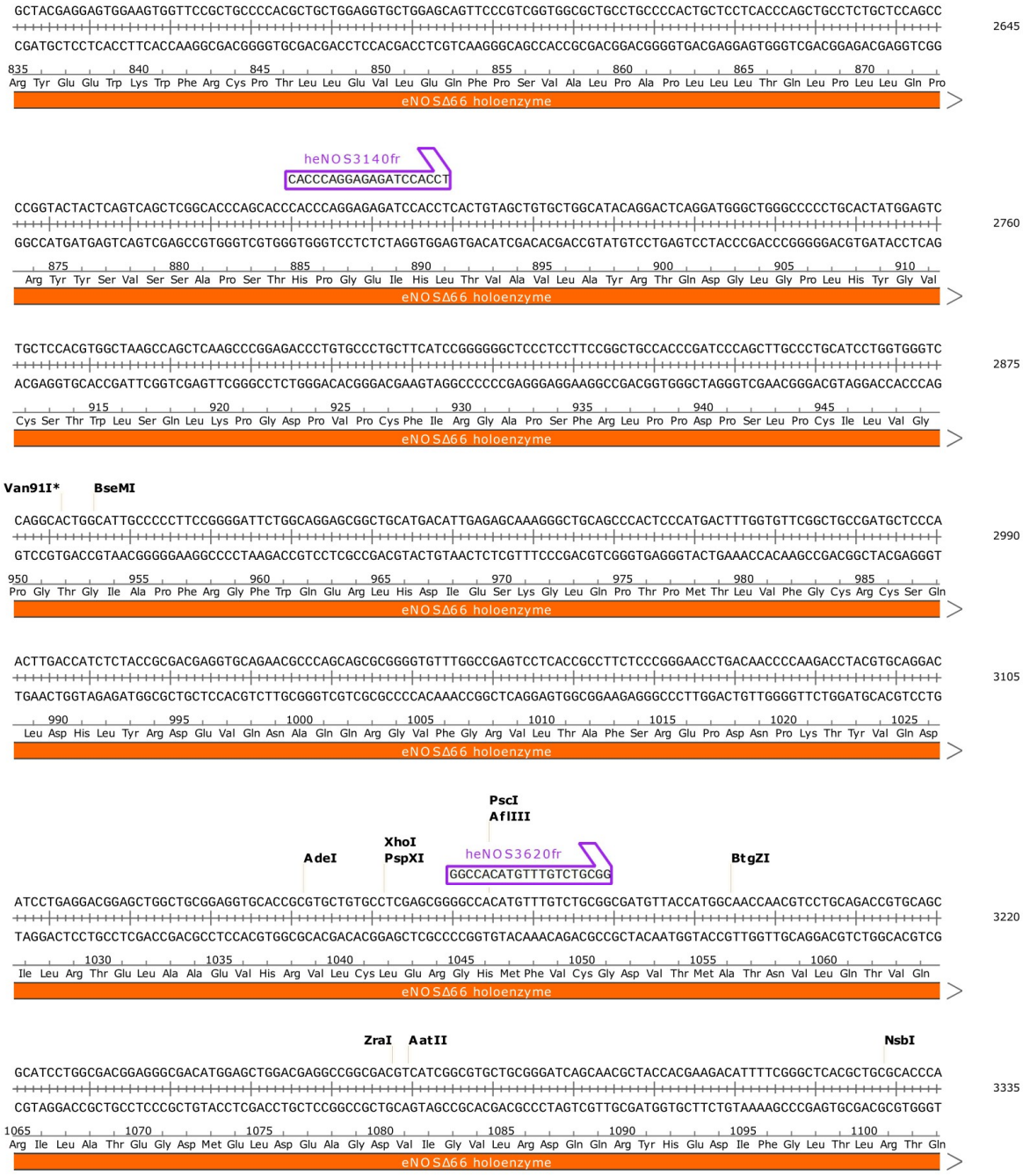

pHeNOShisAmp (cont'd – 5)

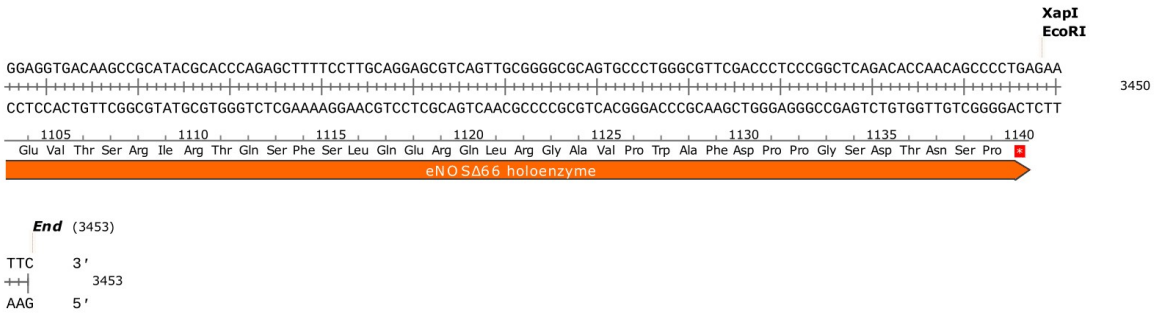

Protein sequence alignment of eNOS (GenPept: P29474.3; Query) and eNOS holoenzyme (Sbjct) aligned using NCBI BLAST.

```
Query  66   PKFPRVKNWEVGSITYDTLSAQAQQDGPCTPRRCLGSLVFPRKLQGRPSPGPPAPEQLLS  125
            PKFPRVKNWEVGSITYDTLSAQAQQDGPCTPRRCLGSLVFPRKLQGRPSPGPPAPEQLLS
Sbjct  1    PKFPRVKNWEVGSITYDTLSAQAQQDGPCTPRRCLGSLVFPRKLQGRPSPGPPAPEQLLS   60

Query  126  QARDFINQYYSSIKRSGSQAHEQRLQEVEAEVAATGTYQLRESELVFGAKQAWRNAPRCV  185
            QARDFINQYYSSIKRSGSQAHEQRLQEVEAEVAATGTYQLRESELVFGAKQAWRNAPRCV
Sbjct  61   QARDFINQYYSSIKRSGSQAHEQRLQEVEAEVAATGTYQLRESELVFGAKQAWRNAPRCV  120

Query  186  GRIQWGKLQVFDARDCRSAQEMFTYICNHIKYATNRGNLRSAITVFPQRCPGRGDFRIWN  245
            GRIQWGKLQVFDARDCRSAQEMFTYICNHIKYATNRGNLRSAITVFPQRCPGRGDFRIWN
Sbjct  121  GRIQWGKLQVFDARDCRSAQEMFTYICNHIKYATNRGNLRSAITVFPQRCPGRGDFRIWN  180

Query  246  SQLVRYAGYRQQDGSVRGDPANVEITELCIQHGWTPGNGRFDVLPLLLQAPDEPPELFLL  305
            SQLVRYAGYRQQDGSVRGDPANVEITELCIQHGWTPGNGRFDVLPLLLQAPDEPPELFLL
Sbjct  181  SQLVRYAGYRQQDGSVRGDPANVEITELCIQHGWTPGNGRFDVLPLLLQAPDEPPELFLL  240

Query  306  PPELVLEVPLEHPTLEWFAALGLRWYALPAVSNMLLEIGGLEFPAAPFSGWYMSTEIGTR  365
            PPELVLEVPLEHPTLEWFAALGLRWYALPAVSNMLLEIGGLEFPAAPFSGWYMSTEIGTR
Sbjct  241  PPELVLEVPLEHPTLEWFAALGLRWYALPAVSNMLLEIGGLEFPAAPFSGWYMSTEIGTR  300

Query  366  NLCDPHRYNILEDVAVCMDLDTRTTSSLWKDKAAVEINVAVLHSYQLAKVTIVDHHAATA  425
            NLCDPHRYNILEDVAVCMDLDTRTTSSLWKDKAAVEINVAVLHSYQLAKVTIVDHHAATA
Sbjct  301  NLCDPHRYNILEDVAVCMDLDTRTTSSLWKDKAAVEINVAVLHSYQLAKVTIVDHHAATA  360

Query  426  SFMKHLENEQKARGGCPADWAWIVPPISGSLTPVFHQEMVNYFLSPAFRYQPDPWKGSAA  485
            SFMKHLENEQKARGGCPADWAWIVPPISGSLTPVFHQEMVNYFLSPAFRYQPDPWKGSAA
Sbjct  361  SFMKHLENEQKARGGCPADWAWIVPPISGSLTPVFHQEMVNYFLSPAFRYQPDPWKGSAA  420

Query  486  KGTGITRKKTFKEVANAVKISASLMGTVMAKRVKATILYGSETGRAQSYAQQLGRLFRKA  545
            KGTGITRKKTFKEVANAVKISASLMGTVMAKRVKATILYGSETGRAQSYAQQLGRLFRKA
Sbjct  421  KGTGITRKKTFKEVANAVKISASLMGTVMAKRVKATILYGSETGRAQSYAQQLGRLFRKA  480

Query  546  FDPRVLCMDEYDVVSLEHETLVLVVTSTFGNGDPPENGESFAAALMEMSGPYNSSPRPEQ  605
            FDPRVLCMDEYDVVSLEHETLVLVVTSTFGNGDPPENGESFAAALMEMSGPYNSSPRPEQ
Sbjct  481  FDPRVLCMDEYDVVSLEHETLVLVVTSTFGNGDPPENGESFAAALMEMSGPYNSSPRPEQ  540

Query  606  HKSYKIRFNSISCSDPLVSSWRRKRKESSNTDSAGALGTLRFCVFGLGSRAYPHFCAFAR  665
            HKSYKIRFNSISCSDPLVSSWRRKRKESSNTDSAGALGTLRFCVFGLGSRAYPHFCAFAR
Sbjct  541  HKSYKIRFNSISCSDPLVSSWRRKRKESSNTDSAGALGTLRFCVFGLGSRAYPHFCAFAR  600

Query  666  AVDTRLEELGGERLLQLGQGDELCGQEEAFRGWAQAAFQAACETFCVGEDAKAAARDIFS  725
            AVDTRLEELGGERLLQLGQGDELCGQEEAFRGWAQAAFQAACETFCVGEDAKAAARDIFS
Sbjct  601  AVDTRLEELGGERLLQLGQGDELCGQEEAFRGWAQAAFQAACETFCVGEDAKAAARDIFS  660

Query  726  PKRSWKRQRYRLSAQAEGLQLLPGLIHVHRRKMFQATIRSVENLQSSKSTRATILVRLDT  785
            PKRSWKRQRYRLSAQAEGLQLLPGLIHVHRRKMFQATIRSVENLQSSKSTRATILVRLDT
Sbjct  661  PKRSWKRQRYRLSAQAEGLQLLPGLIHVHRRKMFQATIRSVENLQSSKSTRATILVRLDT  720

Query  786  GGQEGLQYQPGDHIGVCPPNRPGLVEALLSRVEDPPAPTEPVAVEQLEKGSPGGPPPGWV  845
            GGQEGLQYQPGDHIGVCPPNRPGLVEALLSRVEDPPAPTEPVAVEQLEKGSPGGPPPGWV
Sbjct  721  GGQEGLQYQPGDHIGVCPPNRPGLVEALLSRVEDPPAPTEPVAVEQLEKGSPGGPPPGWV  780
```

eNOS holoenzyme alignment (cont'd – 2)

```
Query  846  RDPRLPPCTLRQALTFFLDITSPPSPQLLRLLSTLAEEPREQQELEALSQDPRRYEEWKW  905
            RDPRLPPCTLRQALTFFLDITSPPSPQLLRLLSTLAEEPREQQELEALSQDPRRYEEWKW
Sbjct  781  RDPRLPPCTLRQALTFFLDITSPPSPQLLRLLSTLAEEPREQQELEALSQDPRRYEEWKW  840

Query  906  FRCPTLLEVLEQFPSVALPAPLLLTQLPLLQPRYYSVSSAPSTHPGEIHLTVAVLAYRTQ  965
            FRCPTLLEVLEQFPSVALPAPLLLTQLPLLQPRYYSVSSAPSTHPGEIHLTVAVLAYRTQ
Sbjct  841  FRCPTLLEVLEQFPSVALPAPLLLTQLPLLQPRYYSVSSAPSTHPGEIHLTVAVLAYRTQ  900

Query  966  DGLGPLHYGVCSTWLSQLKPGDPVPCFIRGAPSFRLPPDPSLPCILVGPGTGIAPFRGFW 1025
            DGLGPLHYGVCSTWLSQLKPGDPVPCFIRGAPSFRLPPDPSLPCILVGPGTGIAPFRGFW
Sbjct  901  DGLGPLHYGVCSTWLSQLKPGDPVPCFIRGAPSFRLPPDPSLPCILVGPGTGIAPFRGFW  960

Query  1026 QERLHDIESKGLQPTPMTLVFGCRCSQLDHLYRDEVQNAQQRGVFGRVLTAFSREPDNPK 1085
            QERLHDIESKGLQPTPMTLVFGCRCSQLDHLYRDEVQNAQQRGVFGRVLTAFSREPDNPK
Sbjct  961  QERLHDIESKGLQPTPMTLVFGCRCSQLDHLYRDEVQNAQQRGVFGRVLTAFSREPDNPK 1020

Query  1086 TYVQDILRTELAAEVHRVLCLERGHMFVCGDVTMATNVLQTVQRILATEGDMELDEAGDV 1145
            TYVQDILRTELAAEVHRVLCLERGHMFVCGDVTMATNVLQTVQRILATEGDMELDEAGDV
Sbjct  1021 TYVQDILRTELAAEVHRVLCLERGHMFVCGDVTMATNVLQTVQRILATEGDMELDEAGDV 1080

Query  1146  IGVLRDQQRYHEDIFGLTLRTQEVTSRIRTQSFSLQERQLRGAVPWAFDPPGSDTNSP  1203
             IGVLRDQQRYHEDIFGLTLRTQEVTSRIRTQSFSLQERQLRGAVPWAFDPPGSDTNSP
Sbjct  1081  IGVLRDQQRYHEDIFGLTLRTQEVTSRIRTQSFSLQERQLRGAVPWAFDPPGSDTNSP  1138
```

Analytical digests were performed to verify subcloning success. Results from restriction enzymes experiments were corroborated by nucleotide sequences aligned with corresponding entries on the GenBank database.

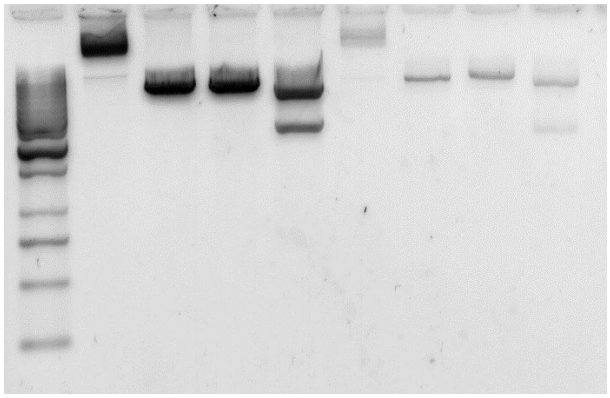

Table B3. Analytical digests of successful pHnNOSoxyFMN (6973 bp) and pHeNOSoxyFMN (6934 bp) constructs. Lanes from L-R: (1) Ladder, (2) pHnNOSoxyFMN no enzyme control, (3) pHnNOSoxyFMN EcoRI single digest, (4) pHnNOSoxyFMN NdeI single digest, (5) pHnNOSoxyFMN EcoRI and NdeI double digest, (6) pHeNOSoxyFMN no enzyme control, (7) pHeNOSoxyFMN EcoRI single digest, (8) pHeNOSoxyFMN NdeI single digest, (9) pHeNOSoxyFMN EcoRI and NdeI double digest. Because the plasmid lengths are approximately the same size, the fragment lengths appear similar on the gel. Single digests yield fragments of 7.0 kbp; double digests, 5.0 and 2.0 kbp.0.5 µg of GeneRuler 1kb DNA Ladder was used.

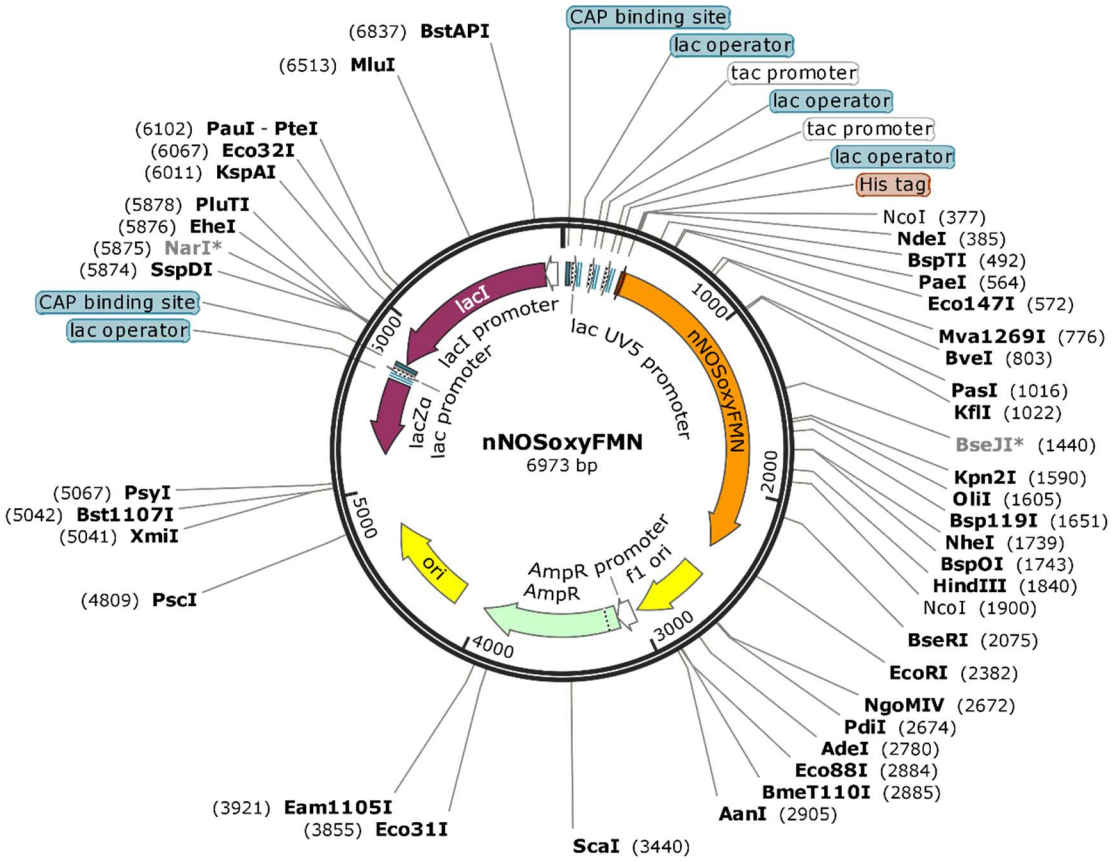

Table B4. Plasmid map of pHnNOSoxyFMN. This plasmid contains the truncated human nNOS oxyFMN sequence subcloned into pCWori via ligation. It is ampicillin-resistant and uses the moderate-expression promoter tac. Restriction enzymes EcoRI and NdeI were used to validate subcloning success.

pHnNOSoxyFMNhisAmp (p541) – Human nNOSΔ290 oxyFMN with N-terminal polyhistidine tag in pCWori, cloned between NdeI and EcoRI. Mutation relative to PubMed sequence P29475.2: G438W.

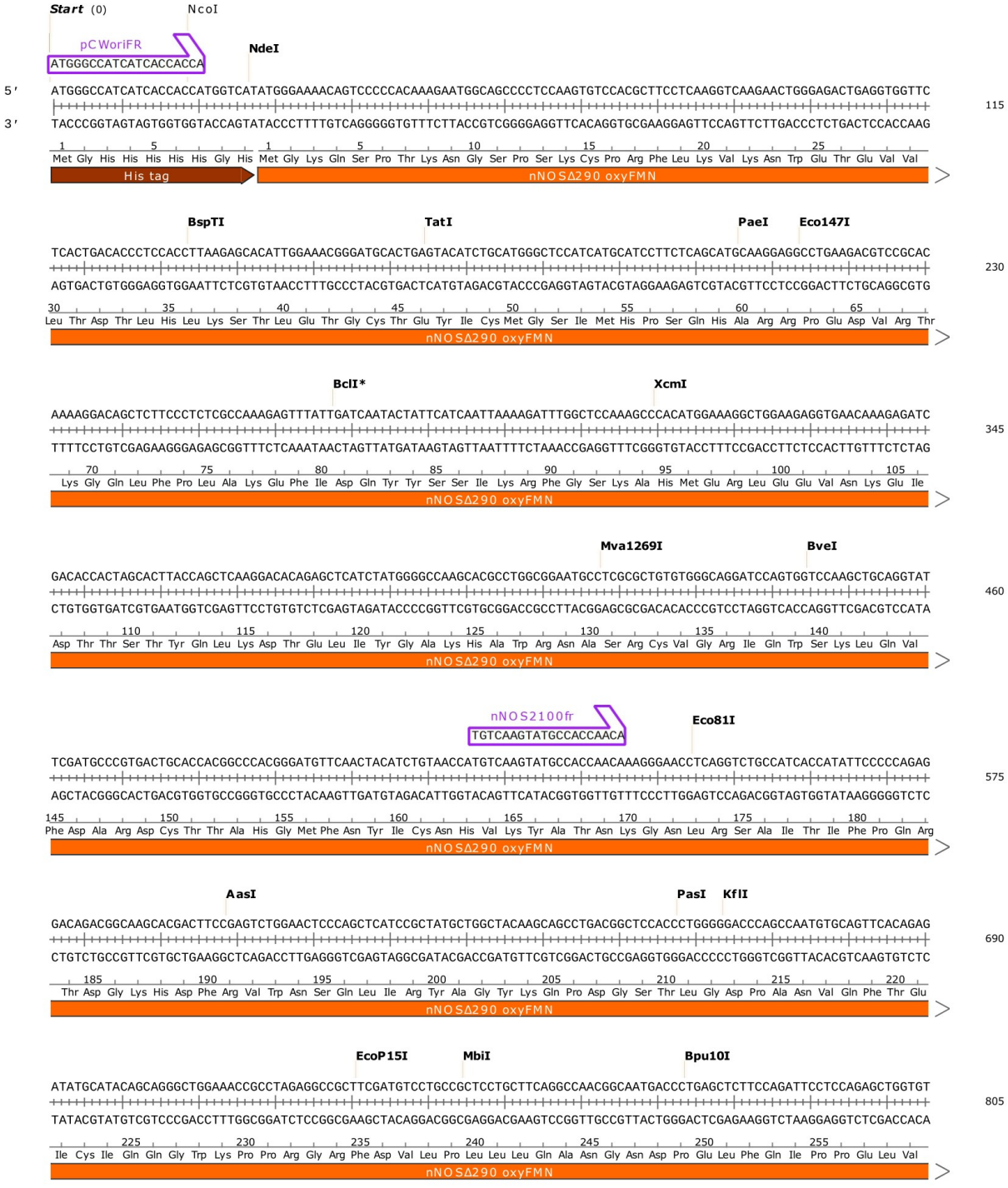

pHnNOSoxyFMNhisAmp (cont'd – 2)

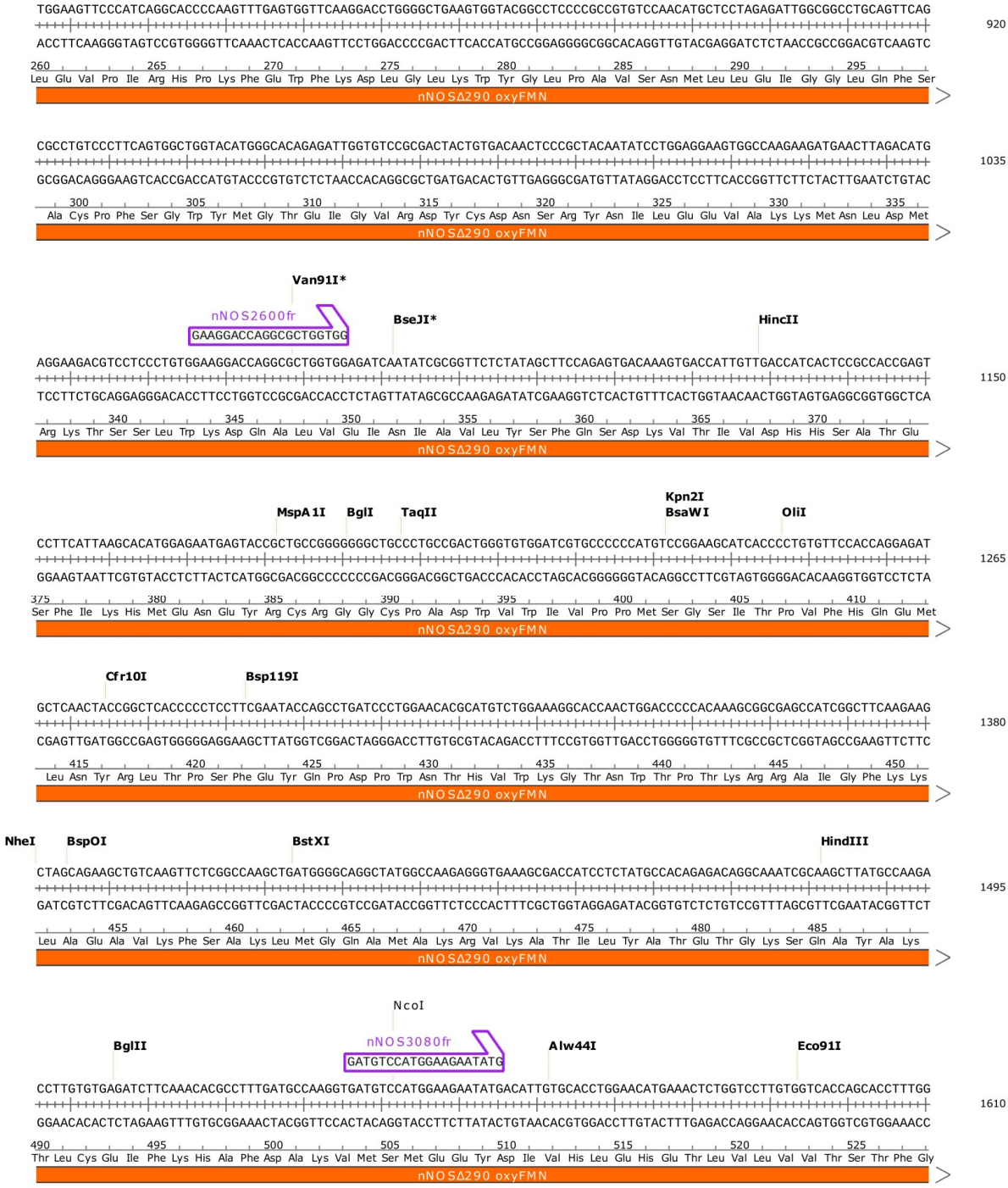

pHnNOSoxyFMNhisAmp (cont'd – 3)

Protein sequence alignment of nNOS (GenPept: P29475.2; Query) and nNOSoxyFMN (Sbjct) aligned using NCBI BLAST.

```
Query  289  GKQSPTKNGSPSKCPRFLKVKNWETEVVLTDTLHLKSTLETGCTEYICMGSIMHPSQHAR  348
            GKQSPTKNGSPSKCPRFLKVKNWETEVVLTDTLHLKSTLETGCTEYICMGSIMHPSQHAR
Sbjct  1    GKQSPTKNGSPSKCPRFLKVKNWETEVVLTDTLHLKSTLETGCTEYICMGSIMHPSQHAR  60

Query  349  RPEDVRTKGQLFPLAKEFIDQYYSSIKRFGSKAHMERLEEVNKEIDTTSTYQLKDTELIY  408
            RPEDVRTKGQLFPLAKEFIDQYYSSIKRFGSKAHMERLEEVNKEIDTTSTYQLKDTELIY
Sbjct  61   RPEDVRTKGQLFPLAKEFIDQYYSSIKRFGSKAHMERLEEVNKEIDTTSTYQLKDTELIY  120

Query  409  GAKHAWRNASRCVGRIQWSKLQVFDARDCTTAHGMFNYICNHVKYATNKGNLRSAITIFP  468
            GAKHAWRNASRCVGRIQWSKLQVFDARDCTTAHGMFNYICNHVKYATNKGNLRSAITIFP
Sbjct  121  GAKHAWRNASRCVGRIQWSKLQVFDARDCTTAHGMFNYICNHVKYATNKGNLRSAITIFP  180

Query  469  QRTDGKHDFRVWNSQLIRYAGYKQPDGSTLGDPANVQFTEICIQQGWKPPRGRFDVLPLL  528
            QRTDGKHDFRVWNSQLIRYAGYKQPDGSTLGDPANVQFTEICIQQGWKPPRGRFDVLPLL
Sbjct  181  QRTDGKHDFRVWNSQLIRYAGYKQPDGSTLGDPANVQFTEICIQQGWKPPRGRFDVLPLL  240

Query  529  LQANGNDPELFQIPPELVLEVPIRHPKFEWFKDLGLKWYGLPAVSNMLLEIGGLEFSACP  588
            LQANGNDPELFQIPPELVLEVPIRHPKFEWFKDLGLKWYGLPAVSNMLLEIGGL+FSACP
Sbjct  241  LQANGNDPELFQIPPELVLEVPIRHPKFEWFKDLGLKWYGLPAVSNMLLEIGGLQFSACP  300

Query  589  FSGWYMGTEIGVRDYCDNSRYNILEEVAKKMNLDMRKTSSLWKDQALVEINIAVLYSFQS  648
            FSGWYMGTEIGVRDYCDNSRYNILEEVAKKMNLDMRKTSSLWKDQALVEINIAVLYSFQS
Sbjct  301  FSGWYMGTEIGVRDYCDNSRYNILEEVAKKMNLDMRKTSSLWKDQALVEINIAVLYSFQS  360

Query  649  DKVTIVDHHSATESFIKHMENEYRCRGGCPADWVWIVPPMSGSITPVFHQEMLNYRLTPS  708
            DKVTIVDHHSATESFIKHMENEYRCRGGCPADWVWIVPPMSGSITPVFHQEMLNYRLTPS
Sbjct  361  DKVTIVDHHSATESFIKHMENEYRCRGGCPADWVWIVPPMSGSITPVFHQEMLNYRLTPS  420

Query  709  FEYQPDPWNTHVWKGTNGTPTKRRAIGFKKLAEAVKFSAKLMGQAMAKRVKATILYATET  768
            FEYQPDPWNTHVWKGTN TPTKRRAIGFKKLAEAVKFSAKLMGQAMAKRVKATILYATET
Sbjct  421  FEYQPDPWNTHVWKGTNWTPTKRRAIGFKKLAEAVKFSAKLMGQAMAKRVKATILYATET  480

Query  769  GKSQAYAKTLCEIFKHAFDAKVMSMEEYDIVHLEHETLVLVVTSTFGNGDPPENGEKFGC  828
            GKSQAYAKTLCEIFKHAFDAKVMSMEEYDIVHLEHETLVLVVTSTFGNGDPPENGEKFGC
Sbjct  481  GKSQAYAKTLCEIFKHAFDAKVMSMEEYDIVHLEHETLVLVVTSTFGNGDPPENGEKFGC  540

Query  829  ALMEMRHPNSVQEERKSYKVRFNSVSSYSDSQKSSGDGPDLRDNFESAGPLANVRFSVFG  888
            ALMEMRHPNSVQEERKSYKVRFNSVSSYSDSQKSSGDGPDLRDNFESAGPLANVRFSVFG
Sbjct  541  ALMEMRHPNSVQEERKSYKVRFNSVSSYSDSQKSSGDGPDLRDNFESAGPLANVRFSVFG  600

Query  889  LGSRAYPHFCAFGHAVDTLLEELGGERILKMREGDELCGQEEAFRTWAKKVFKAACDVFC  948
            LGSRAYPHFCAFGHAVDTLLEELGGERILKMREGDELCGQEEAFRTWAKKVFKAACDVFC
Sbjct  601  LGSRAYPHFCAFGHAVDTLLEELGGERILKMREGDELCGQEEAFRTWAKKVFKAACDVFC  660

Query  949  VGD  951
            VGD
Sbjct  661  VGD  663
```

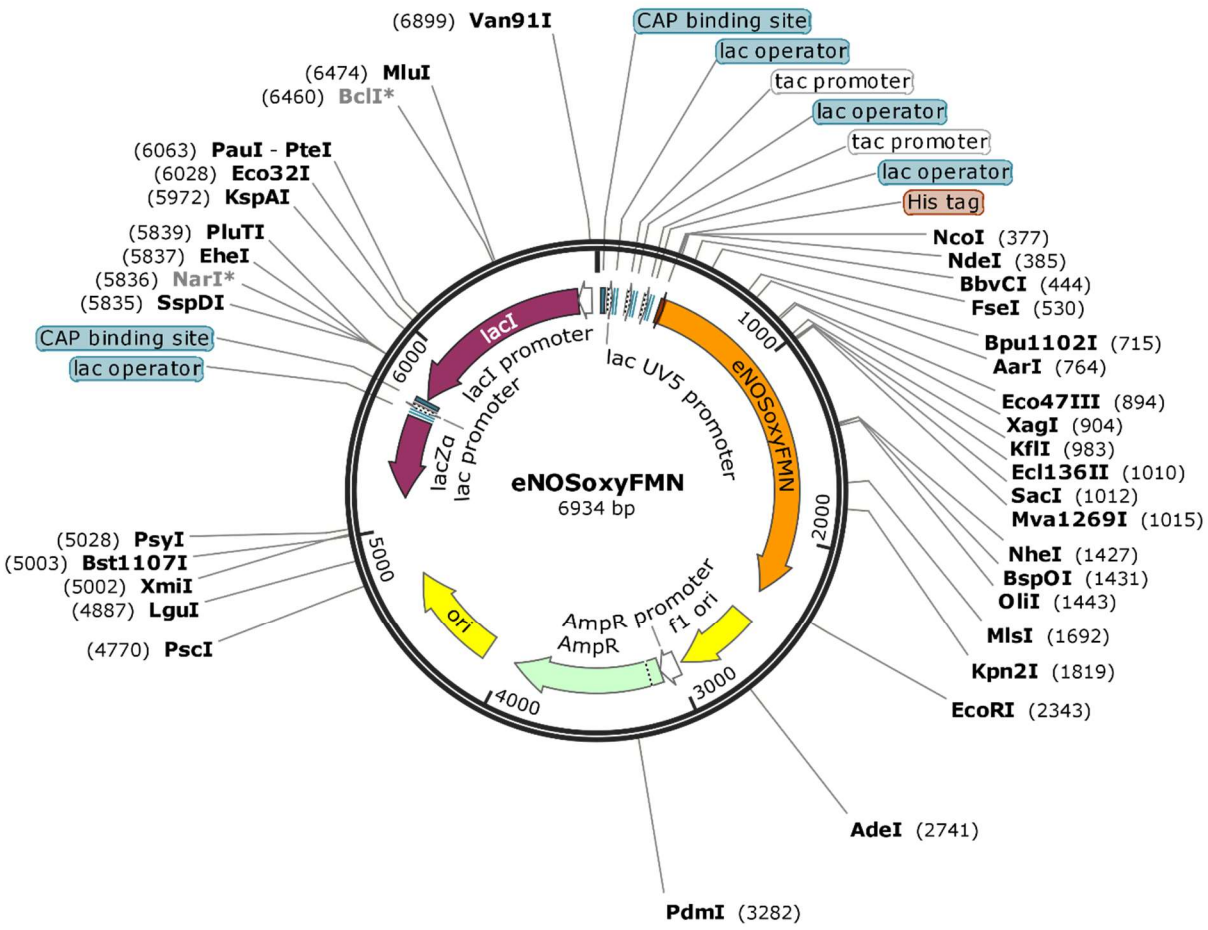

Table B5. Plasmid map of pHeNOSoxyFMN. This plasmid contains the truncated human eNOS oxyFMN sequence subcloned into pCWori via ligation. It is ampicillin-resistant and uses the moderate-expression promoter tac. Restriction enzymes EcoRI and NdeI were used to validate the subcloning process.

pHeNOSoxyFMNhisAmp (p535) – Human eNOSΔ66 oxyFMN with N-terminal polyhistidine tag in pCWori, cloned between NdeI and EcoRI.

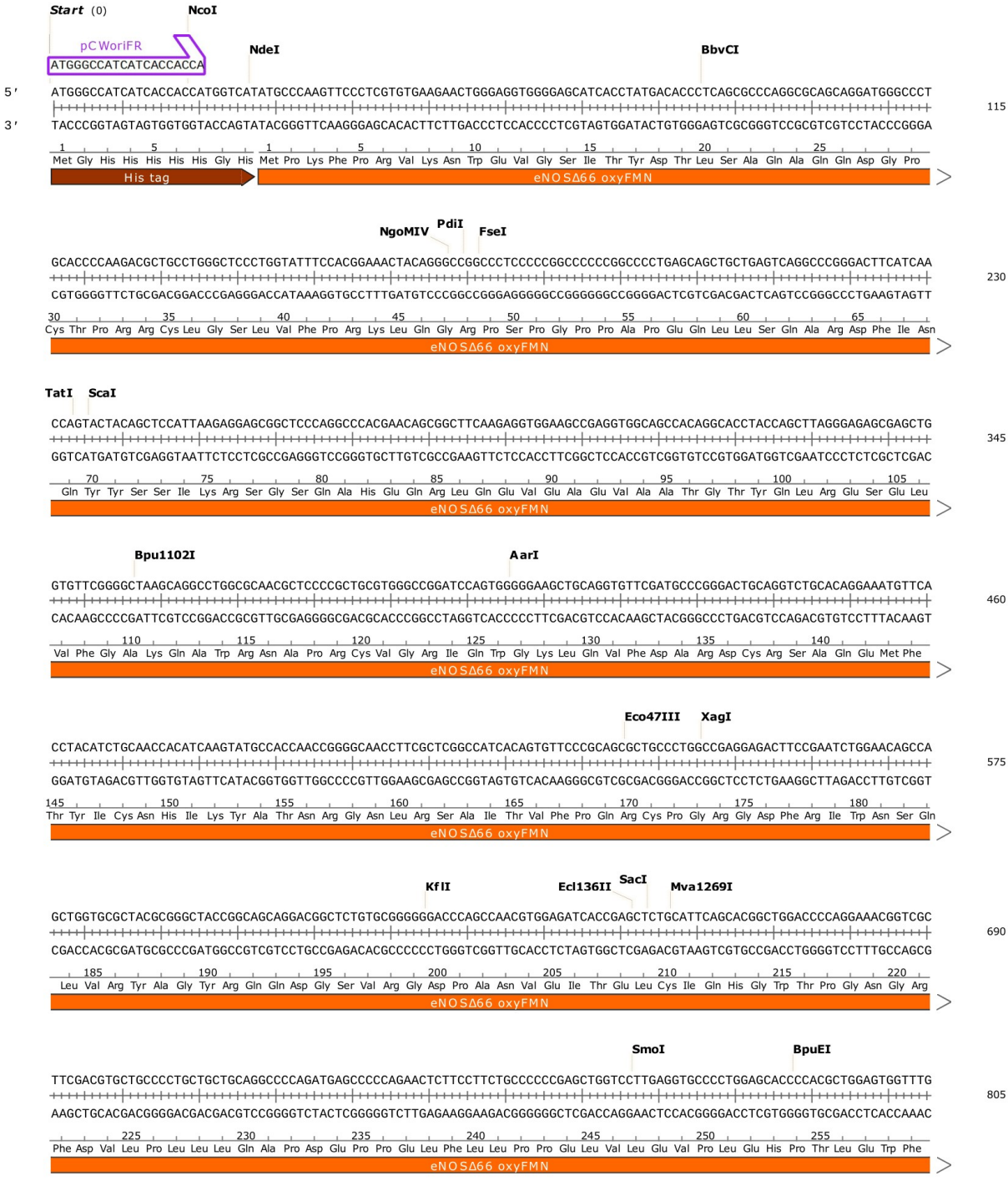

pHeNOSoxyFMNhisAmp (cont'd – 2)

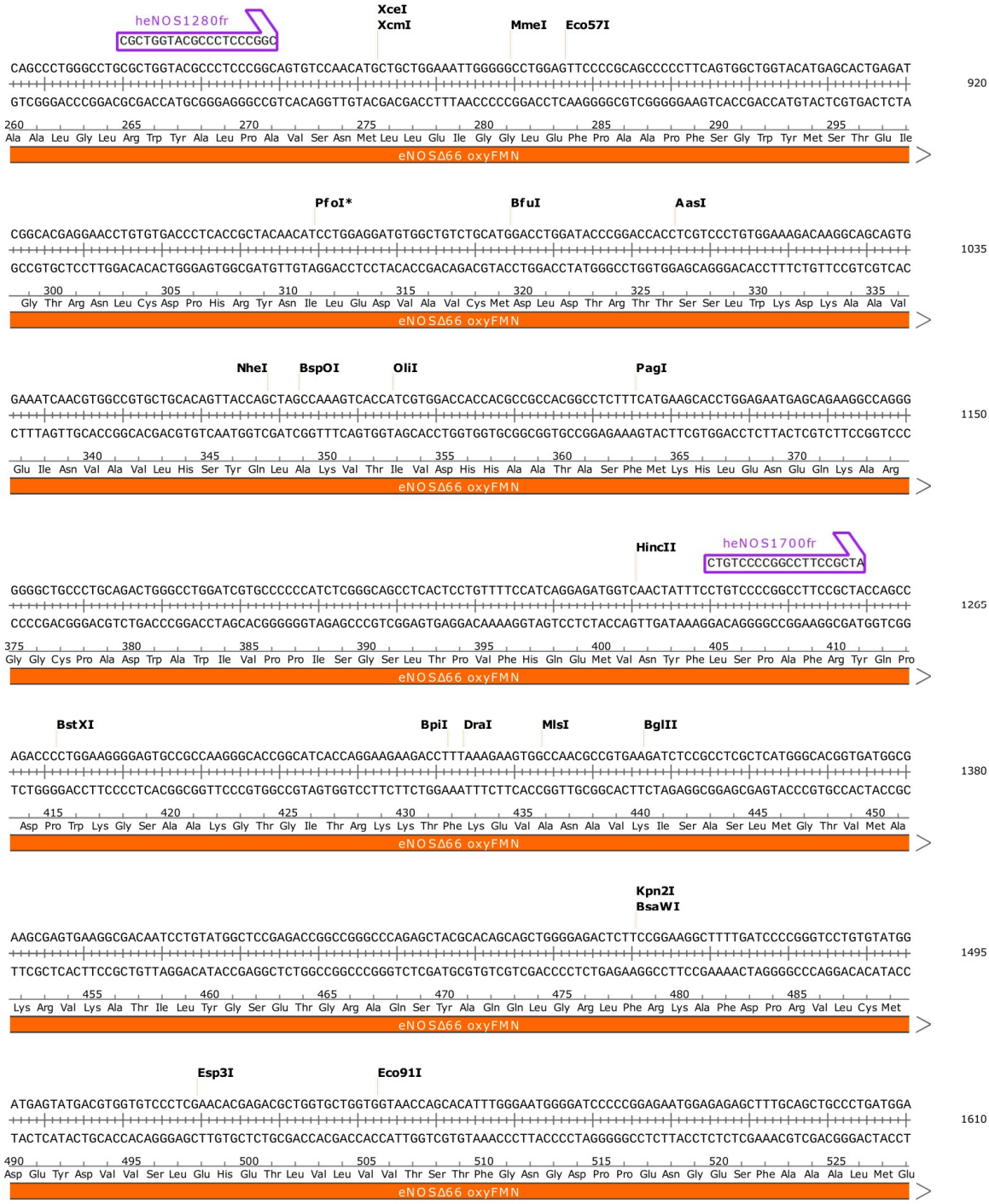

pHeNOSoxyFMNhisAmp (cont'd – 3)

Protein sequence alignment of eNOS (GenPept: P29474.3; Query) and eNOSoxyFMN (Sbjct) aligned using NCBI BLAST.

```
Query  66    PKFPRVKNWEVGSITYDTLSAQAQQDGPCTPRRCLGSLVFPRKLQGRPSPGPPAPEQLLS  125
             PKFPRVKNWEVGSITYDTLSAQAQQDGPCTPRRCLGSLVFPRKLQGRPSPGPPAPEQLLS
Sbjct  4     PKFPRVKNWEVGSITYDTLSAQAQQDGPCTPRRCLGSLVFPRKLQGRPSPGPPAPEQLLS  183

Query  126   QARDFINQYYSSIKRSGSQAHEQRLQEVEAEVAATGTYQLRESELVFGAKQAWRNAPRCV  185
             QARDFINQYYSSIKRSGSQAHEQRLQEVEAEVAATGTYQLRESELVFGAKQAWRNAPRCV
Sbjct  184   QARDFINQYYSSIKRSGSQAHEQRLQEVEAEVAATGTYQLRESELVFGAKQAWRNAPRCV  363

Query  186   GRIQWGKLQVFDARDCRSAQEMFTYICNHIKYATNRGNLRSAITVFPQRCPGRGDFRIWN  245
             GRIQWGKLQVFDARDCRSAQEMFTYICNHIKYATNRGNLRSAITVFPQRCPGRGDFRIWN
Sbjct  364   GRIQWGKLQVFDARDCRSAQEMFTYICNHIKYATNRGNLRSAITVFPQRCPGRGDFRIWN  543

Query  246   SQLVRYAGYRQQDGSVRGDPANVEITELCIQHGWTPGNGRFDVLPLLLQAPDEPPELFLL  305
             SQLVRYAGYRQQDGSVRGDPANVEITELCIQHGWTPGNGRFDVLPLLLQAPDEPPELFLL
Sbjct  544   SQLVRYAGYRQQDGSVRGDPANVEITELCIQHGWTPGNGRFDVLPLLLQAPDEPPELFLL  723

Query  306   PPELVLEVPLEHPTLEWFAALGLRWYALPAVSNMLLEIGGLEFPAAPFSGWYMSTEIGTR  365
             PPELVLEVPLEHPTLEWFAALGLRWYALPAVSNMLLEIGGLEFPAAPFSGWYMSTEIGTR
Sbjct  724   PPELVLEVPLEHPTLEWFAALGLRWYALPAVSNMLLEIGGLEFPAAPFSGWYMSTEIGTR  903

Query  366   NLCDPHRYNILEDVAVCMDLDTRTTSSLWKDKAAVEINVAVLHSYQLAKVTIVDHHAATA  425
             NLCDPHRYNILEDVAVCMDLDTRTTSSLWKDKAAVEINVAVLHSYQLAKVTIVDHHAATA
Sbjct  904   NLCDPHRYNILEDVAVCMDLDTRTTSSLWKDKAAVEINVAVLHSYQLAKVTIVDHHAATA
1083

Query  426   SFMKHLENEQKARGGCPADWAWIVPPISGSLTPVFHQEMVNYFLSPAFRYQPDPWKGSAA  485
             SFMKHLENEQKARGGCPADWAWIVPPISGSLTPVFHQEMVNYFLSPAFRYQPDPWKGSAA
Sbjct  1084  SFMKHLENEQKARGGCPADWAWIVPPISGSLTPVFHQEMVNYFLSPAFRYQPDPWKGSAA
1263

Query  486   KGTGITRKKTFKEVANAVKISASLMGTVMAKRVKATILYGSETGRAQSYAQQLGRLFRKA  545
             KGTGITRKKTFKEVANAVKISASLMGTVMAKRVKATILYGSETGRAQSYAQQLGRLFRKA
Sbjct  1264  KGTGITRKKTFKEVANAVKISASLMGTVMAKRVKATILYGSETGRAQSYAQQLGRLFRKA
1443

Query  546   FDPRVLCMDEYDVVSLEHETLVLVVTSTFGNGDPPENGESFAAALMEMSGPYNSSPRPEQ  605
             FDPRVLCMDEYDVVSLEHETLVLVVTSTFGNGDPPENGESFAAALMEMSGPYNSSPRPEQ
Sbjct  1444  FDPRVLCMDEYDVVSLEHETLVLVVTSTFGNGDPPENGESFAAALMEMSGPYNSSPRPEQ 1623

Query  606   HKSYKIRFNSISCSDPLVSSWRRKRKESSNTDSAGALGTLRFCVFGLGSRAYPHFCAFAR  665
             HKSYKIRFNSISCSDPLVSSWRRKRKESSNTDSAGALGTLRFCVFGLGSRAYPHFCAFAR
Sbjct  1624  HKSYKIRFNSISCSDPLVSSWRRKRKESSNTDSAGALGTLRFCVFGLGSRAYPHFCAFAR 1803

Query  666   AVDTRLEELGGERLLQLGQGDELCGQEEAFRGWAQAAFQAACETFCVGED  715
             AVDTRLEELGGERLLQLGQGDELCGQEEAFRGWAQAAFQAACETFCVGED
Sbjct  1804  AVDTRLEELGGERLLQLGQGDELCGQEEAFRGWAQAAFQAACETFCVGED 1953
```

pCaM$_{1234}$DNKan (p542) – CaM$_{1234}$DN in pET9d, cloned between NcoI and BamHI. Mutations relative to PubMed sequence AAA40864.1: D20N, D56N, D93N and D129N.

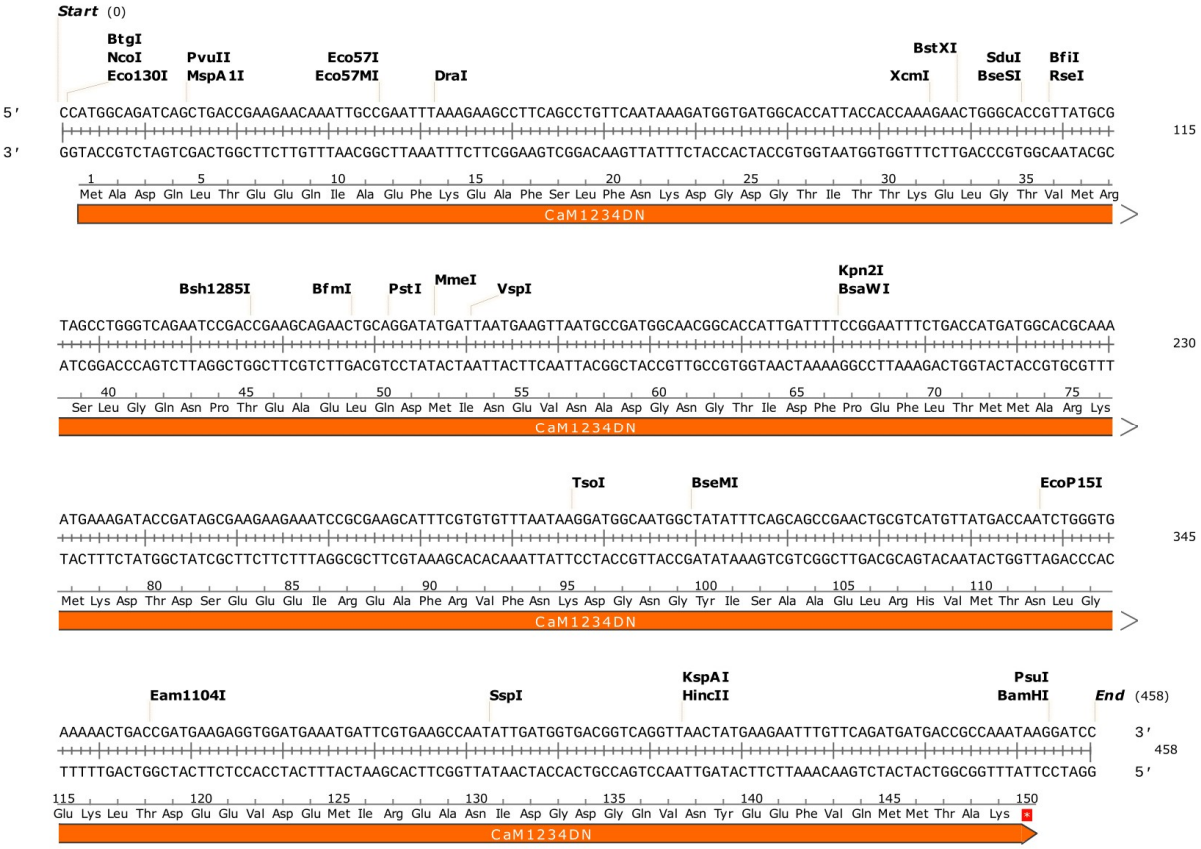

Protein sequence alignment of CaM (GenPept: AAA40864.1**; Query) and CaM$_{1234}$DN (Sbjct) aligned using NCBI BLAST.**

```
Query  1    MADQLTEEQIAEFKEAFSLFDKDGDGTITTKELGTVMRSLGQNPTEAELQDMINEVDADG  60
            MADQLTEEQIAEFKEAFSLF+KDGDGTITTKELGTVMRSLGQNPTEAELQDMINEV+ADG
Sbjct  1    MADQLTEEQIAEFKEAFSLFNKDGDGTITTKELGTVMRSLGQNPTEAELQDMINEVNADG  60

Query  61   NGTIDFPEFLTMMARKMKDTDSEEEIREAFRVFDKDGNGYISAAELRHVMTNLGEKLTDE  120
            NGTIDFPEFLTMMARKMKDTDSEEEIREAFRVF+KDGNGYISAAELRHVMTNLGEKLTDE
Sbjct  61   NGTIDFPEFLTMMARKMKDTDSEEEIREAFRVFNKDGNGYISAAELRHVMTNLGEKLTDE  120

Query  121  EVDEMIREADIDGDGQVNYEEFVQMMTAK  150
            EVDEMIREA+IDGDGQVNYEEFVQMMTAK
Sbjct  121  EVDEMIREANIDGDGQVNYEEFVQMMTAK  150
```